

High Resolution Electron Impact Study of the FUV Emission Spectrum of Molecular Hydrogen

Xianming Liu,[†] Syed M. Ahmed,[†] Rosalie A. Multari[†],
Geoffrey K. James and Joseph M. Ajello

Jet Propulsion Laboratory
California Institute of Technology
4800 Oak Grove Drive
Pasadena, CA 91109

Submit to *Astrophysical Journal Supplement*

March 1995

[†] National Research Council-Jet Propulsion Laboratory Associate

ABSTRACT

The emission spectrum of molecular hydrogen produced by electron impact excitation at 100eV has been measured in the wavelength range 1140 to 1675 Å. High resolution optically thin spectra ($\Delta\lambda=0.136\text{Å}$) of the FUV Lyman and Werner band systems have been obtained with a newly constructed 3 meter spectrometer. Synthetic *spectral intensities* based on the transition probabilities calculated by Abgrall *et al* (1987, 1989, 1993a&b) are in very good agreement with *experimentally* observed intensities. Previous modeling utilizing Allison-Dalgarno (1970) band transition probabilities with Hönl-London factors breaks down when the transition moment has significant J *dependence* or when rotational-vibrational coupling is significant. Rotation-vibration perturbation between $v=14$ of the B $^1\Sigma_u^+$ state and $v=3$ of the C $^1\Pi_u$ state and the rotational *dependence* of the transition moment in (6, 12) and (7, 1 3) bands of the Lyman system are examined, Complete high resolution reference experimental FUV spectra, together with the model synthetic spectra based on the Abgrall transition probabilities, are *presented*. An improved calibration standard is obtained and an accurate calibration of the 3-meter spectrometer has been achieved.

Subject headings: laboratory spectra - transition probabilities - ultraviolet: spectra (molecular hydrogen)

I. INTRODUCTION

Electron interaction with H_2 is a major factor that governs the ambient radiation field, temperature and state of ionization in molecular clouds and certain stellar atmospheres. The ambient UV radiation field of molecular clouds consists of Lyman and Werner band emission which partly determines the chemical composition of the molecular clouds. The vacuum ultraviolet (VUV) spectrum of H_2 is also of *fundamental* interest for planetary studies. Voyager and IUE flights have clearly showed that H_2 excitation by electron impact is the primary VUV emission process in the atmospheres of outer planets (Broadfoot *et al.* 1979, 1981; Clarke *et al.* 1980). Since the launch of the Hubble Space Telescope (HST), there have been several investigations of the aurora and dayglow phenomena of Jupiter by observing its H_2 emission spectra with the on board Goddard High Resolution Spectrometer (GHRS) and Faint Object Spectrometer (FOS) (Clarke *et al.* 1994; Trafton *et al.* 1994).

This paper describes the acquisition of high resolution optically thin H_2 spectra of the Lyman and Werner band systems in the far ultraviolet region with a newly constructed 3 meter spectrometer. Analysis of the high resolution spectra yields *refinements* of a previous model of the *excitation* of hydrogen molecule by electron. Previous models of the H_2 band applied to laboratory, astrophysical, and planetary emission analysis (Shemansky *et al.* 1983; Ajello *et al.* 1982, 1984, 1988; Trafton *et al.* 1994) contain minimal correction for perturbation, in addition, the J-dependence of electronic transition moment was *neglected*. Emission cross sections for B $^1\Sigma_u^+ \rightarrow X^1\Sigma_g^+$, C $^1\Pi_u \rightarrow X^1\Sigma_g^+$, B $^1\Sigma_u^+ \rightarrow X^1\Sigma_g^+$, B $^1\Sigma_u^+ \rightarrow X^1\Sigma_g^+$, D $^1\Pi_u \rightarrow X^1\Sigma_g^+$, and D $^1\Pi_u \rightarrow X^1\Sigma_g^+$ electronic transitions of H_2 have been obtained using the same model (Ajello *et al.* 1982, 1984, 1988; Shemansky *et al.* 1985).

While the model used by Shemansky and Ajello appears adequate for modeling spectra measured at 4-5 Å

resolution, significant discrepancies appear at higher resolution. Firstly, the experimental and theoretical work by Roncin *et al.* (1984) Roncin & Launay (1994), Senn *et al.* (1988), and Abgrall *et al.* (1987) have demonstrated the presence of perturbations between a number of excited energy levels. In addition, studies performed by Ford *et al.* (1974 & 1975a), and Abgrall *et al.* (1987, 1993b & 1993c) have shown that the relative intensities of some P(J+1) and R(J-1) branches deviate significantly from the rotational line strength ratios of the P(J+1) to R(J-1) in the presence of perturbations and a centrifugal potential. (Lefebvre-Brion & Field, 1986) Moreover, Senn *et al.* and Abgrall *et al.* (1993a) have revealed that incorrect assignments were made to several perturbed rotational levels prior to their work. These mis-assignments were, unfortunately, used in the works of Shemansky *et al.* (1983 & 1984), and many others. The P/R relative intensity deviations, together with the mis-assignments, can result in positional shifts and significant band shape changes in the synthetic spectra at high resolution. High resolution measurement under optically thin condition can precisely identify both effects. Finally, since the rotational constant of H₂ is very large (60-30 cm⁻¹), the centrifugal distortion potential cannot be neglected. Consequently, the electronic transition moment may exhibit a significant J-dependence. It is important to determine the effect of perturbations and variations in the transition moment on the excitation and emission cross sections at higher resolution.

Many theoretical studies have been performed on the H₂ molecule. Accurate *ab initio* calculations of the energy levels, wave functions, and transition moments for the lowest few excited electronic states of H₂ have been carried out. Allison and Dalgarno (AD) obtained band transition probabilities for the Lyman and Werner systems using the *ab initio* potential energy surfaces and transition moments obtained by Kolos and Wolniewicz (Allison & Dalgarno 1971; Kolos & Wolniewicz 1965, 1968, 1964, 1966; Kolos 1967; Wolniewicz 1969). Subsequently, Stephens and Dalgarno (SD) extended the previous work to obtain the vibrational band and total transition probabilities by including the Lyman continuum. (Stephens & Dalgarno 1972). Julienne (1973) also included the rotation-vibration coupling between B and C states to obtain the line emission probability of the Lyman and Werner band systems. Ford (1974, 1975a) considered the effect of the rotation-vibration perturbation between B and C states on the rotational line strength, and showed conclusively that coupling profoundly alters the intensity ratio of the P and R branches. More recently, Senn *et al.* calculated J=0(1)-6 rotation-vibration levels of the B, C, B' and D states by employing the *ab initio* potential energy surfaces of Wolniewicz and Dressler (1985), and numerically solving the coupled four state Schrödinger equation. The accuracy of this calculation allowed Senn *et al.* to revise a few previous assignments of rotational levels. Utilizing a semi-*ab initio* approach, Abgrall and co-workers (1993a; 1993b & 1993c) not only extended the work of Senn *et al.* to higher rotational levels, but also calculated the transition probability from each rotational level of the B and C states to its counterpart of the ground state and the total transition probabilities from the B and C states (Abgrall *et al.* 1992). Their calculations have revealed that a few dozen rotational levels of the B' Σ_g^+ state are strongly coupled to their counterparts of the C $^1\Pi_u$ state. Spectroscopically, the coupling is revealed by an energy positional shift and intensity deviation. Abgrall *et al.* (1987) have attempted to test their calculations by comparison to

experimental transition frequencies. However, because of the uncertainties in the initial population of the discharge, together with the effect of possible self-absorption, it was difficult to accurately compare the calculated and measured intensities.

Motivated by the strong astrophysical and theoretical interest, many experimental studies of H_2 have been performed since the pioneering works of Lyman, Wcmer, Dieke and Hopfield. Huber and Herzberg (1979) have provided an extensive tabulation of the experimental study performed prior to 1979. More recently, Dabrowski & Herzberg (1974), Dabrowski(1984) and Roncin *et al* (1984), Roncin & Launay(1994) have performed extensive high resolution emission studies of H_2 . Aided by their semi-ab *initio* calculations of the transition frequencies and transition probabilities, Abgrall & Roueff(1989), Abgrall *et al.* (1 993b & 1993c, 1994), and Roncin *et al.* (1 994) have provided extended rotational assignments of the $B^1\Sigma_u^+ \rightarrow X^1\Sigma_g^+$, $C^1\Pi_u \rightarrow X^1\Sigma_g^+$, $B^1\Sigma_u^+ \rightarrow X^1\Sigma_g^+$, $D^1\Sigma_u^+ \rightarrow X^1\Sigma_g^+$ transitions. Most of the recent experimental work on the Lyman and Werner systems has been published in Table and Atlas formats.

Optically thin high resolution experimental spectra of the H_2 molecule are needed to verify the accuracy of the various theoretical calculations. Electron impact induced fluorescence spectroscopy is a technique well suited for accurate measurement of the optically thin spectrum. Because the impact interaction is a single scattering process, accurate measurements of the relative emission intensities are possible. Moreover, the interaction between the molecule and the exciting electron can be modeled quantitatively.

The electron impact induced emission spectrum of H_2 is also an ideal and convenient primary standard for the calibration of VUV spectrometers(Ajello *et al.* 1988). The H_2 emission spectrum covers very wide wavelength range, from 800 to 1700 Å, and consists of more than 70,000 rotational lines from seven electronic transitions. A more accurate calibration (better than 10%) can be achieved with an H_2 model which takes both perturbation and transition moment variation into account.

This paper presents the results of an electron impact study of the optically thin high resolution (FWHM 0.064-0.136 Å) FUV (1200-1675 Å) emission spectrum of H_2 measured at 100 eV excitation energy. The objectives are to examine the accuracy of the calculated transition probabilities, refine the H_2 spectral model and improve the H_2 calibration standard. Section II describes the high resolution experimental apparatus and procedures used in the spectral measurements. Section III begins with a discussion of the theoretical model which uses AD and SD transition probabilities to generate the synthetic spectrum, and is followed by a description of the approximations used in the model. A procedure is presented to correct the deficiencies in the model with the line transition probabilities of Abgrall and co-workers. Section IV first examines the relative accuracy of the AD and Abgrall transition probabilities by comparing the calculated and observed spectra, then performs an iterative calibration of the experimental spectra by taking into account perturbations and the rotational dependence of the transition moment. The calibration provides a more accurate model spectrum that can be used as a calibration standard at high resolution. Section VI summarizes

the refinements in the new model and in the synthetic emission spectrum of H_2 as a calibration standard, Section VI also briefly discusses astrophysical applications of the new model for hot spectra.

II. EXPERIMENTAL SETUP

High resolution UV spectrometers ($\lambda/\Delta\lambda = 10^5$) on board orbiting spacecraft are now capable of observing emission spectra from astrophysical objects under a variety of gaseous regimes. Laboratory instrumentation is needed to match this high resolution capability. This is the first laboratory program equipped to measure high resolution UV spectra under optically thin conditions with the goal of measuring rotational line emission cross sections which can be used to infer other important atomic physics parameters: rotational line oscillator strengths, predissociation yields, branching ratios and resonances. A custom designed 3.0-m UV spectrometer in tandem with an electron collision chamber mounted at the entrance slit provide a highly sensitive optical system.

An Acton VM-523-SG 3.0-m vacuum ultraviolet spectrometer has been used for these measurements. This UV spectrometer is equipped with three exit slit assemblies capable of interchangeable mounting of either single pixel or custom designed FUV or EUV CODACON array detector (McClintock *et al.* 1982). To our knowledge it is the highest resolution single scattering instrument in the U.S. This is the latest addition to our laboratory which is already equipped with a medium resolution 1.0-m spectrometer (Ajello *et al.* 1989) and a low resolution 0.2-m spectrometer (Ajello *et al.* 1982). The optical system employed in the high resolution instrument is a normal incidence mounting of concave 1200 grove/mm² grating with a horizontal aperture ratio of 31. The spectrometer is equipped with an indexable kinematic dual grating holder assembly which allows grating to be interchanged without re-alignment or adjustment after initial alignment in the instrument. The 1200 grooves/mm grating has an Al+MgF₂ coating blazed at 1200 Å, whereas the 2400 grooves/mm grating has iridium surface blazed at 600 Å. The spectrometer has two entrance ports. Two gratings cover the spectral region from 300 to 3700 Å. Any one of the slit ports can be selected or deselected during the experiment without breaking the vacuum using external diverter mirror feed throughs. The optical path of the photons produced during an electron-target impact event is shown in the top view diagram of the collision chamber (Figure 1). This diagram also displays the electron gun, collision chamber and focussing mirror. The retractable focussing mirror is coated with iridium and located opposite to the entrance slit producing an intensity enhancement of about 60% by reflecting more of the emitted photons and enabling greater filling of the grating surface. The top view of the experimental set-up is shown in Figure 11.

Emitted photons are detected by the high resolution spectrometer at an angle of 90° to the plane containing the crossed electron and target beams. No corrections for polarization of the radiation are made, since polarization is expected to be small for H_2 molecular transitions at 100 eV excitation energy.

The electron-beam source used in the present set-up is essentially similar to the one described in detail by Ajello *et al.*, 1990. Thermionic electrons are produced by heating a pure tungsten or thoriated tungsten filament. The energy

resolution of the electron beam is 0.3 eV, The assembly diagram of the electron gun and the block diagram of the electronics for the high voltage 0-2.5 keV ramp, electron gun and lenses are shown in Figs. I and II, respectively, of Ajello *et al.* (1990). The electron beam is collimated by an axially symmetric magnetic field (~ 100 Gauss) which is generated by a solenoid system. A Faraday cup designed to minimize back scattered electrons is used to monitor the electron beam current. It also prevents the escape of secondary electrons generated inside the cup at high accelerating energies. Constant electron beam currents can be obtained in the electron energy region varying from few eV to 2.5 keV.

The instrument is entirely automated for repetitive spectral scans and is interfaced with a IBM PC/compatible computer. Wavelength scans are performed using an API motor indexer to provide channel advance pulses for the multichannel scaler which in turn drives the stepper motor. The stepper motor rotates the diffraction grating so as to sweep the dispersed radiation to be scanned in the exit slit plane. Detailed description of the electronics used in the present measurements is shown in block diagram form in Figure 111.

The data are taken in two operating modes: 1). Fixed grating and linear scanning of electron beam energy between programmable start and stop energies. 2). Fixed electron beam energy with programmable wavelength sweeps. The latter mode was used in this experiment. The spectral scans are performed with a *crossed beam* geometry. In this mode, a magnetically collimated electron beam, whose energy can be selected in the range 1.0 eV to 2.5 keV is crossed with a target gas beam formed by a capillary array at a background pressure range of 8×10^{-8} to 4×10^{-4} Torr. The two beams intersect at 90° . This geometry establishes a point emission source ($\sim 2 \text{ mm}^3$) collision region, Optimization of the signal can be achieved by (1) aligning the position of gas beam with respect to the electron beam using an x,y,z manipulator, and (2) rotating the focus mirror. Alternatively, cross section measurements are conducted in a *swarm mode* geometry. A uniform static gas sample can be admitted to the chamber over the same pressure range forming a cylindrical line source collision region of approximately 4 cm in length and 2 mm in diameter for the excitation function measurements.

The instrumental resolution measured from an extended source discharge lamp, together with the experimental values obtained from the crossed beam point source are given in Table 1. For the case of a point source (c + molecule/atom) the complete efficiency of the grating could not be utilized due to underlining of the grating, and hence, the attainable resolution is lower. A simple calculation shows that without the focussing mirror only 22% of the available width of the 1200 grooves/mm grating is utilized for the present geometry with a 1 mm^3 emission source. The present observations are made at an instrumental resolution limit of 0.136 Å corresponding to 40 microns slit width. This represents a 37-fold improvement compared to the 0.2-m spectrometer used to obtain electron-impact emission spectra from the Rydberg series of H_2 at 5.0 Å resolution (Ajello *et al.*, 1984) and a two-fold improvement compared to the 1.0-m spectrometer used for measuring the emission cross sections of the b', c' states of N_2 at 0.3 Å (Ajello *et al.*, 1989). However the best resolution of 0.024 Å ($\lambda/\Delta\lambda=50,000$ at 10 microns slit width) is used for the

electron-impact hydrogen Lyman-alpha line in the third order. The instrument transmission function is shown in a paper by Ajello *et al* (1995).

Two single channel detectors (a channel electron multiplier (CEM) and a photomultiplier with a CsI photocathode and MgF₂ window) are installed on two of the three available exit ports. The present measurements are made with a commercially available Galileo Electro-Optics model 4503 CEM with a cesium iodide coating deposited at our laboratory to extend the spectral response from 1400 to 1800 Å. Dark counts increased from 1 count per 50 sec to 1 count per 10 sec following the CSI deposition. The photomultiplier tube spectral range spans the 1150-3500 Å region, while a CODACON 1024-array detector will be used on the focal plane exit slit port in future work,

III. THEORY

In an electron-impact induced emission experiment, a molecule initially in the ground state $|X, v'', J''\rangle$ is excited to the excited state $|\alpha, v, J\rangle$ as a result of inelastic collision with the impact electrons, the molecule subsequently emits a photon by a radiative decay to the final state $|X, v_f, J_f\rangle$. The photo-emission intensity is proportional to excitation rate $g(\alpha, v, J, E_e)$ and emission branch ratio:

$$I(X, \alpha, v_f, v, J_f, J) = \frac{A(X, \alpha, v, v, J, J)}{A(X, \alpha, v, J)} g(\alpha, v, J, E_e) \quad (1a)$$

$$A(X, \alpha, v, J) = \sum_{v_f, J_f} A(X, \alpha, v_f, v, J_f, J) \quad (1b)$$

where $A(X, \alpha, v_f, v, J_f, J)$ is the Einstein A coefficient for spontaneous transition from the excited state $|\alpha, v, J\rangle$ to the level $|X, v_f, J_f\rangle$ of the $X^1\Sigma_g^+$ state, and $A(X, \alpha, v, J)$ is the total emission probability. The excitation rate, $g(\alpha, v, J, E_e)$, is proportional to the population of the molecule in the initial level, the excitation cross-section, and the impact electron flux. The excitation cross-section can be calculated from a known transition probability and a measured excitation function (Shemansky *et al.* 1985a & 1985 b).

Three distinct mechanisms, resonance, cascade, and direct excitation, have been identified in the electron impact excitation of the B and C states of H₂. The resonance contribution arises from the formation of a short-lived negative molecular ion, which subsequently decays to the B and C states. The cascade arises from excitation from the X state to the $E, F^1\Sigma_g^+$ state, followed by radiative relaxation to the B state. Although excitation is forbidden by the dipole selection rule, the cascade process contributes about ~ 12% of the total emission cross section of the B state at 100-300 eV. Cascade contributes primarily to the $v=0-4$ of the B state. Both resonance and cascade contributions become important at low electron impact energy (12 ~ 19 eV) when direct excitation is small. For excitation energies above 20 eV, the direct excitation contribution dominates,

Because the cascade affects only a few low vibrational levels of the B state and is much less important than direct

excitation at 100 eV, most of the previous studies treated cascade with a very simple model. Shemansky and Ajello, for example, calculated the cascade with a constant electronic transition moment and the Frank-Condon factors calculated by Lin (1974) together with the experimental results of Ajello *et al* (1984). A similar approach is adopted in the present work.

In past modeling of the direct excitation contribution used the band and total transition probabilities calculated by AD and SD. A detailed formulation has been presented in a number of publications (Shemansky *et al* 1983, Ajello *et al* 1984, Trafton *et al* 1994). The model involved calculation of the excitation rate, $g(\alpha, \nu, j, E_e)$, with the calculated oscillator strength and measured excitation function as well as the replacement of $A(X, \alpha, \nu, v, J_p, J)$ and $A(X, \alpha, \nu, J)$ in Eq.(1) with the band and total transition probabilities calculated by AD and SD.

In general, the transition probabilities in Eq.(1) depends on rotational, vibrational and electronic quantum numbers. Since the AD oscillator strengths and transition probabilities were calculated without consideration of rotational coupling interferences, any model which utilizes these transition probabilities has to make two assumptions: the transition moment does not depend on rotational quantum number; and the relative intensity of the P and R branches originating from the same rotational level is given by the ratio of Hönl-London factors. The approximations are applied for both excitation and emission process.

The model is, however, expected to yield poor results when either or both of the assumptions break down. Both rotational dependence of the transition moment due to the centrifugal potential and local perturbations between $B^1\Sigma_u^+$ and $C^1\Pi_u$ states can invalidate the assumptions. The presence of the centrifugal potential, $J(J+1)/2\mu R^2$, makes it impossible to achieve a complete separation of rotation from vibrational motion. Because of the large rotational constant of H_2 , the electronic transition moment may display a significant J-dependence. Even if the J-dependence of the transition moment is negligible, the centrifugal distortion can cause the relative intensity of P(J'+1) and R(J'-1) to deviate from Hönl-London factors as it mixes different vibrational wave functions for $J''=J'+1$ and $J''=J'-1$ (Abgrall *et al*, 1987). A local perturbation produces mixing of the two perturbing levels and therefore alters the transition probabilities of the two levels, though the sum of the transition probabilities remains unchanged. The relative intensities of the P and R transitions from each of the perturbing levels can be changed profoundly. The line transition probabilities calculated by Abgrall *et al* (1993b& 1993c) have revealed that the transition moment (A/ν^3) is J-dependent, and both band and line transition probabilities can be changed significantly by a local perturbation.

We have developed a simple procedure using the Abgrall transition probabilities to account for perturbations and correct the deficiency in the model. The correction is performed in three steps: one for emission probability, one for the excitation probability, and the other for total transition probability. Following Ford (1975a), we attribute the overall perturbation effect to an "effective" rotational line strength. In each step, the correction factor is obtained from the ratio of the perturbation-corrected to an unperturbed transition probabilities. Since the J=0 level of the $B^1\Sigma_u^+$ state is not perturbed by the $^1\Pi_u$ component of the $C^1\Pi_u$ state, the calculated transition probability of P(J''=1) can be used

as an unperturbed transition probability for the Lyman transition. Similarly, the Q-branch of the Werner system arises from or reaches to the ${}^1\Pi_u^+$ component, which is not perturbed by the $B\ ^1\Sigma_u^+$ state, so the calculated transition probability for Q(J) can be used as the unperturbed value for both P(J+1) and R(J-1) branches. For the Werner bands the rotational line strengths are J+1, 2J+1, and J for R(J-1), Q(J), and P(J+1), respectively. Rotational line strengths for the Lyman transitions are J, and J+1 for R(J-1) and P(J+1), respectively. The effective correction factor for each perturbed emission transition can thus be written as

$$CP(J+1)_W = \frac{(2J+1)A_{P(J+1)}}{JA_{Q(J)}} \quad CR(J-1)_W = \frac{(2J+1)A_{R(J-1)}}{(J+1)A_{Q(J)}} \quad (2a)$$

$$CP(J+1)_L = \frac{(2J+1)A_{P(J+1)}}{(J+1)A_{P(J=1)}} \quad CR(J+1)_L = \frac{(2J+1)A_{R(J-1)}}{JA_{P(J=1)}} \quad (2b)$$

where CP and CR are the correction factors for P and R branches, the subscript identifies the type of transition involved, and A is the rotational line transition probability calculated by Abgrall & Roueff (1989). Since the eigenfunction of each perturbed state will have a portion of the zeroth-order property of the other state, the "eigen" dipole matrix element is a linear combination of the zeroth-order parallel and perpendicular dipole matrix elements. However, we treated it as if it were either only parallel or only perpendicular. The correction factor CP and CR must be understood to be *effective* or numerically equivalent correction values, which are conveniently employed to measure the relative deviations of the corrected line intensities from the "unperturbed" values.

CP and CR yield the correction factor for emission directly. The correction for the excitation step, however, is slightly different. Since excitation via both P(J+1) and R(J-1) transitions lead to the same excited level J, the correction factors for P(J+1) and R(J-1) must be *weighted* according to line strength and the population of the $J''=J+1$ and $J''=J-1$ levels. The overall correction for the line transition probabilities is the product of the correction factors for excitation and emission.

Rotation-vibrational coupling also modifies the value of the total transition probability, $A(J,v)$. In general, $A(J,v)$ consists of the contributions from emissions to both discrete and continuum levels. The discrete component of $A(J,v)$ can be obtained from a summation of the relevant line transition probabilities calculated by Abgrall *et al.* The continuum contribution can be obtained from the calculation by Stephens and Dalgarno. When complete line transition probabilities are not available, the approximate $A(J,v)$ can be obtained in the following manner. Assuming that the coupling occurs primarily between the B and C states, and that the mixing coefficient of the eigenfunction for this interaction is β , the corrected $A(J,v)$ is given by the zeroth-order transition probabilities $A^{(0)}(J,v_C)$ and $A^{(0)}(J,v_B)$ as (Glass-Maujean *et al* 1984)

$$A(J, \nu_C) \approx (1 - \beta^2) A^{(0)}(J, \nu_C) + \beta^2 A^{(0)}(J, \nu_B) \quad (3a)$$

$$A(J, \nu_B) \approx (1 - \beta^2) A^{(0)}(J, \nu_B) + \beta^2 A^{(0)}(J, \nu_C) \quad (3b)$$

where the mixing coefficient β is given by Senn *et al.* (1988), and Abgrall & Roueff (1989). The calculation performed by Senn *et al.*, and subsequently by Abgrall & Roueff also considered non-adiabatic coupling between the B, C, B', and D states. However, since the perturbations that affect transition in the FUV region are mainly due to the rotation-vibrational coupling between the B and C states, Eq.(3) should be a very good approximation. The zeroth-order $A^{(0)}(J, \nu_C)$ and $A^{(0)}(J, \nu_B)$ can be taken from Tables 2 and 5 of SD. Since the numerical values of $A^{(0)}(J, \nu_C)$ and $A^{(0)}(J, \nu_B)$ for the coupled levels are very similar, the correction of the total transition probability amounts to only a 1 ~7% change.

IV. ANALYSIS AND RESULTS

Using the model described in Section III and the transition probabilities of Allison and Dalgarno and Stephens and Dalgarno, a synthetic spectrum can be generated for the Lyman and Werner band systems of H₂. After convolution of the synthetic data file with the appropriate experimental line profile, the data can, in principle, be compared to the experimentally observed spectrum.

However, several factors need to be considered before the convolved synthetic spectrum can be directly compared to the experimental spectrum. Firstly, the experimental parameters such as electron beam current and gas pressure can fluctuate during a long scan. In addition, the experimental data must be calibrated to take into account systematic spectral sensitivity variation since the efficiencies of individual instrumental components such as the grating and detector are wavelength-dependent. Since the overall instrumental sensitivity is known only with large uncertainties, the experimental spectrum must be calibrated using the synthetic spectral data. However, the synthetic spectral data itself can have errors due to the approximations used in building the model as well as inaccuracies of the input parameters used. Since most of the errors in the model spectrum are unknown until it is compared to the experimental data, the uncertainties introduced by neglecting perturbation and rotational dependence of the transition moment must be carefully examined.

A. Accuracy of the Theoretical Transition Probabilities

The relative intensities of the observed transitions can be measured very accurately even though measurement of the absolute intensities is difficult. When the observed transitions are close enough to each other that the experimental spectral sensitivity change is not significant, the observed relative intensities can be used to check the consistency of the calculated transition probabilities.

We first determine the uncertainties in the calculated transition probability. The transition probabilities calculated by AD and SD were obtained under the assumption that the effects of perturbation and a centrifugal potential can be

neglected. The dependence of the electronic dipole moment on the internuclear distance was not explicitly considered in the work of AD. Schmoranzcr, Imschweiler, and Nell (1984) reported that their experimentally measured radiative lifetime were about 8% and 15% longer than the theoretical lifetimes of the B and C states obtained by SD. However, a more extensive *ab initio* calculation of the electronic transition moment by Dressler and Wolniewicz (1985) yielded essentially same results as those of SD, Glass-Maujean *et al* and Dressler *et al* suggested that radiation trapping may explain the difference between the measured and calculated lifetimes, Since the spectrum is obtained at low pressure (10^{-4} torr) and the emission bands in FUV region involve final state with $v'' \neq 0$, radiation trapping is not significant in the present experimental configuration. Hence, the calculated band and total transition probabilities used in the model should be sufficiently accurate for the Q-branches and for most of the P- and R-branches when coupling is absent and the state involved is not very close to the dissociation limit Nevertheless, it is important to remember that the model utilizing AD transition probabilities will breakdown when a local perturbation exists between the C and B states.

Discrete line transition probabilities calculated by Abgrall *et al* are obtained by solving a system of four coupled Schrödinger equations for the B, C, B' and D states and by using the *ab initio* transition moment calculated by Dressier *et al* (1986), Ford *et al* (1975b) and Rothenberg *et al* (1967). Abgrall *et al* have adjusted the *ab initio* potentials of Wolniewicz and Dressier slightly so that the calculated frequencies of the lowest J levels agree with the experimental observation.

Figure IV shows an over-plot of a region of the high resolution experimental H_2 spectrum measured at 100eV electron impact energy (solid line) and the convolved synthetic spectrum (dotted line) based on the transition probabilities of Allison *et al* and Stephens *et al*. The assignment of each observed transition is indicated in the figure. The absolute wavelength scale of the experimental spectra is established by using the known wavelength of the H Lyman α emission from dissociative excitation of H_2 1215.685 Å, while the spectral intensity is normalized to the Q(1) transition of the (3,7) Werner band at 1229.981 Å. The Q(1) transition is chosen because the rotational levels of the $C^1\Pi_u^+$ ($C^1\Pi_u^f$) state, which connect to the rotational levels of the ground state $X^1\Sigma_g^+$ via A J=0 transitions, are not perturbed by any rotational levels of the $B^1\Sigma_u^+$ state. No intensity calibration is made for the experimental spectrum in the Figure since the overall spectral sensitivity of the system change by less than 2% over the range 1225-1237 Å.

It is clear from Figure IV that several prominent synthetic spectral features differ significantly from the experimental observations in both position and intensity. All the calculated strong transitions between 1227 and 1236 Å appear to be shifted toward the blue. This positional shift is, however, not uniform: the low-J transitions of the Lyman (14,7) band shift by 1.22- 1.5Å, whereas those of the Werner (3,7) band shift by 0.13-0.43 Å. Moreover, the predicted relative intensities are strikingly different from the experimental observations. In general, the model underestimates the relative intensity of the Lyman (14,7) band, and overestimates that of the Werner (3,7) band. An

apparent **discrepancy** in relative intensity between the **theory** and experiment, involves the P(3) line of the Werner (3,7) band at 1234.09 Å whose intensity is overestimated by a factor of 2.5. The worst numerical disagreement occurs at 1228.48 Å, corresponding to the R(0) transition of the (14,7) Lyman band, where the model underestimates its intensity by a factor of 45.

These intensity and positional discrepancies can be explained. Firstly, *ab initio* calculations performed by Senn *et al* and Abgrall *et al* have suggested that the previous assignments for J= 1 and 2 of $v_c=3$ need to be interchanged with the J=1 and 2 levels of $v_B=14$. After this re-assignment is adopted in the synthetic spectrum, the calculated peak position moves closer to that in the observed spectrum. However, significant differences in peak position still remain. Further examination indicates that spectroscopic constants used in the program for the (14,7) and (3,7) bands were obtained without consideration of perturbations and possibly involved other mis-assignments. Indeed, none of the wavelengths for the low J (<5) transitions of both bands were predicted correctly by the program. When the experimentally observed frequencies obtained by Roncin & Launay(1994) are used, the peak positions of the calculated spectrum are in agreement with the experiment. The calculations by Senn *et al* and Abgrall *et al* have also indicated that J= 1 and 2 of the $v_B= 14$ level of the B state are strongly coupled to their counterparts in the $v_c=3$ level of the C state. The eigenstate of the J= 1 levels have ~27% mixture of the other zeroth-order character, while for J=2 levels have ~ 13% character of its zero-order perturbing partner. Moreover, the spontaneous transition probability calculations by Abgrall and co-workers have shown that the relative Einstein A coefficient of the P and R branches for J=1 and 2 of ($v_c=3, v_x$) and ($v_B= 14, v_x$) deviate from the ratios of Hönl-London factors.

The relative intensities of the synthetic spectrum are obtained under the assumption that the relative intensities of P(J+1) and R(J- 1) branches equals the ratios of their Hönl-London factors. When coupling is significant, however, the relative intensities can deviate significantly from these line strength ratios. Since the rotational line transition probabilities for the Lyman and Werner bands have been calculated extensively by Abgrall and co-workers, we can use their transition probabilities to measure the degree of "deviation" and model the spectrum, Good agreement between the experimental and synthetic spectra based on the rotational line transition probability demonstrates the accuracy of the calculations by Abgrall and co-workers.

The second and third columns of Table II list the emission correction factors for the rotational lines of the Lyman (14,0) and (14,7) and Werner (3,0) and (3,7) bands obtained using the procedure described in Section III and the line transition probabilities calculated by Abgrall *et al* (1993b& 1993c). The fifth and sixth columns list the correction factors for excitation and total transition probability. The last column displays the overall correction factor for the observed transition. For comparison, the fourth column of the Table lists the correction factors published by Ford (1975a), where available. While some differences exist between the two sets of correction factors, our experimental spectrum can not distinguish one from the other for most of the transitions in Figure 1 V. In the present work, we have used the correction factors listed in the second column of Table II, which are based on the Abgrall *et al*'s transition

probabilities.

Figure V shows an **overplot** of experimental and synthetic spectra based on the correction factors in Table II. The overall correction factors are obtained by multiplication of the excitation and emission correction factors, followed by a **division** of the correction factors of the total transition probability. The **corrected intensity** is obtained by the product of the model output intensity and **the** overall correction factor. The R(0) transition of the (14,7) Lyman band, for instance, arises from excitation from ($v''=0, J''=0$) via an R transition and ($v''=0, J''=2$) via a P transition to ($v'=14, J'=1$) of the B state, followed by a radiative **decay** to $J'=0$ of the $v'=7$ level of the X state. The emission correction factors for 0(14,0)R Lyman and 2(14,0)P Lyman are calculated to be 0.1243 and 2.187, respectively, from Eq.(2), the excitation correction factor of the 0(14,0)R Lyman transition is **determined to be** 0.6765 by averaging the two emission correction factors over the population and line strengths. Meanwhile, the emission correction factors for the 0(14,7)R Lyman transition and the total transition probability are calculated to be 74.09 and 1.075, respectively from Eq.(2) and (3). The overall correction factor is thus as $0.6765 \times 74.09 / 1.075 = 46.63$. So, if the line transition probability **calculated** by Abgrall *et al* is accurate, the old model underestimates the intensity of the 0(14,7) R Lyman transition by a factor of approximately 47.

The experimental **spectrum** and model spectrum corrected on the basis of the Abgrall transition probabilities are again normalized to the Q(1) transition of the (3,7) band of the Werner system in Figure V. It can be seen that the agreement between the observed and calculated intensities is now extremely good. Therefore, the line transition probabilities calculated by Abgrall and co-workers appear very accurate, at least for the (14,7) Lyman and (3,7) Werner bands.

The intensity **disagreements** in Figure IV are almost exclusively due to the effects of coupling between the B and C states. The centrifugal potential arising from rotational interaction is small when J'' is small. For the (3, 0) and (3,7) bands of the Werner system, the transition dipole matrix element of the Q-branch changes by less than 1 % as J'' increases from 1 to 4, according to the calculations of Abgrall *et al*.

We now consider a different region of the FUV spectrum of H_2 around 1580 Å. The synthetic model that utilizes the AD transition probabilities is also expected to breakdown when the **J-dependence** of the transition moment is significant. Since the centrifugal potential is proportional to $J(J+1)/2\mu R^2$, the rotational dependence of the transition moment is normally **expected to be** observed at high J levels. At moderate temperature, the Boltzmann thermal distribution does not populate the high J levels and **the J-dependence** of the transition moment can **not be** easily detected. Nonetheless, when the energy level is very close to the asymptotic dissociation limit, the variation of the transition moment with J can be significant because of the non-radiative **processes** and non-adiabatic couplings that result from an extremely high density of state near the **limit**. The strong molecular hydrogen emissions that display observable **J-dependence** of the transition moment typically originate from the $v=6, 7,$ and 8 levels of the B state and terminate in the $v=12, 13,$ and 14 levels of the X state.

Figure VI shows an overplot of experimentally observed and synthetic spectra based on AD transition probabilities for the (7,13) and (6,12) bands of the Lyman system. Both spectral traces are normalized to the P(1) branch of the Lyman (7,13) band at 1579.18 Å. Since all the observed transitions in the Figure belong to the Lyman system, the label “L” is dropped from each of the assignment labels in the Figure. Once again, no sensitivity calibration has been applied to the observed spectrum as the instrumental sensitivity is not expected to change more than 2% over the wavelength change 1575.5 Å to 1586 Å. The decrease in the baseline with wavelength is due to falling intensity of the Lyman continuum, which is modeled fairly accurately with the transition probabilities calculated by SD.

For the (7,13) Lyman band, Figure VI shows that the agreement between the observed and calculated intensities becomes poorer as J increases. For example, the model based on the band transition probabilities of AD underestimates the observed relative intensities by 0% (assumed), ~25%, ~40%, and ~65% for P(1), P(3), P(4), and P(5) transitions, respectively. A similar trend can also be seen for the (6,12) band, where the model underestimates the intensities of P(3), P(4) and P(5) (not shown in Fig. VI) by about ~65%, -120%, and -160%, respectively.

Intensity differences in Figure VI are due to the J-dependence of the transition moment as well as the break-down of Hönl-London factor ratios. While J-dependence of the transition moment is significant in both excitation and emission processes for the (6,12) and (7,13) bands, it is more important in the emission process. Figure VII is a plot of the sum of P(J+1) and R(J-1) line transition probabilities of the (6,12), together with the total transition probabilities of rotational levels of v'=6 with the excited state J. The sum of the transition probabilities for P(J+1) and R(J-1) increases by a factor of 4 as J increases from 0 to 9. Total transition probabilities, on the other hand, decrease by only 7%. Figure VIII compares Abgrall line transition probabilities (A_p & A_R) with the “line” transition probabilities (A_p' & A_R') obtained from AD band probabilities using Hönl-London factors. In addition to the increase of the Abgrall line transition probabilities, Figure VIII clearly shows the ratio $A_{R(J-1)}/A_{P(J+1)}$ (obtained from Abgrall line transition probabilities) is significantly different to the Hönl-London factor ratio, $J/(J+1)$.

Figure IX compares the observed spectra and synthetic spectra obtained with the line transition probabilities of Abgrall and co-workers. The agreement between the observed and calculated spectra is very good. Table 111 shows the correction factors for the (6,0), (6,12), (7,0) and (7,13) bands. As can be seen from the Table, the centrifugal potential due to rotational motion has a profound effect on the relative intensities of rotational transitions of a given vibronic transition. For example, the P(3) and P(5) transitions of the (6,12) band are enhanced by factor of about 1.7 and 3, and the P(3) and P(5) transitions of the (7,13) band by 1.4 and 1.7, respectively. Strong J-dependence of the transition probability is also observed for the (5,14), (6,13), (7,12), (7,14), (8,14) and (10,13) bands of the Lyman system. Since all these bands are strong or moderately strong transitions, consideration of the rotational dependence of the transition moment is extremely important for accurate modeling of the FUV emission spectrum. The effect will become even more important for solar and outer planetary studies, where the ambient temperature ranges from several

the transition frequency (ν_0), the local perturbation merely result in an intensity **re-distribution** between the two interacting states and between the **corresponding** P and R branches. As long as A/ν_0 is much smaller than 1, the **total** emission intensities of the two perturbing states is conserved, Since almost all the local perturbations meet this condition, the calibration error due to neglecting **local** coupling is minimized provided the spectral interval includes all the branch transitions of the two interacting states.

The selection of the spectral range for calibration is a compromise between minimizing the calibration error due to local perturbation and being able to recognize their presence from the differences between the calculated and calibrated observed spectra. While a **large** spectral range that accommodates both P and R transitions of the perturbed levels reduces the calibration errors arising from neglecting local perturbations, it also tends to obscure the real difference **between** the observed and calculated spectra, This can **become very** significant between 1520Å and 1600 Å, where the Lyman continuum is strong and small differences in the “baseline” can result in large variations in the calibrated intensities of the spectral peaks corresponding to discrete transitions. A large spectral range (30-40 Å) is used for the initial calibration, whereas a small spectral interval (15-40Å) is used **after** strong local perturbations have been considered. In general, a **small** spectral interval is selected for strong spectral transition regions while a large interval is chosen for weak transition regions.

The H₂FUV spectrum spans about 530 Å. Complete **overplots** of the observed and synthetic spectra cover 53 pages. Since it is impractical to present all this information in **this** paper, these additional figures are presented in a supplement form (Appendix A) and form a data base which may prove useful in the interpretation of high resolution astrophysical observations. **Spectral** data in electronic form can be obtained by contact one of us (X.L or J. M. A.).

Figure X shows the spectral sensitivity curve of the experimental apparatus obtained by comparing the observed and calculated spectra. The shape of the spectral sensitivity curve is primarily determined by two factors. The monotonic decline in sensitivity from 1250 to 1650 Å is largely due to the decrease in quantum efficiency of the CsI **coated** channel electron multiplier detector. The increase in sensitivity from 1150 to 1250 Å is a superposition in the **increase** of the **reflectance** of the diverter mirror and the change in the **quantum efficiency** of the detector. The sensitivity curve is well-represented by a polynomial.

The calibration error over the **specified** spectral region is estimated to be less than 9%. The maximum error for a few **discrete** transitions, however, may be much larger. The largest relative error in the calibration of a discrete transition probably arises from uncertainties of the Lyman continuum, whose accuracy is hard to assess. The effects of **local** perturbation and **J-dependence** of the transition moment on the continuum emission are not known and are also **difficult** to assess. In addition, the detector noise and the error in background subtraction complicate calibration, but they affect the continuum emission much more significantly than discrete transitions. Another error in the calibration is the **uncertainty** in the estimation of cascade from the E,F state, which is modeled with a constant electronic transition moment without consideration of the **J-dependence**. Just as these assumptions can fail for the Lyman and Werner

transitions, they can equally breakdown for the E,F \leftrightarrow B transition,

C. Calibration Standard

Table IV compares the integrated spectral intensities of the refined model spectrum with those of the observed spectrum in specified wavelength intervals. We divide the FUV spectrum into 29 spectral regions with intervals identical to those used by *Ajello et al*, (1989), as listed in the first column of the Table. The fifth column tabulates the relative integrated theoretical intensities for each interval. For comparison, the sixth column lists the available relative integrated experimental intensities measured by *Ajello et al* using a double monochromator technique. As these experimental measurements were performed at a FWHM of 4\AA , the theoretical spectrum was convolved with a triangular transmission function at this experimental resolution before summing the intensities over the spectral regions,

The uncertainty in the relative experimental intensities measured by *Ajello et al* was estimated to be less than 25%. As can be seen from **Table IV**, the differences between the relative intensities of all the regions (except 33) are within this experimental uncertainty. The 33rd feature, which has an error of 37%, spans a region where the spectral intensities are very weak and errors in the background subtraction can produce significant error in the experimental intensity.

The values listed in the fifth column of **Table IV** can be used for a coarse calibration of the low resolution ($\lambda \geq 4\text{\AA}$) spectra. However, a more convenient and versatile approach is to use the model output file directly for calibration. The model output file from 1150 to 1750 \AA at $T=300\text{ K}$ and 100 CV electron impact energy is available upon request.

V. DISCUSSION

We have examined the relative accuracy of the band transition probabilities calculated by AD, and the rotational line transition probabilities of *Abgrall* and co-workers. In general, the AD band transition probability can be applied to a specific rotational level if there is no significant mixing with other states and when neither of the radial parts of the wavefunction depends strongly on rotational motion. The *Abgrall* line transition probabilities generally differ from AD transition probabilities a few percent when these two conditions are fulfilled.[†] In particular, all the Q-branch transitions of the Werner band system and all the P(1) transitions of the Lyman system appear to meet these requirements and the AD transition probabilities yield a good description for these transitions.

Although we can not examine the total transition probabilities directly with our observed spectrum, we have found that the SD total transition probabilities are consistent with the observed spectrum and with the line transition

[†]When the transition probability is small, the transition probability calculated by *Abgrall et al* may differ significantly from that of Allison and Dalgarno even when the two conditions are met. However, this type of transition is generally too weak to cause any significantly observable difference

probabilities calculated by Abgrall *et al.* Although the total transition probabilities calculated by SD are also obtained without consideration of the centrifugal potential, the total transition probabilities should not be as sensitive to perturbation and J-dependence of the transition moment as the line transition probabilities. Firstly, since the total transition probability involves a summation over the P and R branches, the effects of perturbation which alter the P/R ratio will be “diluted” after the summation. Moreover, as the perturbing ro-vibrational levels of the B and C states have similar (zeroth-order) total transition probabilities, even a strong perturbation is not likely to change the value of the total transition probability significantly. Finally, as the total transition probability consists of the summation over all the vibrational levels of the ground state, its J-dependence, which typically occurs at high v'' and high J'' , will be averaged out.

We can consider a few numerical examples to demonstrate that the SD total transition probabilities are sufficient for modeling the Lyman and Werner band systems. For the case of emission from $v'=3$ of the C state and from $v'=6$ of the B state, the $v'=3$ of the C state interacts strongly with $v'=14$ of the B state. A summation of the Q-branch emission line probabilities of Abgrall *et al.* over all the discrete v'' levels yields 1.121×10^9 , 1.120×10^9 , 1.119×10^9 , and 1.117×10^9 Sec^{-1} , for $J' = 1, 2, 3$, and 4 , respectively, of $v'=3$ of the $C^1\Pi_u$. The overall variation is less than 0.4%, suggesting that the transition moment is essentially independent of J' . A similar summation of the appropriate P and R branches gives 9.052×10^8 , 1.031×10^9 , 1.088×10^9 , and 1.221×10^9 sec^{-1} for $J' = 1, 2, 3$, and 4 , respectively. However, the $J' = 1, 2$, and 3 levels have a significant component of the B state character from $v'=14$ and the contribution to the Lyman continuum from the $v'=14$ is also very significant. The mixed part of the Lyman continuum must be added to the above values. (The Werner continuum, on the other hand, is very weak and can be safely neglected) Using Eq.(3) we find that the Lyman continuum contributes 1.504×10^8 , 0.6348×10^8 , and 0.2222×10^8 sec^{-1} for $J' = 1, 2$, and 3 levels, respectively, yielding total transition probabilities of 1.056×10^9 , 1.099×10^9 , 1.110×10^9 sec^{-1} , respectively. In comparison with the SD value of 1.121×10^9 sec^{-1} , they correspond to -6%, -2%, -1%, and +9% differences, respectively. These differences would have been smaller had the continuum contribution from each J' level been known. Another example that illustrates the insensitivity of the total transition probability to the variation of the transition moment is the $v'=6$ level of the B state. The total transition probability from $v'=6$ of the B state of H_2 to all the discrete vibrational levels of the X state was calculated to be 1.261×10^9 sec^{-1} by SD. A summation of the line transition probabilities calculated by Abgrall *et al.* shows that the same quantity for $J'=0, 1, 2$, and 3 are 1.261×10^9 , 1.257×10^9 , 1.247×10^9 and 1.227×10^9 sec^{-1} , respectively, which correspond to 0%, 0.3%, 1%, and 2.7% decreases. Again, these changes would be smaller if the contributions from each J level to the continuum were considered individually.

The AD band transition probabilities were obtained without considering the rotational motion. The intensities calculated by extending the probability to other rotational levels are, therefore, incorrect whenever coupling alters the magnitude of the band transition probability. Moreover, the model partitions the band probability into P and R branches according to the Herzberg factor ratio, However, $P(J'+1)/R(J'-1)$ deviates from the Hönl-London ratio

wherever appreciable coupling between different electronic states is present. Even if the local coupling is not significant, global non-adiabatic coupling may be important in some *regions*. Further deviation can arise from the centrifugal potential, $J(J+1)/2\mu R^2$, which mixes different vibrational wave functions of the X state for P(J+1) and R(J-1) transitions (Abgrall *et al* 1987). Hence, even if the magnitude of the band probability is not changed significantly by perturbation, the relative intensities of the P and R branches can still be incorrect because the perturbation causes re-distribution of the intensity. The correction factors in Table II, obtained using Eq. (2), is a direct appraisal of the deviation of the model based on Hönl-London factor when strong local coupling is present. As can be seen from the Table, perturbation can enhance or weaken either or both P and R branches.

Just as perturbation will cause the relative intensity of the P(J+1) and R(J-1) branches to differ from the ratio of the Hönl-London factors, the J-dependence of the transition moment will result in a similar deviation, as the transitions involve different J's. For the Lyman and Werner band systems of H₂, the Frank-Condon factors are small for excitation from the v'=0 of the X state to high vibrational levels of the B and C states. The dipole selection rule for ΔJ, together with the small population of high J' levels of the ground state make excitation to high J' levels insignificant. For those two reasons, the J-dependence of the transition moment is insignificant in the excitation process and is generally not observable in photoabsorption studies. The ΔJ selection rule also restricts the emission from the B and C states to the low J' levels of the X state. Hence, the J-dependence of the transition moment is significant only in transitions to high vibrational levels of the ground state. Since the populated C states have small Frank-Condon overlap with the high vibrational levels of the ground state, the effect of J-dependence is not likely to be observed in the Werner system. On the other hand, the vibrational wavefunctions of the v' = 6, 7, and 8 levels of the B state have significant overlap with the high vibrational levels, v''=12, 13, and 14, of the ground state. The J-dependence of the transition moment is hence observable for those strong emissions.

Our spectrum has shown that the J-dependence of the transition moment causes the abnormal intensity differences shown in Figure VI. From this Figure, we see that the model using a constant transition moment, in general, underestimates the relative intensity of the higher rotational levels. Furthermore the model underestimates the intensity of the P(J+1) branch more than that of the R(J-1) transition. Cascade and non-radiative processes such as predissociation can, therefore, be ruled out immediately. The difference can not be explained by local coupling between the B and C states since v'=7 vibrational level of the B state lies about 420 cm⁻¹ below the v=0 level of the C state and energy difference is 1530 cm⁻¹ for the v=6 level of the B state. The perturbation matrix elements would have to be of the order of these energy differences in order to produce such a large intensity variation, and such large interactions should be easily detected as positional shifts in energy. Moreover, if the intensity variation arises from coupling between the B and C states, then emission from the C state to v=12 and 13 of the X state should also have been observed in the same region with comparable intensity as J increases. Experimentally, however, neither the positional shifts or the emissions from the C state have been observed. Indeed, the calculations by Abgrall and Roueff

(1989) have shown that the low J levels of $v=6$ and 7 of the B state are not perturbed and the wavefunctions are almost pure (>99.5%).

The present study shows unambiguously the presence of strong **J-dependence** of the transition moment for certain Lyman emissions to high vibrational **levels** of the ground state. For the observed rotational lines of the (6, 12) and (7,13) bands of the Lyman system, Figures VII& VIII show that the emission probability is observed to increase as J increases and the intensity ratio of $P(J+1)/R(J-1)$ deviates from the ratio of the corresponding Hönl-London factors. In fact, the calculated sums of the squared dipole matrix element for P and R branches, $(A_R/v_R^3 + A_P/v_P^3)$, for $J'=1, 2, 3, 4, 5, 6$, and 7 of the (6,12) band, was found to increase by factor of 1.08, 1.25, 1.51, 1.88, 2.37, 2.95 and 3.58, respectively, in comparison to that of $J'=0$. The second column of Table III shows that the intensity of the R branch is significantly reduced, while that of the P branch is greatly enhanced.

The variation of the electronic transition moment with the rotational motion has a profound effect on the emission cross section of the Lyman band system at high temperature. Since the centrifugal potential is proportional to $BJ(J+1)$ and the rotational constant of the H_2 is very large, centrifugal distortion changes the transition probability significantly even at moderately high J levels, as illustrated by the (6,12) and (7,13) bands of the Lyman system. At room temperature, the Boltzmann distribution strongly discriminates against population of the high J levels. The **J-dependence** of the transition moment, while it may drastically alter the transition probability, does not have a significant effect on the overall observed intensities. When the temperature approaches 1000-2000 K, the variation of the transition moment can have a large effect on the intensities of spectra. For example, at $T=300$ K, the states which lie above $J=4$ of the $v''=0$ of the X state contribute only 10% to the overall partition function; this contribution rapidly increases to 170% at 1000 K; and to 58% at $T=2000$. Considering the relatively strong intensities of the emissions to $v''=12, 13$, and 14 of the ground electronic state, it is imperative to consider the J dependence of the transition moment for the Lyman band system even at temperature of a few hundred K.

We have also examined the relative accuracy of the line transition probabilities calculated by Abgrall *et al.* The Abgrall transition probabilities correctly predicted the observed relative intensities of all the perturbed transitions that have moderate intensities. While our experimental method is insensitive to weak transitions, the Abgrall transition probabilities also reproduce the relative intensities of the observed perturbed weak transitions very satisfactorily within our experimental error limit. We have also shown that Abgrall *et al.* have correctly predicted the J-dependence of the transition moment involved in the discrete transitions. The total discrete transition probabilities derived from the calculated line probabilities are consistent with our experimental observations and are also consistent with the calculations of SD. Obviously, the line transition probabilities calculated by Abgrall *et al.* yield a more accurate description of the Lyman and Werner bands of molecular hydrogen and will become even more useful when used to model astrophysical observations of molecular clouds and the atmospheres of the outer planets.

The calibration standard achieved in the present study is more accurate than that obtained by Ajello *et al.* because

we now have access to more accurate transition wavelengths and more reliable transition probabilities. Errors in the wavelength **affect** the calibration in two ways. Spurious intensities results when the transition is actually inside/outside a chosen region, but is considered as outside/inside by the model. In addition, an incorrect **center** of intensity of a selected interval (i.e. wavelength position weighted by intensity) generates an incorrect spectral sensitivity value when the model uses inaccurate transition wavelengths. The former typically occurs when a **large** wavelength error exists, whereas the latter occurs when systematic wavelength differences are present between experiment and the model. The present study has reduced wavelength error in two ways. Firstly, **the wavelength error** related to $v=14$ of the B state and $v=3$ of the C state have been eliminated in the present analysis. **Secondly**, small wavelength errors due to the utilization of the analytical formula are removed from the present model by substituting the observed wavelengths of Roncin and co-workers. The importance of such substitution increases at high temperature, when the higher rotational levels are populated, and in the EUV region, where perturbations from higher Rydberg states make application of analytical **formulae** to some rotational levels inappropriate.

In addition to the improvement in the calibration procedure achieved by using **correct** transition wavelengths, more reliable transition probabilities are also used. The previous model used by Ajello *et al* partitions the AD band transition probabilities into rotational line transition probabilities according to Hönl-London ratios. As we have seen in Figure IV and Table II, this partitioning can be inaccurate by as much as a factor of 46 when local perturbation is present. The calculations by Abgrall and co-workers has shown that the intensity ratio $P(J+1)/R(J-1)$ does not generally agree with Hönl-London ratios even when significant local perturbation is absent. Although coupling merely re-distributes the intensity between P and R branches (and between the interacting levels) and although the effect of neglecting perturbation can be minimized by dividing the spectrum into appropriate spectral regions, the intensity re-distribution **nevertheless** introduces **similar** uncertainties into the calibration as the inaccuracies of the transition wavelengths discussed in the previous paragraph. Moreover, it is possible to select a spectral region that fails to include all the relevant perturbed transitions. Finally, the uncertainties arising from neglecting the J-dependence of the transition moment can only be accounted for when the correct transition probabilities are used. While only a few Lyman bands are observed to display such J-dependence, they nevertheless contribute a relatively large fraction of the spectral intensity **between** 1550 and 1650 Å.

The present study has also **achieved** an improved calibration for the **experimental** FUV spectrum. Firstly, a more reliable model and synthetic spectrum is used. In addition, the spectral sensitivity of the CsI coated channel electron multiplier detector used **decreases** monotonically with the wavelength. This avoids the complications arising from the use of a FUV **photomultiplier** for which the efficiency initially increases rapidly with wavelength in the MgF_2 cut-off region, followed by a very slow increase. Finally, since a smaller spectral interval is used, it is possible to reject the weak regions which produces statistically large difference.

VI. CONCLUSION

The first high resolution optically thin FUV emission spectrum of H_2 produced by electron impact at 100 eV has been measured and analyzed. Examination of the relative values of the calculated transition probabilities has shown that the partitioning of the AD transition probabilities into P and R branches according to the Hönl-London factors is invalid. Significant deviations in relative intensity can arise when local coupling is present or when the J-dependence of the transition moment due to the centrifugal potential is neglected. The total transition probabilities calculated by SD is consistent with the experimental observation if the perturbed rotational levels are corrected according to Eq.(3). The transition probabilities calculated by Abgrall and co-workers are consistent with the experimental spectrum, and accurately account for ro-vibronic coupling and the J-dependence of the electronic transition moment. Finally, a more reliable model spectrum has been generated, together with a more accurate calibration.

The excitation of H_2 by electron impact in the atmospheres of the outer planets and in molecular clouds takes place at a variety of thermal kinetic excitation energies and under a variety of optically thick conditions. High resolution laboratory spectra are needed as a basis for identifying atmospheric conditions observed at high resolution from UV space observatories. While the present work deals only with monoenergetic excitation at an electron impact energy of 100 eV, extension to other thermal kinetic energies (> 19eV) is straight forward, provided excitation functions of the Lyman and Werner transitions as well as the E,F states are known.

The primary refinement of the present model results from the accurate description of direct and discrete excitation and emission using the line transition probabilities calculated by Abgrall *et al.* Since the overall spectral intensity also includes the contribution from Feshbach resonances, cascade of the E,F states, and from the Lyman continuum emission from the B state to the higher vibrational levels of the X state, more accurate data on these processes are required before further significant improvements can be made. Work is presently underway to accurately measure and model resonance effects, and the direct excitation function of the Lyman and Werner systems.

VII. ACKNOWLEDGEMENT

The work reported in the present paper was carried out at the Jet Propulsion Laboratory. We wish to acknowledge the financial support of the Air Force Office of Scientific Research, the Acromy Program of the National Science Foundation (ATM-9320589), and the NASA Planetary Atmospheres, Space Physics, and Astronomy Program Offices through an agreement with the National Aeronautics and Space Administration. The authors wish to thank Drs. D. E. Shemansky and H. Hu for their valuable suggestions and assistance in data analysis. We would also like to thank Drs. H. Abgrall, J.-Y. Roncin, E. Roueff, and F. Launay for communicating their experimental and calculated results prior to publication. We thank Chris Wrigley and Brian O. Franklin for their technical assistance. This work was performed while X. Liu, S. M. Ahmed, and R. A. Multari held a National Research Council Associateship at the Jet Propulsion Laboratory

REFERENCES

- Abgrall H., Launay F., Roueff E., & Roncin J.-Y. 1987, *J. Chem Phys.* 87,2036
- Abgrall H., & Roueff E. 1989, *A&AS*, 79,313
- Abgrall H, Le Bourlot J., Pineau des Forêts G., Roueff E., Flower, D. R. & Heck L. 1992, *A&A* 253,525
- Abgrall H., Roueff E., Launay F., Roncin J.-Y., & Subtil J.-L. 1993a, *J. Mol.Spectrosc.* **157,512**
- Abgrall H., Roueff E., Launay F., Roncin J.-Y., & Subtil J.-L. 1993b, *A&AS*, 101,273
- Abgrall H., Roueff E., Launay F., Roncin J.-Y., & Subtil J.-L. 1993c, *A&AS*, 101,323
- Abgrall H., Roueff E., Launay F., & Roncin J.-Y. 1994, *Can. J.Phys.* (in press)
- Ajello J. M., Srivastava S. K., & Yung Y. L, 1982, *Phys.Rev. A.* 25,2485
- Ajello J. M., Shemansky D. E., Kwok T. L., & Yung Y. L. 1984, *Phys.Rev. A.* 29,636
- Ajello J. Met al. 1988, *Appl. Opt.* 27,890
- Ajello, J. M., James, G. K., Franklin, B. O., & Shemansky, D. E. 1989, *Phys.Rev. A.* 40,3524
- Ajello, J. M., James, G. K., Franklin, B. O., & Howell, S. 1990, *J Phys. B.* 23,4355
- Ajell, J. M., Ahmed, S. M., Kanik, I. & Multari, R. 1995, *Phys. Rev. Lett.* (Submitted)
- Allison A. C., & Dalgarno A.)970, *At. Data* 1,289
- Broadfoot A. L. et al. 1979, *Science*, 24,979
- Broad fast, A. L. et al. *J. Geophys. Res.* 86,8259
- Clarke J. T., Moos W. H., Atreya S. K., & Lane A. L.1980, *Ap.J.* **241, 179**
- Clarke J. T., Jaffel, L. B., Vidal-Madjar, A, Gladstone, G. R., Waite, H., Prangé, R., Gerard, J.-C., & Ajello, J., 1994, *ApJ.*, **430**, L73
- Dabrowski I., & Herzberg G. 1974, *Can. J.Phys.* 52, 1110
- Dabrowski I.1984, *Can. J. Phys.* 62, 1639
- Dressler K., & Wolniewicz L. 1986, *J. Chem.Phys.* 85,2821
- Dressler K. & Wolniewicz L. 1985, *J. Chem.Phys.* 82,4720
- Dressler K., & Wolniewicz L. 1982, *J. Chem.Phys.* 82,3861

- Ford A. L. 1974, *J. Mol. Spectrosc.* 53,364
- Ford A. L. 1975a, *J. Mol. Spectrosc.* 56,251
- Ford A. L., Brown J. C., Shipsey E. J., & DeVries P., 1975b *J. Chem. Phys.* 63,362.
- Glass-Maujean M., Quadrelli P., & Dressier K. 1984, *J. Chem. Phys.* 80,4355
- Huber K. P., & Herzberg G. 1979, *Molecular Spectra and Molecular Structure IV, Constants of Diatomic Molecules* (Van Nostrand)
- Julienne P. S. 1973, *J. Mol. Spectrosc.* 48,508
- Kolos W., & Wolniewicz L. 1964, *J. Chem. Phys.* 41,3663
- Kolos W., & Wolniewicz L. 1965, *J. Chem. Phys.* 43,2429
- Kolos W., & Wolniewicz L. 1966, *J. Chem. Phys.*, 45,509
- Kolos W., & Wolniewicz L. 1968, *J. Chem. Phys.*, 48,3672
- Kolos W., 1967, *Int. J. Quant. Chem.* **1**, 169
- Lefebvre-Brion H., & Field R. W. 1986, *Perturbations in the Spectra of Diatomic Molecules* (Academic)
- Lin C. S. 1974, *J. Chem. Phys.* 60,537
- McClintock, M. Barth, C. A., Steele, R. E., Lawrence, & Timothy, J. G. 1982, *Appl. Opt.*, **21,3071**
- Roncin, J.-Y., Launay, F. and Lazillièrè M. 1984 *Can. J. Phys.* 62, 1686.
- Roncin J.-Y., & Launay F. 1994, *Atlas of the Vacuum Ultraviolet Emission Spectrum of Molecular Hydrogen*, *J. Phys. Chem. Ref. Data*. Monograph NO. 4. (ACS, APS)
- Rothenberg S., & Davidson E. R, 1967 *J. Mol. Spectrosc.* 22, 1
- Schmoranzler, H., Imschweiler, J. , and Nell, T. 1984, *Proc. 9th Internat. Conf. on Atomic Physics. Satellite Workshop and Conference Abstracts*. Paper A26.
- Senn P., Quadrelli P., & Dressier K. 1988, *J. Chem. Phys.* 89,7041
- Shemansky D. E., & Ajello J. M. 1983, *J. Geophys. Res.* 88,459
- Shamansky, D. E., Ajello, J. M., & Hall, D. T., 1985a, *ApJ.*, 296,765
- Shamansky, D. E., Ajello, J. M., Hall, D. T., & Franklin, B. 1985b, *ApJ.*, 296,774
- Stephens T. L., & Dalgarno A. 1972, *J. Quant. Spectrosc. Radiat. Transfer.* **12,569**

Trafton, L. M., Gérard, J. C., Munhven G., & Waite Jr., J. H., 1994, *ApJ*, 421,816

Wolniewicz L. 1993, *J. Chem. Phys.* 99, 1851

Wolniewicz L., & Dressier K, 1988, *J. Chem. Phys.* 88,3861

Wolniewicz L., & Dressler K. 1992, *J. Chem. Phys.* 96,6053

Wolniewicz L., & Dressler K. 100, *J. Chem. Phys.* **100,444**

Wolniewicz L. 1969, *J. Chem. Phys.*, 51,5002

Table L Instrumental Resolution of 3M Spectrometer

Grating (Grooves/mm)	Wavelength range (Å)	Spectral Order	Dispersion (Å/mm)	Resolution (FWHM) for 10 μ slits	
				Extended source (mÅ) ^a	Point source (e+ H, (mÅ) ^b
3600	300-1220	1	0.924	15	
2400	300-1850	1	1.386	23	35
	300-9250	2	0.693	12	17.5
1200	300-3700	1	2.771	45	64
	300-1850	2	1.386	23	32
	300-1230	3	0.924	12	21.3

a Measured with ArII at 919 Å

b Zero Order slit function

Table II. Intensity Correction Factors for (3,7) Werner and (14,7) Lyman bands

Transition ^a	Emission Correction ^b	Emission Correction ^c	Ford ^d	Excitation Correction ^e	A(J,v,X, α) Correction ^f	Overall
0(14,0) R L	0.1243	0.1237	0.104	0.6765	1.075	0.08
2(14,0) P L	2.187	2.199	2.158	0.6765	1.075	1.3763
1(14,0) R L	2.797	2.839	2.666	2.579	1.032	6.9898
3(14,0) P L	0.1465	0.1487	0.157	2.579	1.032	0.3661
2(14,0) R L	2.035	2.144	1.912	1.991	1.011	4.0076
4(14,0) P L	0.3591	0.3686	0.374	1.991	1.011	0.7072
3(14,0) R L	1.793	1.811	1.654	1.792	1.006	3.1939
5(14,0) P L	0.4610	0.4799	0.476	1.792	1.006	0.8212
0(14,7) R L	74.09	73.79		0.6765	1.075	46.6250
2(14,7) P L	8.542	8.581		0.6765	1.075	5.3755
1(14,7) R L	8.576	8.557		2.579	1.032	21.4317
3(14,7) P L	11.01	11.15		2.579	1.032	27.5143
2(14,7) R L	0.6662	0.6668		1.991	1.011	1.3120
4(14,7) P L	4.567	4.663		1.991	1.011	8.9940
3(14,7) R L	0.001958	0.00197		1.792	1.006	0.0035
5(14,7) P L	2.376	2.452		1.792	1.006	4.2324
0(3,0) R W	1.131	1.128	1.134	1.050	0.9394	1.2642
2(3,0) P W	0.1665	0.1676	0.164	1.050	0.9394	0.1861
1(3,0) R W	0.4776	0.4742	0.470	0.5204	0.9745	0.2550
3(3,0) P w	1.593	1.608	1.633	0.5204	0.9745	0.8507
2(3,0) R W	0.6174	0.6126	0.610	0.6297	0.991	0.3923
4(3,0) P w	1.448	1.470	1.487	0.6297	0.991	0.9201
3(3,0) R W	0.6664	0.6573	0.690	0.6666	0.9952	0.4464
5(3,0) P w	1.390	1.412	1.424	0.6666	0.9952	0.9310
0(3,7) R W	0.6246	0.6229	0.648	1.050	0.9394	0.6981
2(3,7) P W	0.7758	0.7823	0.848	1.050	0.9394	0.8671

Table II. (continued)

1(3,7) R W	0.9972	0.9911	0.951	0.5204	0.9745	0.5325
3(3,7) P w	0.7522	0.7583	0.724	0.5204	0.9745	0.4017
2(3,7) R W	1.077	1.067	1.030	0.6297	0.991	0.6843
4(3,7) P w	0.8395	0.8485	0.835	0.6297	0.991	0,5334
3(3,7) R W	1.100	1.087	1.050	0.6666	0.9952	0.7368
5(3,7) P w	0.8461	0.8575	0.859	0.6666	0.9952	0.5667

- a. Transition is labelled by $J''(v',v'')$ AJ *a*, where P, Q, R corresponds to $\Delta J = J'' - J' = -1, 0,$ and $+1,$ and *a* is W for Werner and L for Lyman band system.
- b. Calculated according to Eq.(2) with the transition probabilities of Abgrall et al, (1993b&1993c). Direct computer output of the transition probabilities with *4 significant figures* are used.
- c. Same as b except the A is replaced by $A/v^3.$
- d. Ford (1975a)
- e. Assuming $T = 300$ K
- f. Assuming only B-C coupling. The zeroth-order total transition probability from Stephen and Dalgarno (1972), and the character percentage is from Abgrall and Roueff (1 989).

Table III. Intensity Correction Factors for (6,12) and (7,13) Lyman bands

Transition ^a	Emission Correction ^b	Ford ^c	Excitation Correction ^d	Overall
0(6,0) R L	1.0540	1.0530	1.0320	1.0877
2(6,0) P L	0.9714	0.9740	1.0320	1.0025
1(6,0) R L	1.0760	1.0780	1.0650	1.1459
3(6,0) P L	0.9425	0.9500	1.0650	1.0038
2(6,0) R L	1.0930	1.1020	1.0880	1.1892
4(6,0) P L	0.9154	0.9280	1.0880	0.9960
3(6,0) R L	1.1050	1.1240	1.1020	1.2177
5(6,0) P L	0.8906	0.9080	1.1020	0.9814
0(6,12) R L	0.7918			0.8171
2(6,12) P L	1.2240			1.2632
1(6,12) R L	0.7641			0.8138
3(6,12) P L	1.5500		1.0650	1.6508
2(6,12) R L	0.8362		1.0880	0.9098
4(6,12) P L	1.9980		1.0880	2.1738
3(6,12) R L	0.9659		1.1020	1.0644
5(6,12) P L	2.5840		1.1020	2.8476
0(7,0) R L	1.1030	1.1090	1.0610	1.1703
2(7,0) R L	0.9462	0.9450	1.0610	1.0039
1(7,0) R L	1.1410	1.1510	1.1210	1.2791
3(7,0) P L	0.9005	0.8990	1.1210	1.0095
2(7,0) R L	1.1660	1.1830	1.1580	1.3502
4(7,0) P L	0.8638	0.8620	1.1580	1.0003
3(7,0) R L	1.1820	1.2070	1.1810	1.3959
5(7,0) P L	0.8362		1.1810	0.9876
0(7,13) R L	0.9046		1.0610	0.9598
2(7,13) P L	1.0970		1.0610	1.1639

Table III. (continued)

1(7,13) R L	0.9052		1.1210	1.0147
3(7,13) P L	1.2210		1.1210	1.3687
2(7,13) R L	0.9455		1.1580	1.0949
4(7,13) P L	1.3420		1.1580	1.5540
3(7,13) R L	1.0180		1.1810	1.2023
5(7,13) P L	1.4190		1.1810	1.6758

- a. See footnote a of Table 11.
- b. See footnote b of Table II
- c. See footnote d of Table 11
- d. See footnote e of Table 11

Table IV. FUV Calibration Intergrated Intensities from H₂ at 100 eV Impact Energy

Spectral Range #	Wavelength Start (rim)	Wavelength End (nm)	Wavelength Center (rim)	Theoretical Area ^a	Experimental Area ^b	(Th-Exp)/Exp
18	106.1	107.3	06,7	0.4549		
19	107.3	109.4	08.4	0.6881		
20	109.4	111.0	10.1	0.9267		
21	111.0	112.6	11.7	0.7513		
22	112.6	113.8	13.1	0.2175		
23	113.8	115.2	114.6	0.3361		
24	115.3	116.9	116.2	0.8457		
25	116.9	118.5	117.9	0.9108		
26	118.5	119.6	119.0	0.4755		
27	119.6	120.9	120.3	0.5205		
28	121.1	122.6	121.8	0.5952		
29	122.6	123.5	123.0	0.3944	0.4634	-15%
30	123.5	124.3	123.9	0.3489	0.3813	-8%
31	124.3	126.4	125.3	1.1740	1.1429	3%
32	126.4	128.8	127.6	1.0000	1,0000	0%0
33	128.8	132.9	130.3	0.2696	0,4268	-37%
34	132.9	136.0	134.6	0.4648	0.4429	5%
35	136.0	138.6	137.2	0.3520	0.3652	-4%
36	138.6	141.9	140.0	0.3767	0.4214	-11%
37	141.9	144.7	143.6	0.3834	0.3679	4%
38	144.7	146.9	146.0	0.3561	0.3196	11%
39	146.9	150.3	148.4	0.5442	0.5179	5%40
40	150.3	153.4	152,1	0.5338	0.5009	7%
41	153.4	155.6	154.5	0.4428	0.4429	0%40
42	155.6	157.4	156.7	0.7177	0.6045	19%
43	157.4	159.9	158.4	1.1006	1.0179	8%
44	159.9	161.9	160.8	1.0810	0,8929	21%40
45	161.9	165.0	163.2	0.5440	0.4991	9%
46	165.0	168.0	166.3	0.1245	0.1500	-17%40

a. Calculated spectral data convoluted to a triangular lineshape function with FWHM = 4 Å.

b. Double Monochrometer measurement with ±25% uncertainties from Ajello *et al*, *App.Optics*, 27, 890 (1988).

LIST OF FIGURES

- Figure I,** Schematics of electron collision chamber. The retractable focussing mirror located at the bottom of the Figure yields an intensity enhancement of about 600/0 by reflecting back more of the emission and provides greater filling of the grating surface.
- Figure II.** Detailed view of 3-m high resolution spectrometer. In the present experiment, a CSI coated channel electron multiplier detector is placed at the left exit port (where the absorption cell is shown)
- Figure III.** Block electronics diagram of the overall experimental setup.
- Figure IV** Comparison between the model (dotted line) and experimental spectra (solid line) of the (3,7) band of Werner and the (14,7) band of the Lyman system. The model spectral intensities are calculated using Allison & Dalgarno (1970) band transition probabilities partitioned by Hönl-London factors. The synthetic spectrum differs from the experimental spectra in both position and intensity because the model fails to consider the ro-vibronic coupling between the $v=14$ level of the $B^1\Sigma_v^+$ state and the $v=3$ level of the $C^1\Pi_v$ state. (See text)
- Figure V** Comparison between a new model synthesized and experimentally observed spectra. The new model utilizes the experimental wavelength of Roncin & Launay (1994), and the line transition probabilities calculated by Abgrall *et al* (1993b&c). (See text)
- Figure VI** Overplot of the model calculated and experimentally observed spectra of the (6,12) and (7, 13) bands of the Lyman system, The model underestimates the intensities of the high J transitions because it uses the band transition probabilities calculated by Allison and Dalgarno and assumes that the transition probabilities are independent of the rotational motion.
- Figure VII** Band transition probabilities, $A_{P(J+1)} + A_{R(J-1)}$, of the (6, 12) band of the Lyman system calculated by Abgrall *et al* (solid line) and the total transition probabilities $J'=0-9$ levels of $v'=6$ (dotted line). The band transition probabilities, $A_{P(J+1)} + A_{R(J-1)}$, show very strong J-dependence of the electronic transition moment for the (6,12) band. Note that band transition probabilities are scaled by a factor of 108, while the total transition probabilities are scaled by a factor of 109.

Figure VIII Comparison of line transition probabilities of the (6,12) band calculated by Abgrall *et al* (solid line) and calculated using Allison and Dalgarno band transition probabilities partitioned by Honl-London factors (dotted line). The break-down of Hönl-London factors and the variation of the transition moment with J are clearly demonstrated.

Figure IX Same as Figure VI except the (new) model the transition probabilities calculated by Abgrall and co-workers. The rotational dependence of the transition moment has been well taken into account by Abgrall *et al*.

Figure X Relative sensitivity curve of 3M spectrometer and channel electron multiplier.

3 m COLLISION CHAMBER (TOP VIEW)

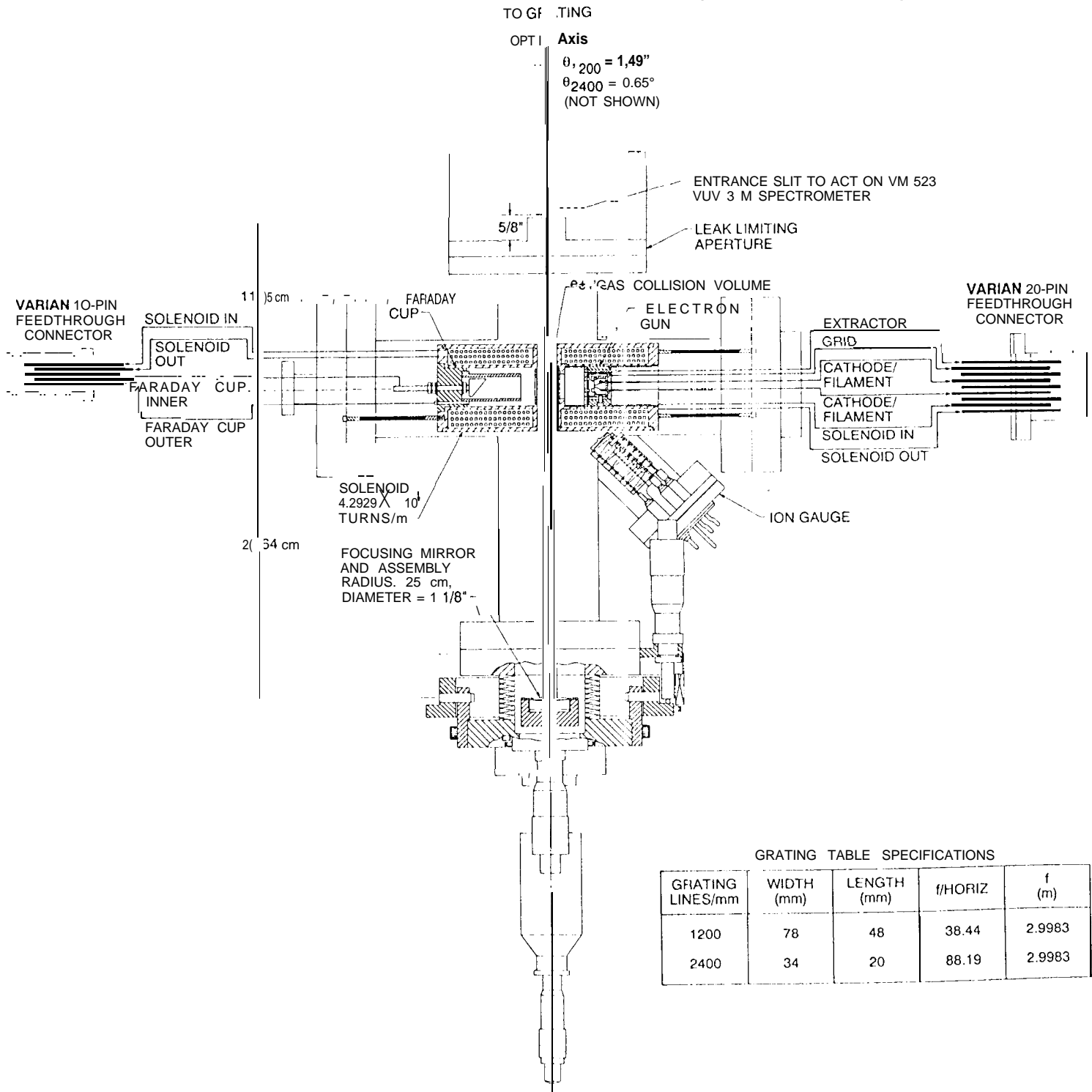


Figure I

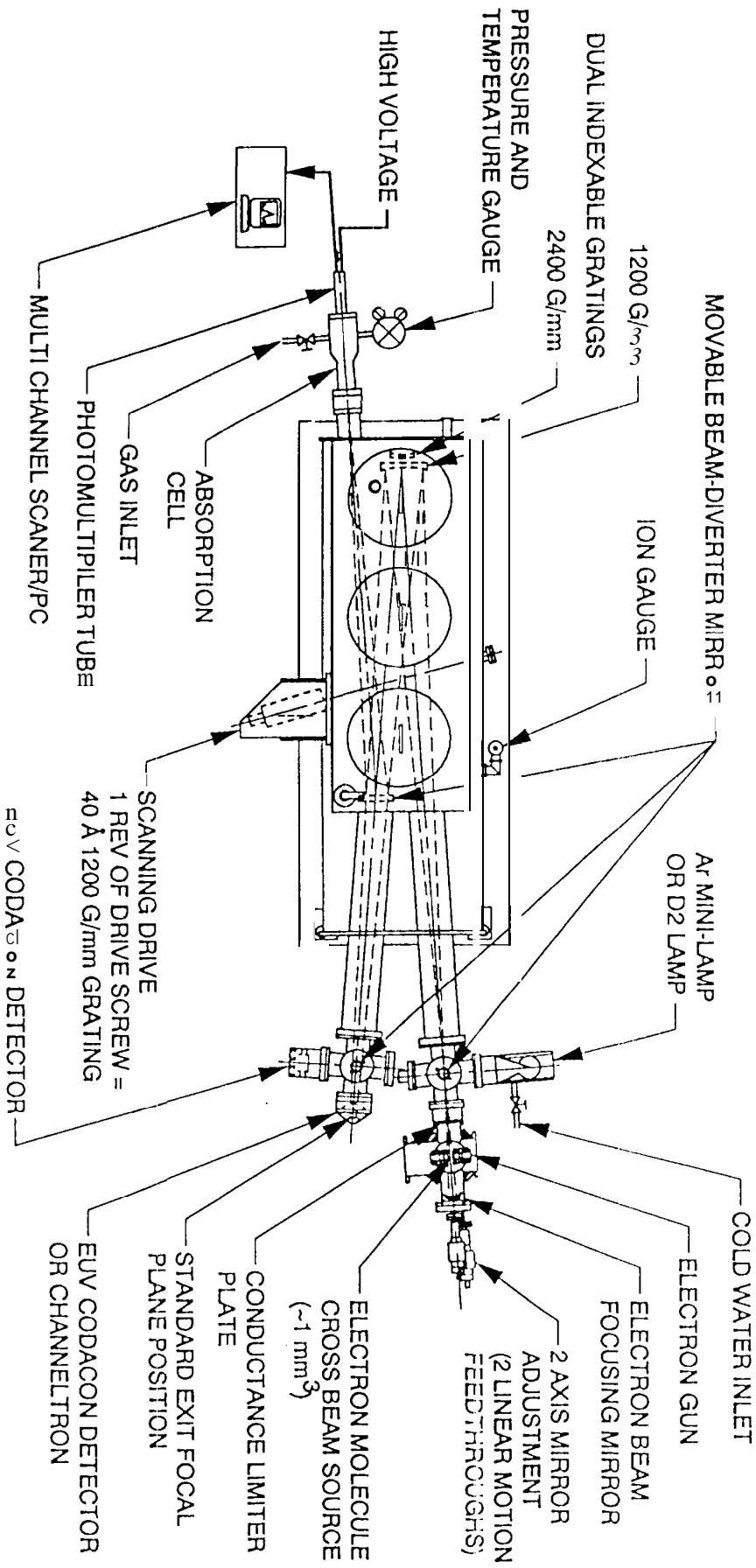


Figure II

3-m UV Spectrometer

Strawman System Block Diagram For Single Pixel Spectrum (Lambda mode)

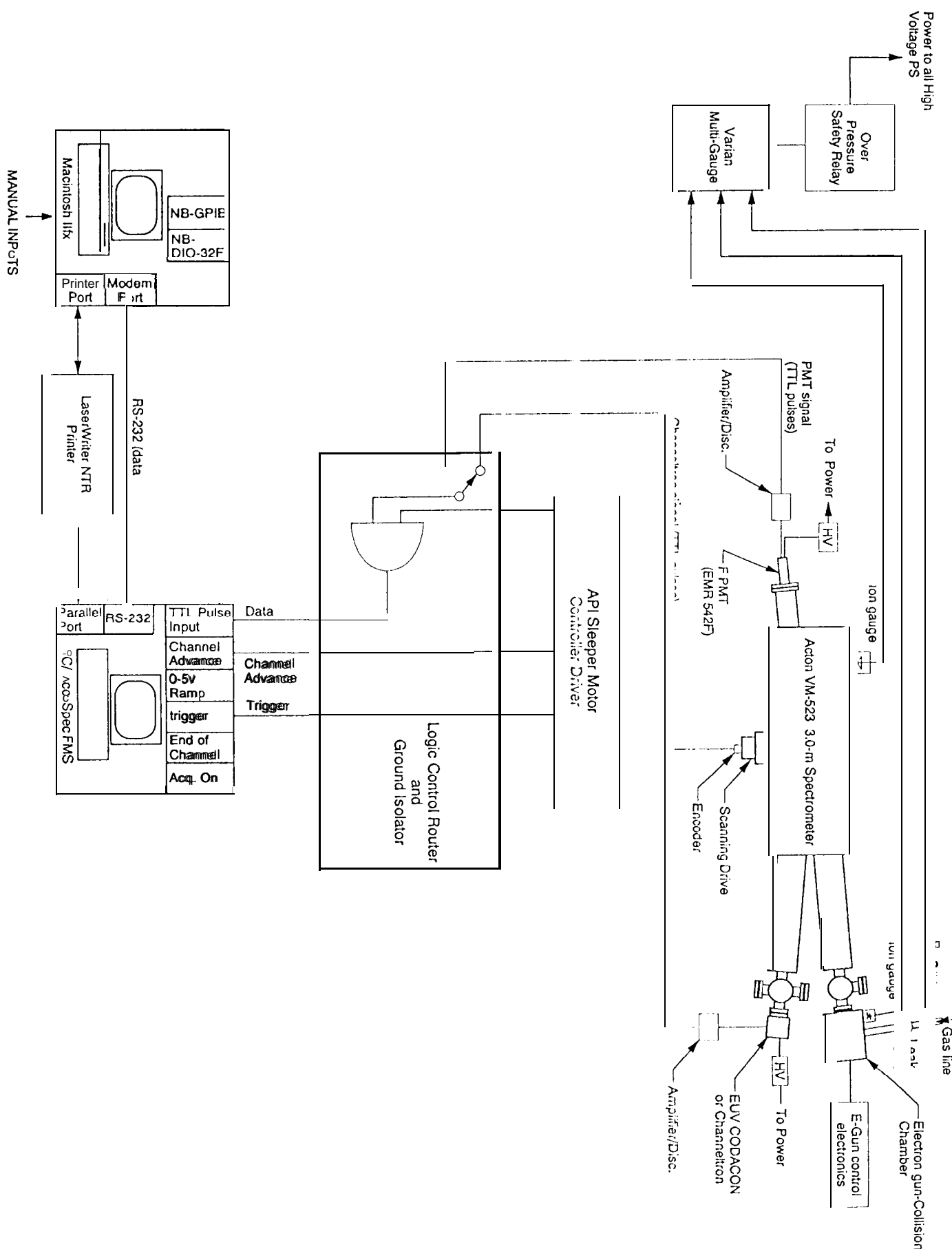


Figure II

e + H₂ (100eV, 300K)

$\Delta\lambda = 0.064 \text{ \AA}$

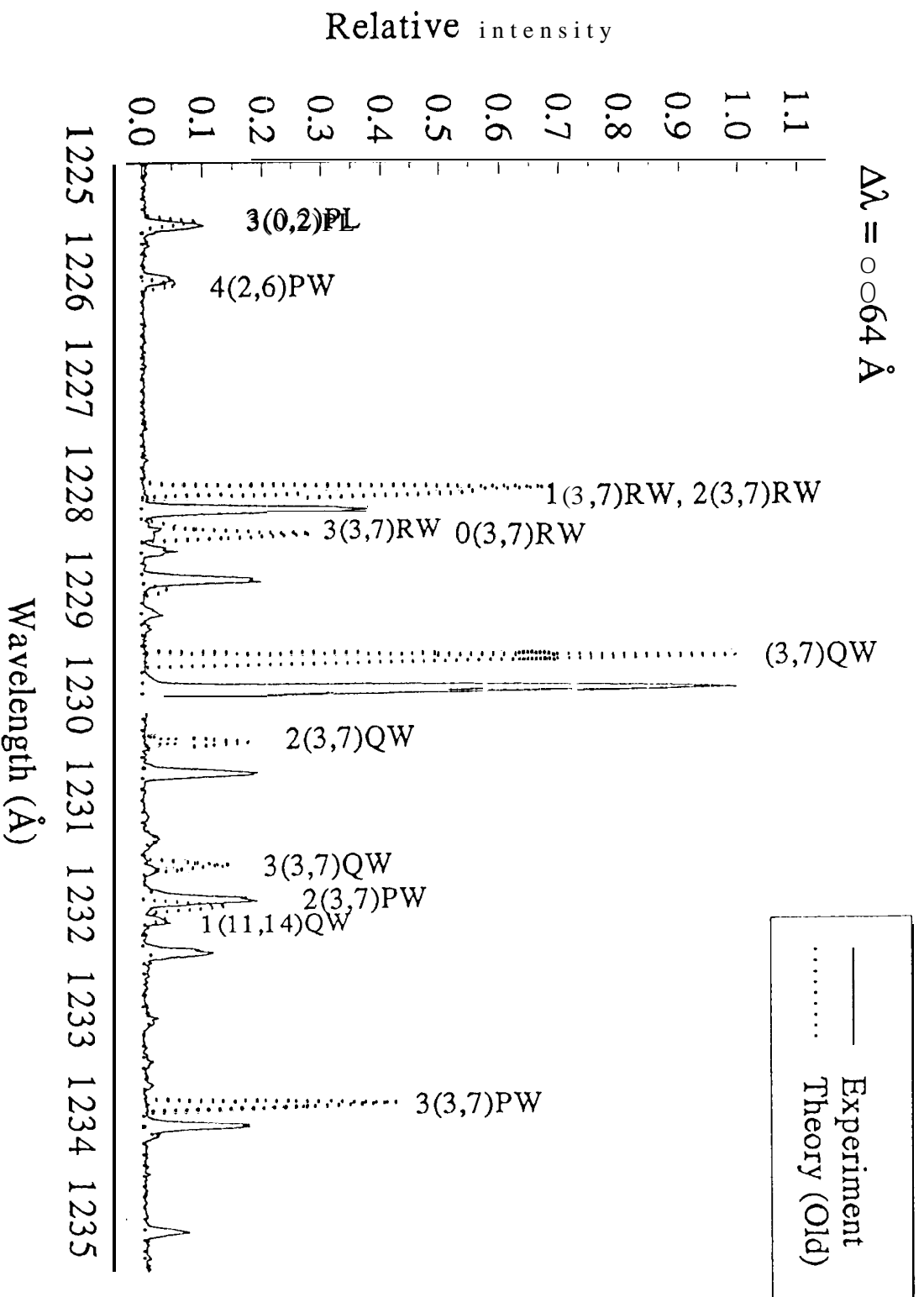


Figure V

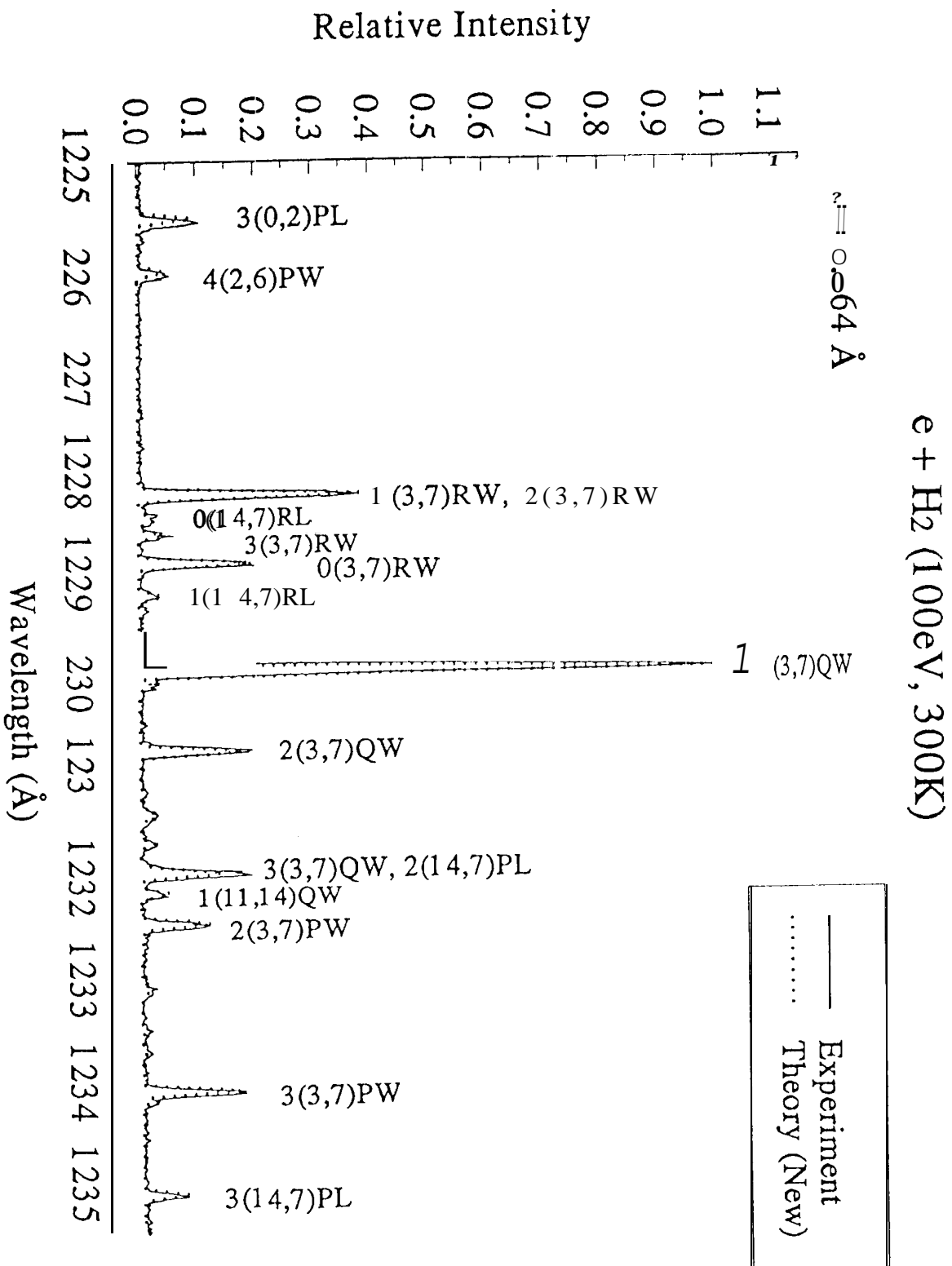


Figure V

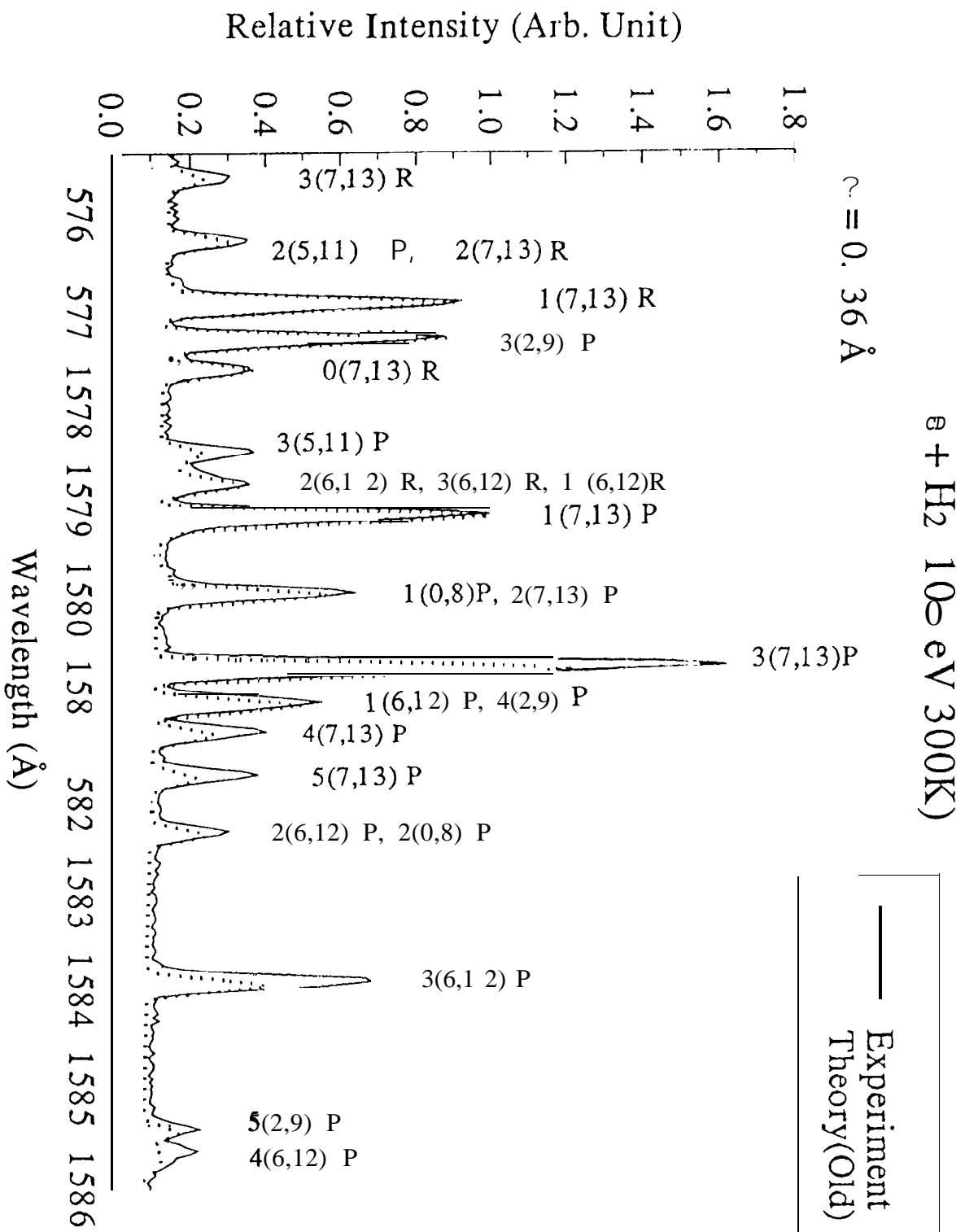


Figure VI

Transition Probabilities of (6,12) Lyman Band

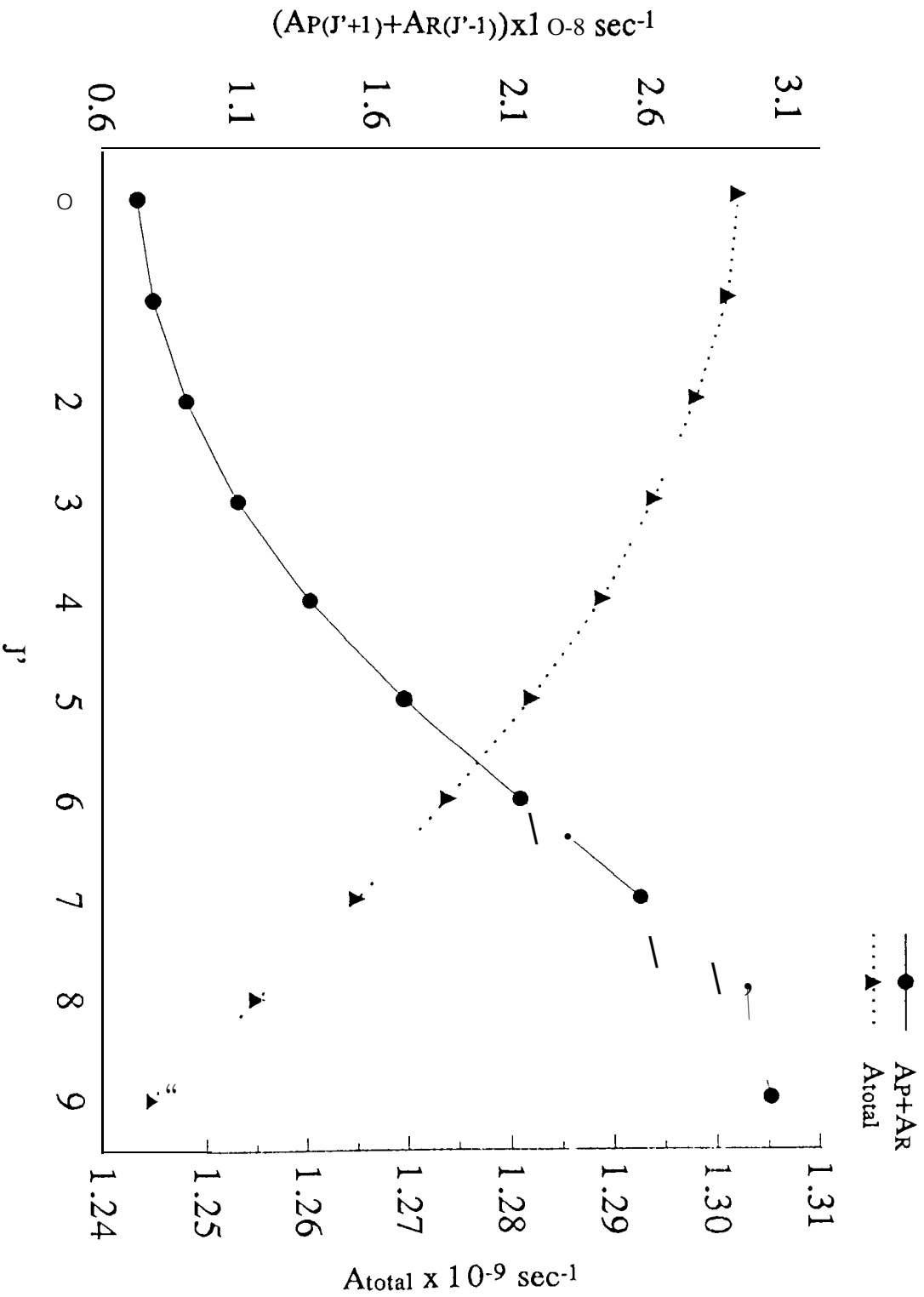


Figure VII

Transition Probabilities of (6,12) Lyman Band

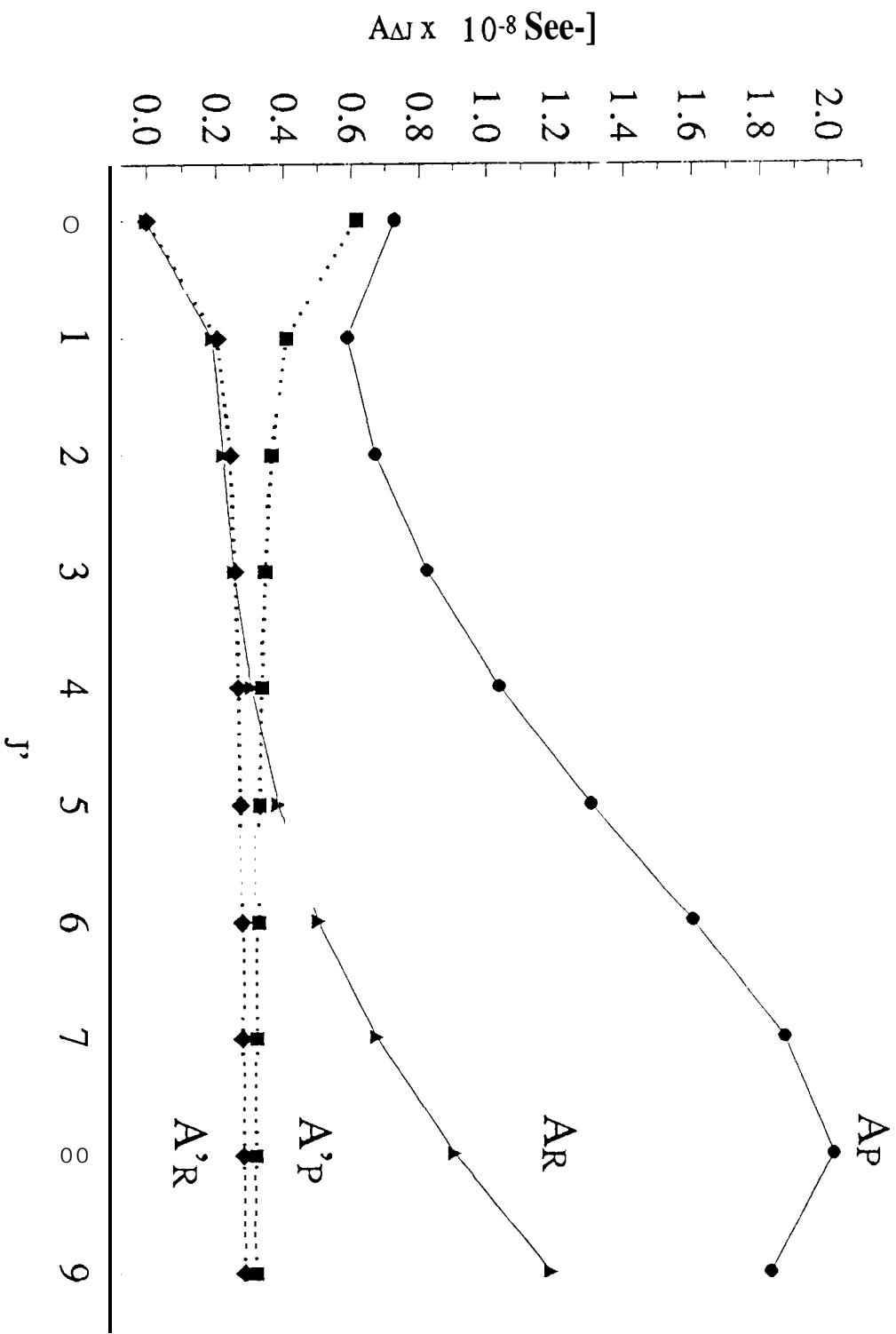


Figure VIII

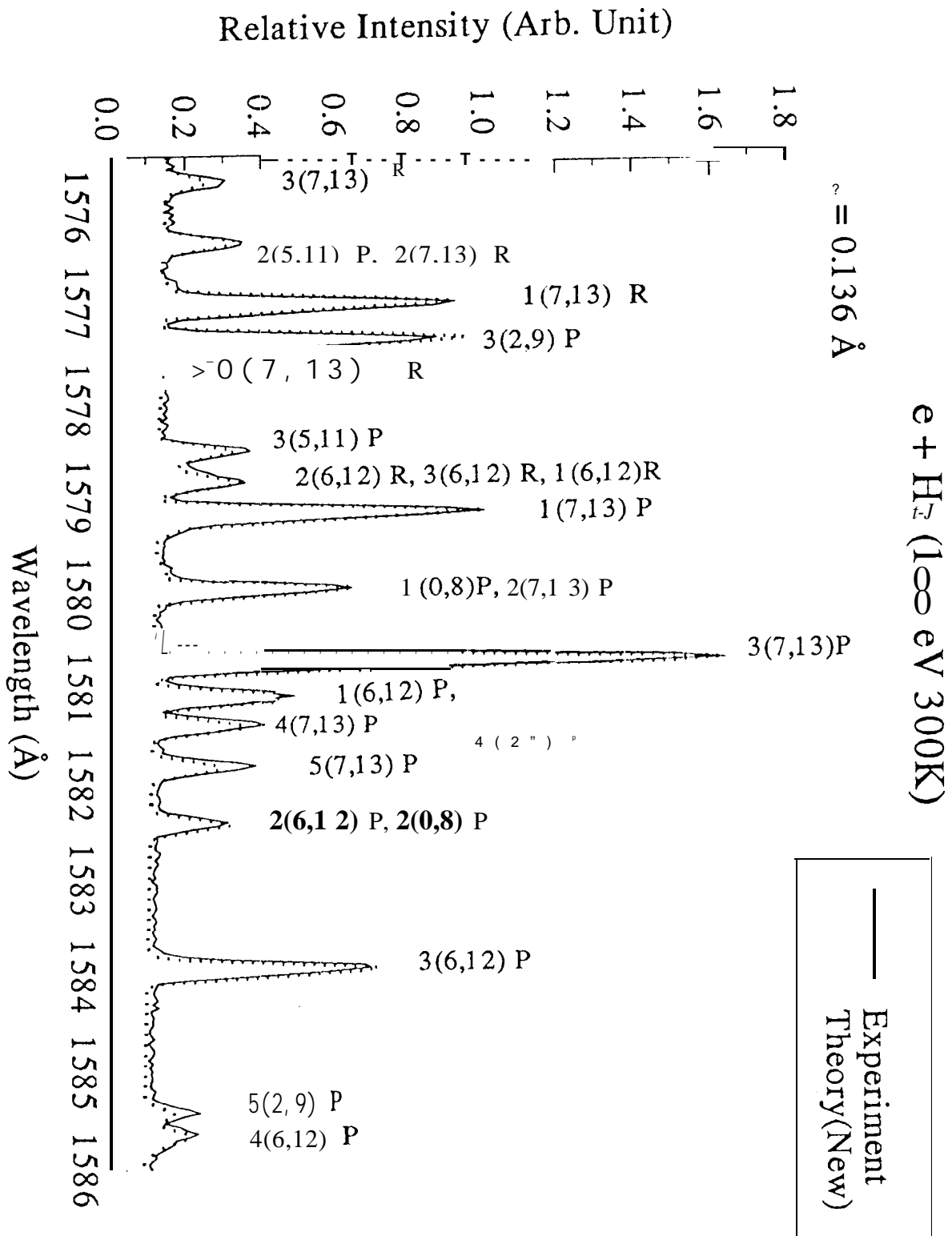


Figure IX

3 M Spectrometer and CEM Calibration

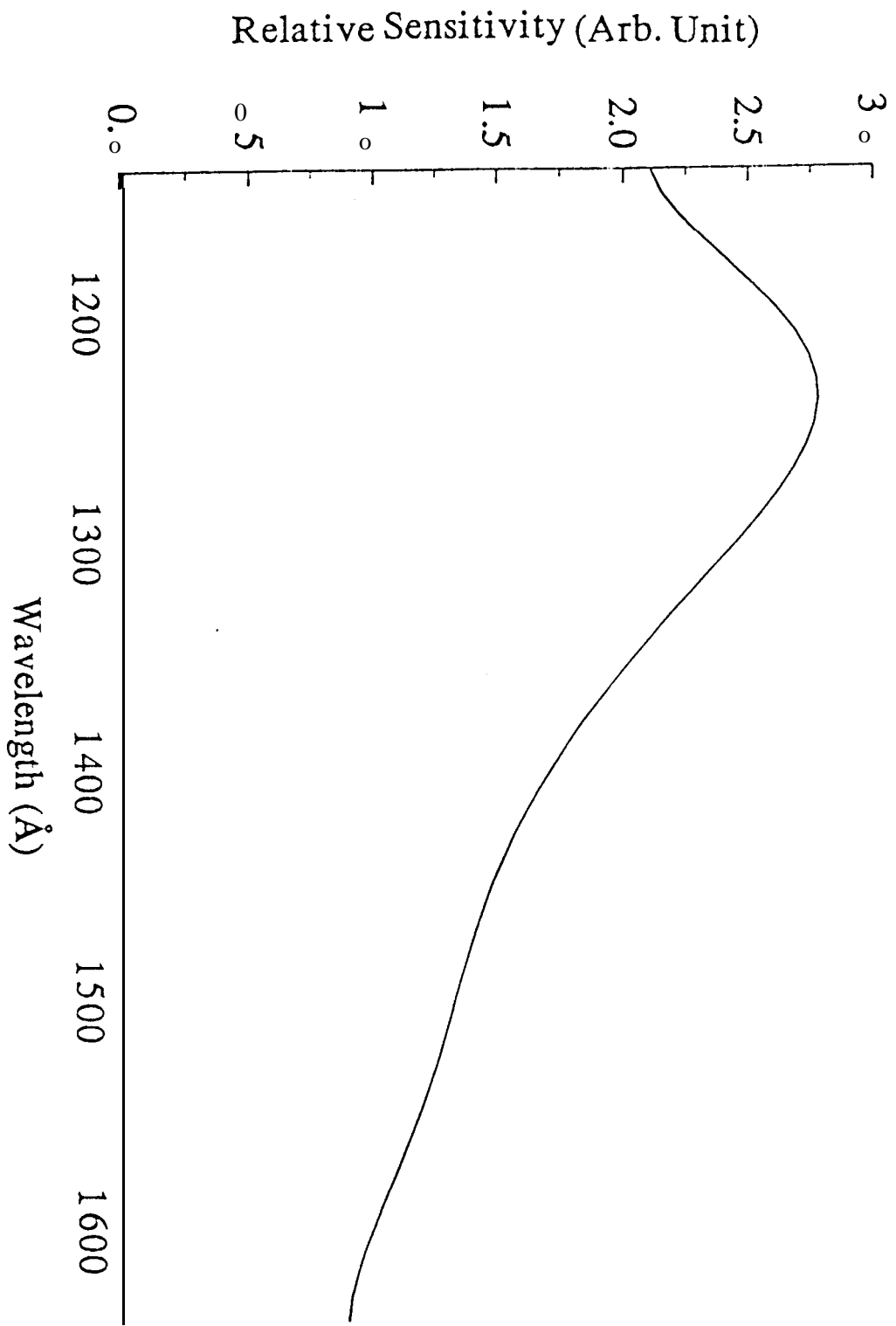
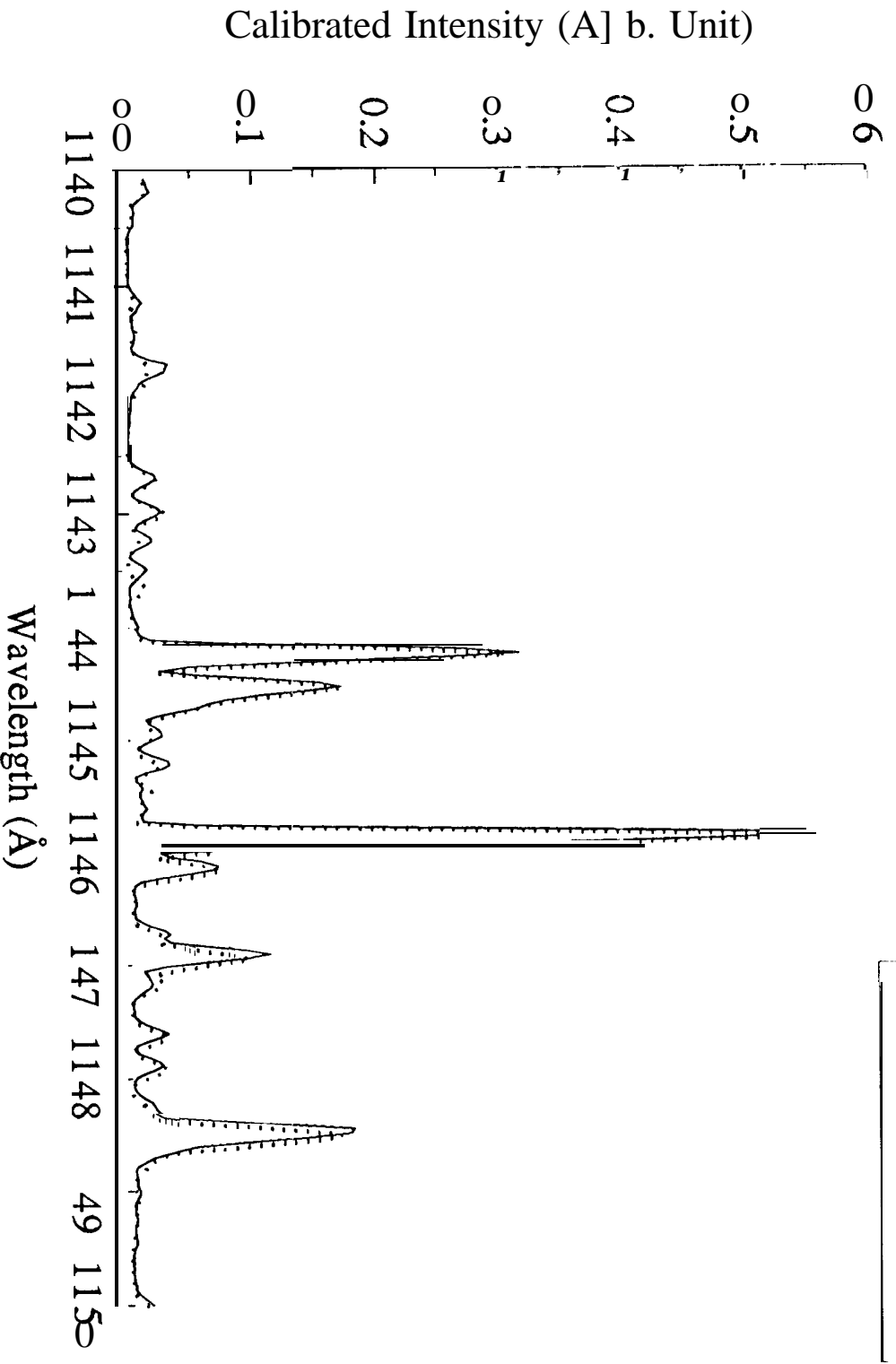


Figure X

Appendix A Overplots of the observed (experiment) and calculated (theory) FUV spectra of H₂. The complete spectra span from 1140 to 1675 Å. The model utilizes the line transition probabilities by Abgrall *et al* (1993b&.1993c) and the total transition probabilities of Stephens and Dalgarno (1972) corrected according to Eq.(3). The strong transition at 121 5.685Å arises from the H Lyman-a emission, which is not considered by the model.

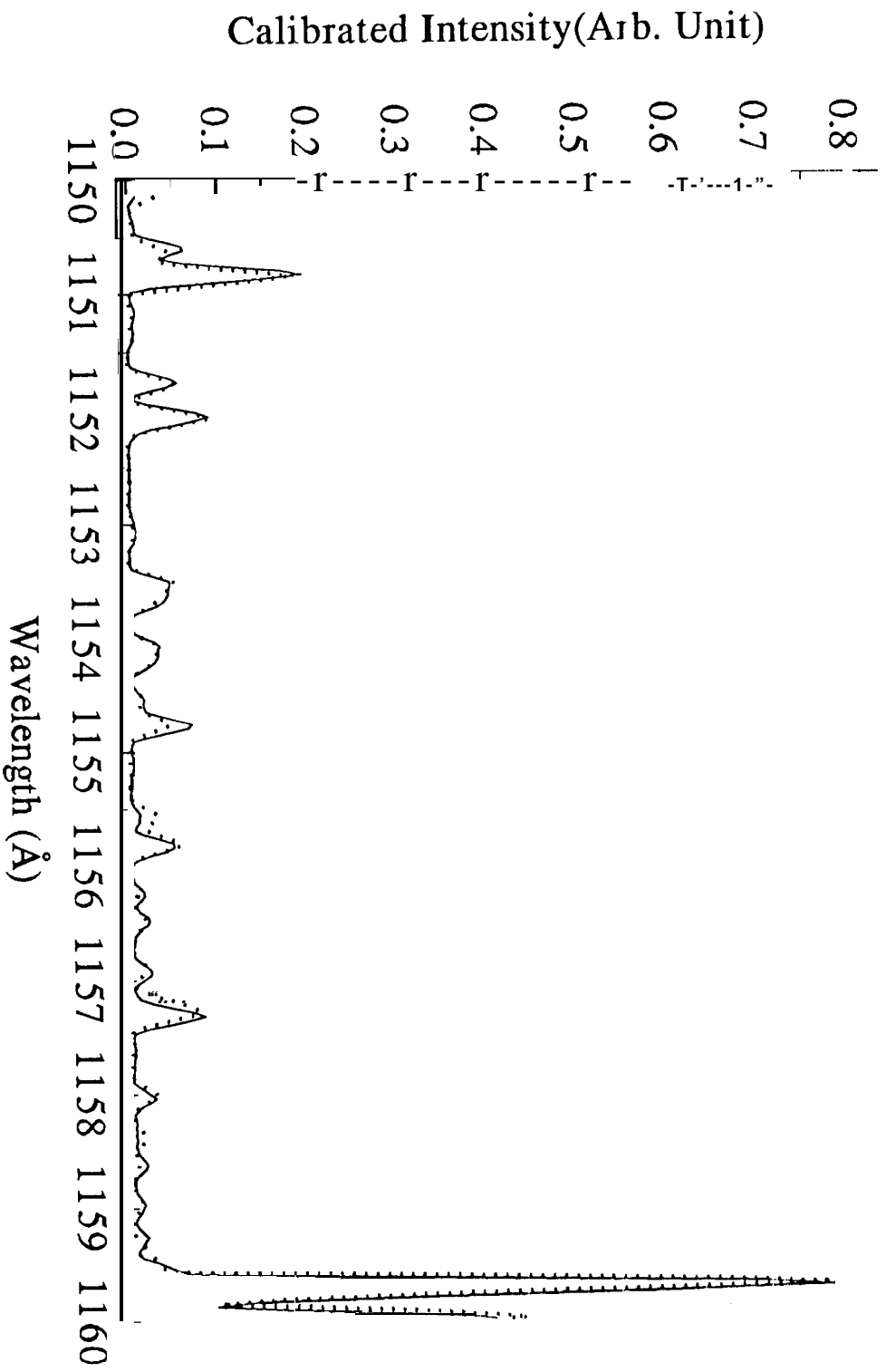
e + H₂ (1∞ eV 300K)

$\lambda = 0.136 \text{ \AA}$



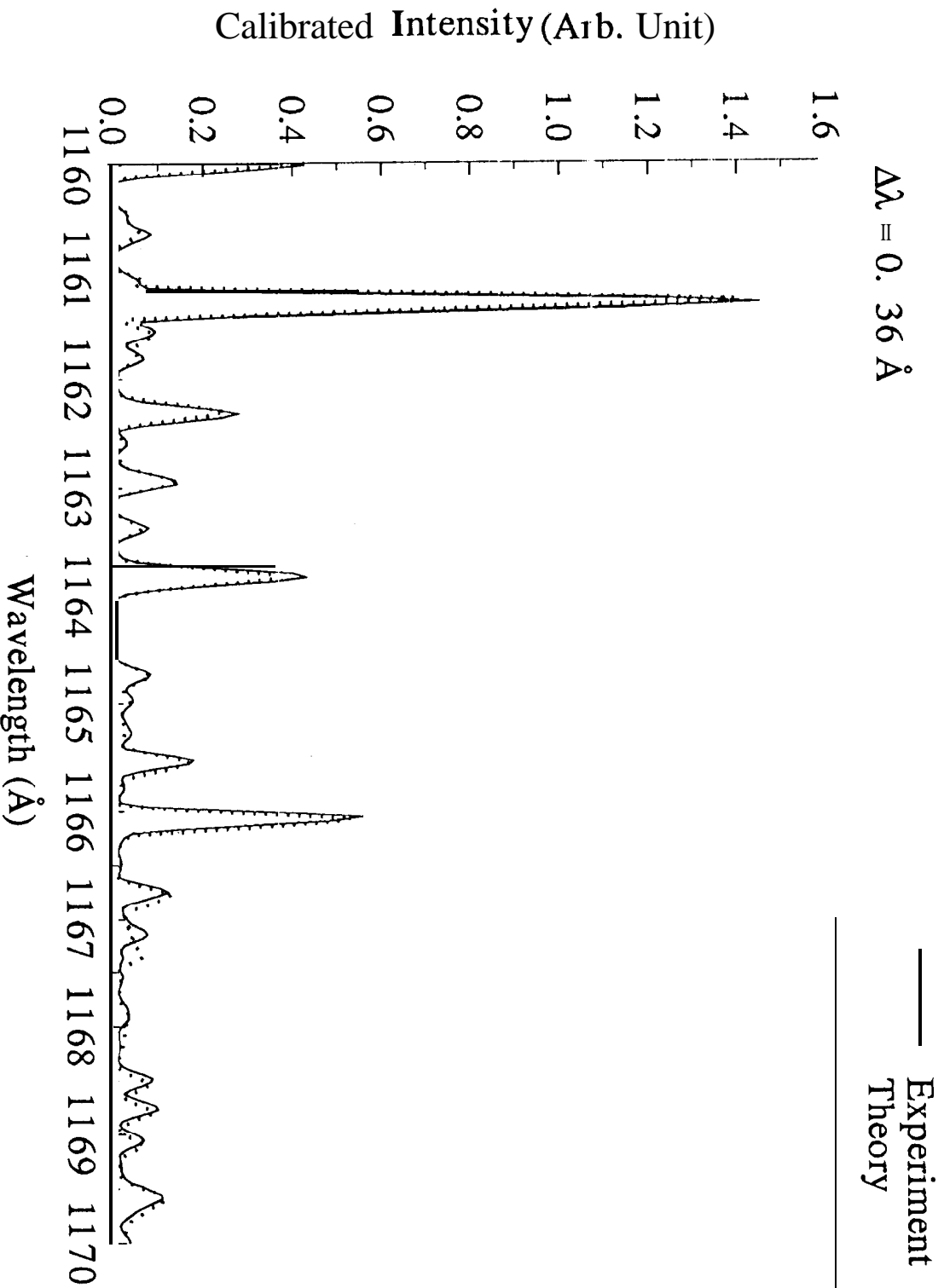
e + H₂ (100 eV 300K)

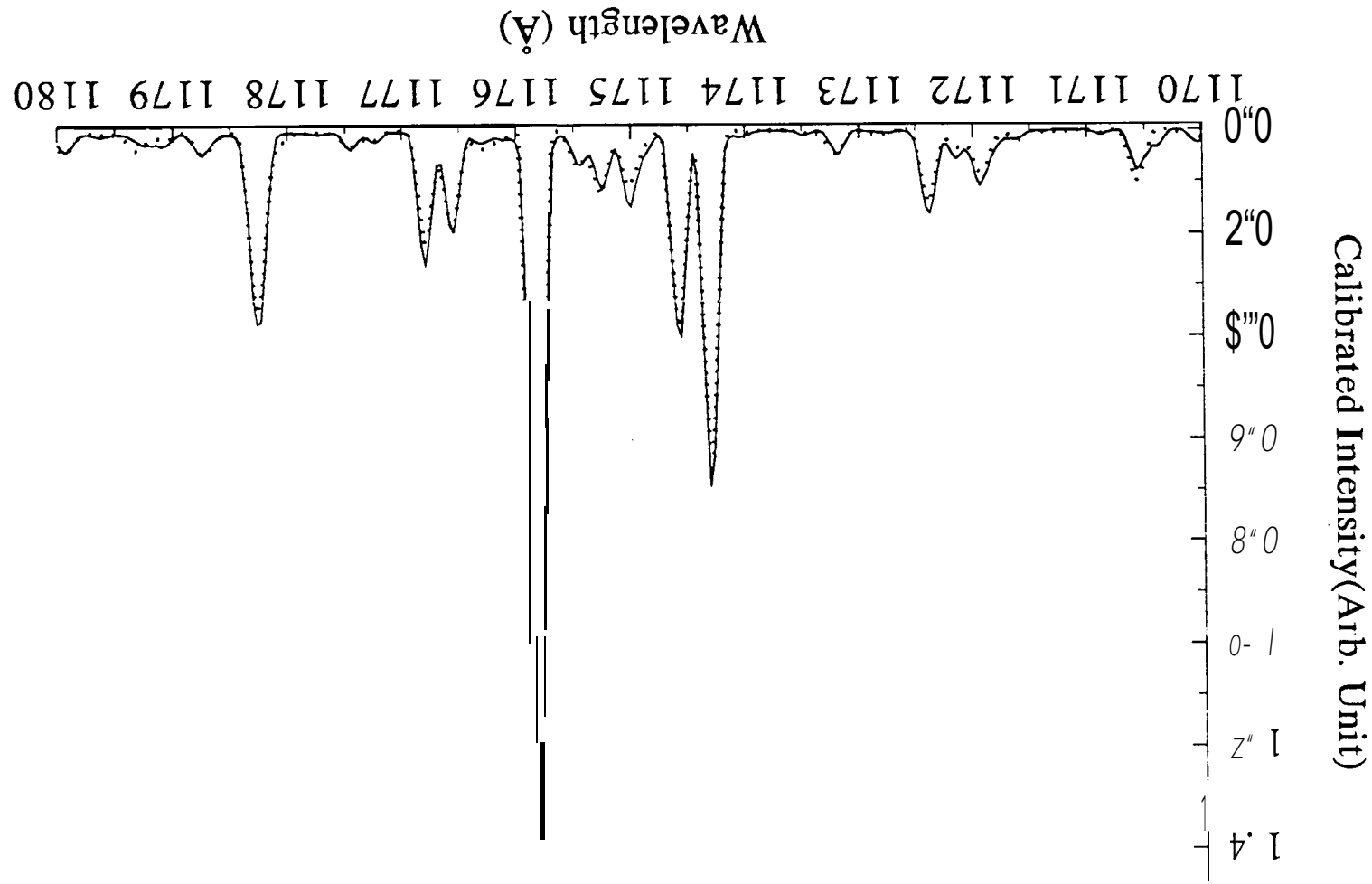
$\Delta\lambda = 0.136 \text{ \AA}$



$\text{S} + \text{H}_2 (1\infty \text{ eV } 300\text{K})$

$\Delta\lambda = 0.36 \text{ \AA}$





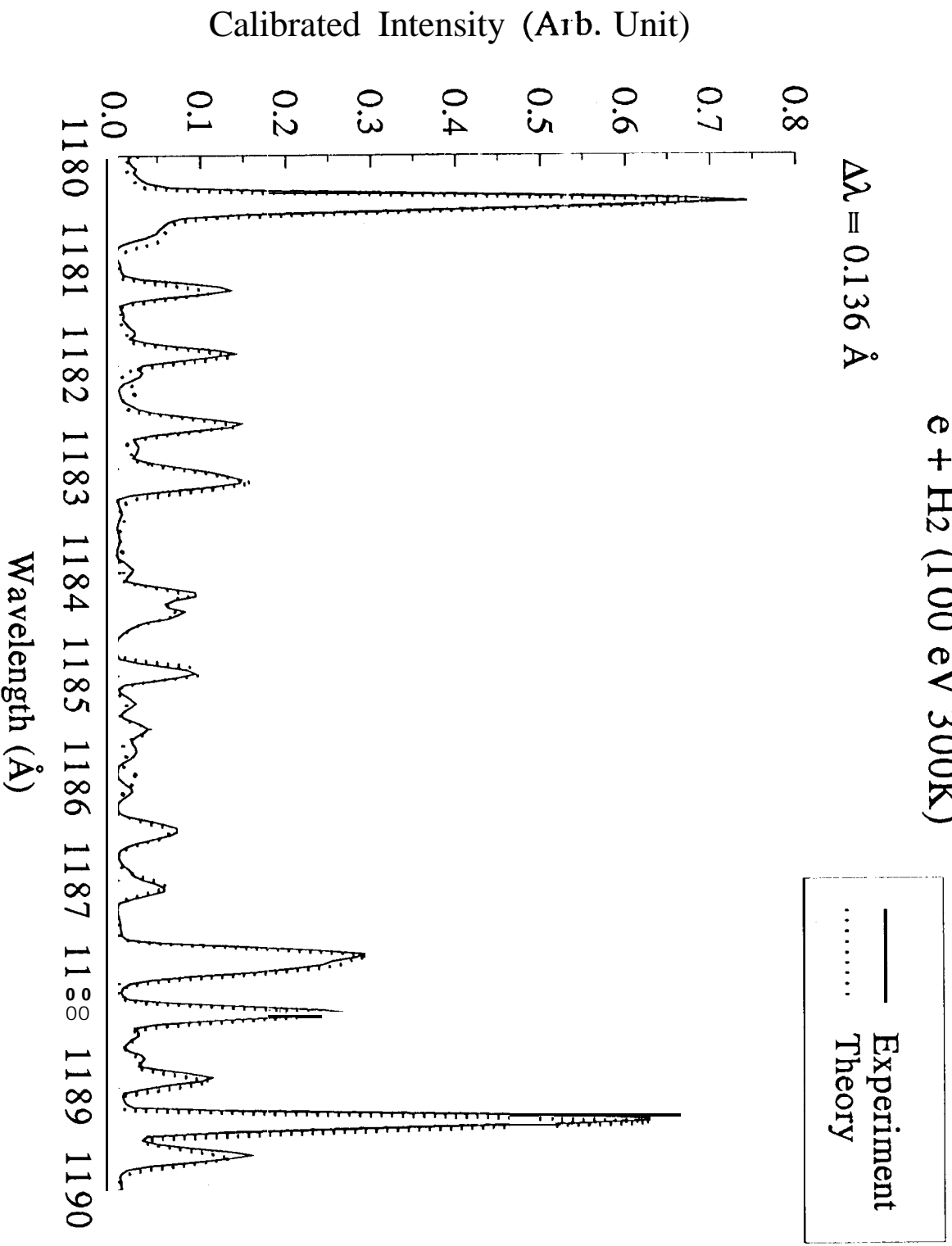
— Experiment
 Theory

$e + H_2$ (100 eV 300K)

$\Delta\lambda = 0.136 \text{ \AA}$

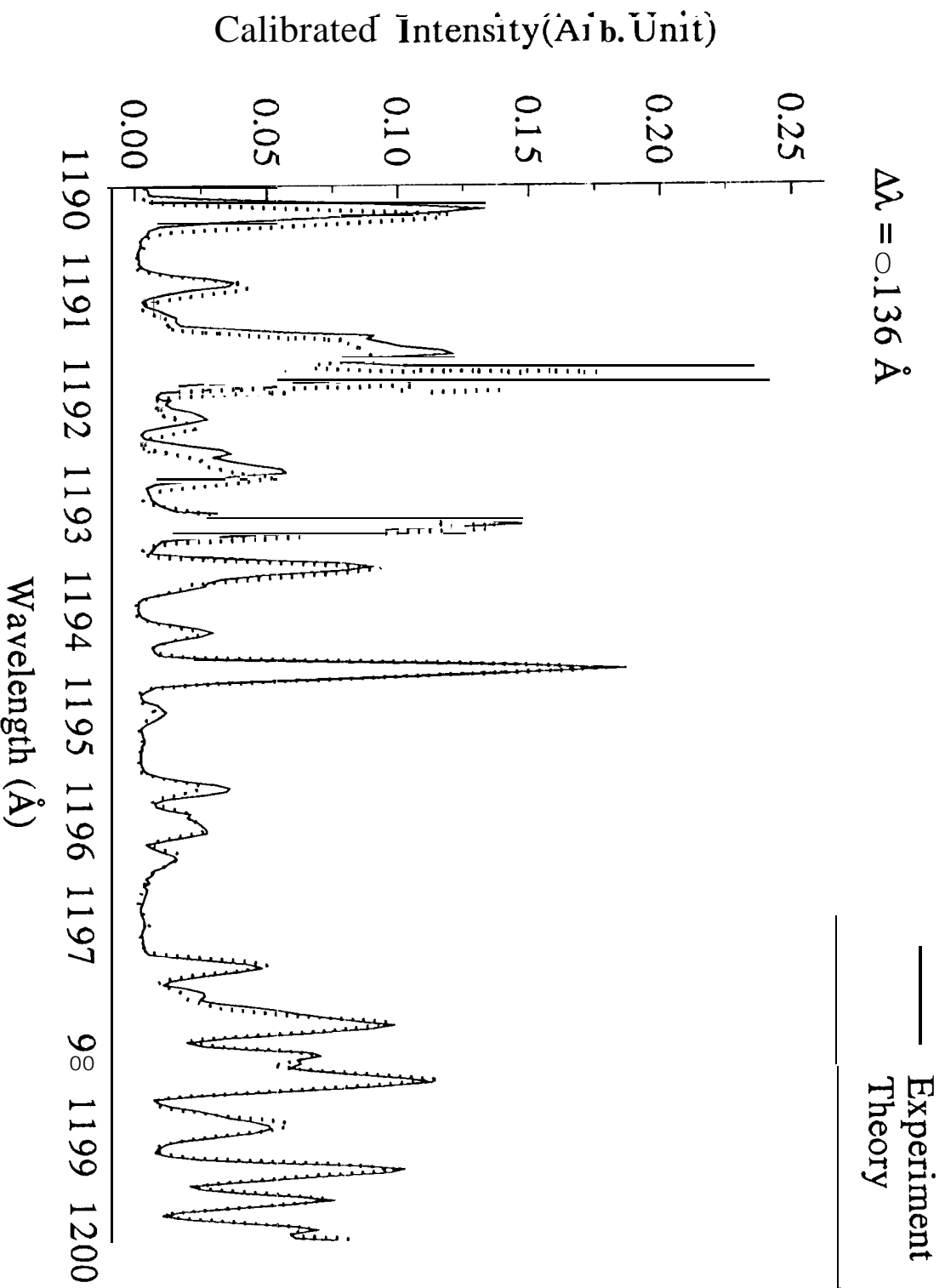
e + H₂ (100 eV 300K)

$\Delta\lambda = 0.136 \text{ \AA}$



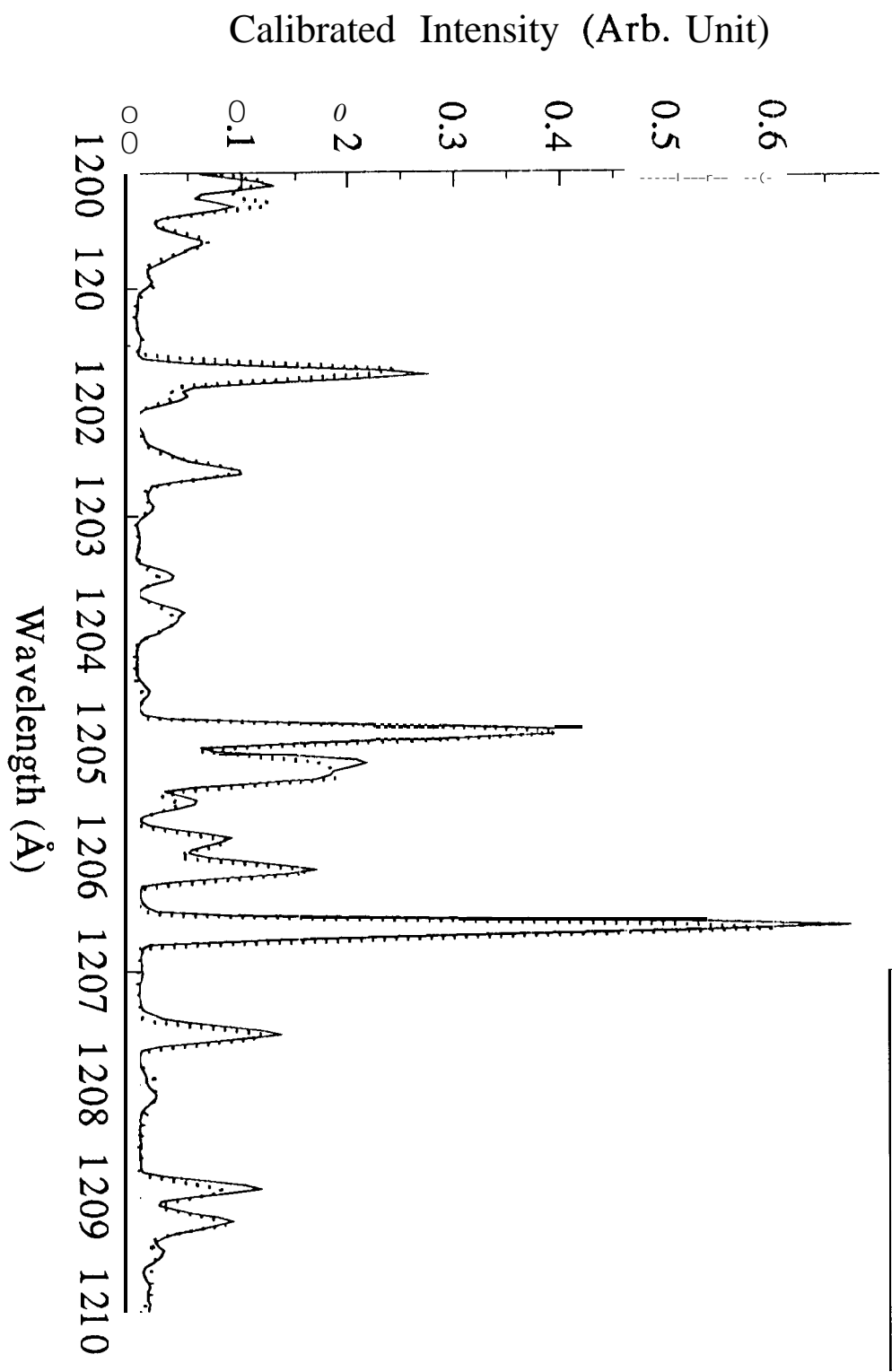
$\text{S} + \text{H}_2$ (100 eV 300K)

$\Delta\lambda = 0.136 \text{ \AA}$



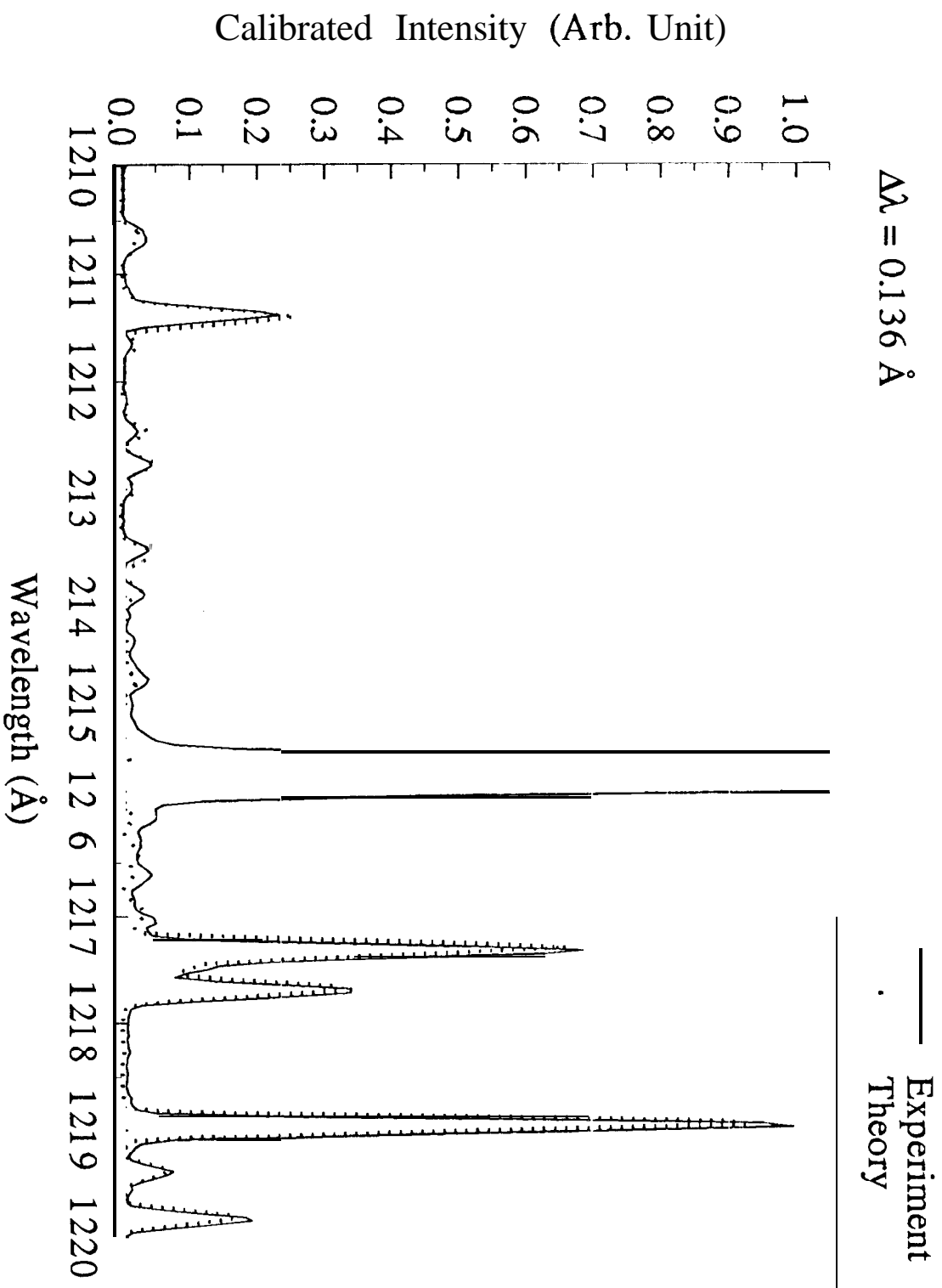
e + H₂ (100 eV, 300K)

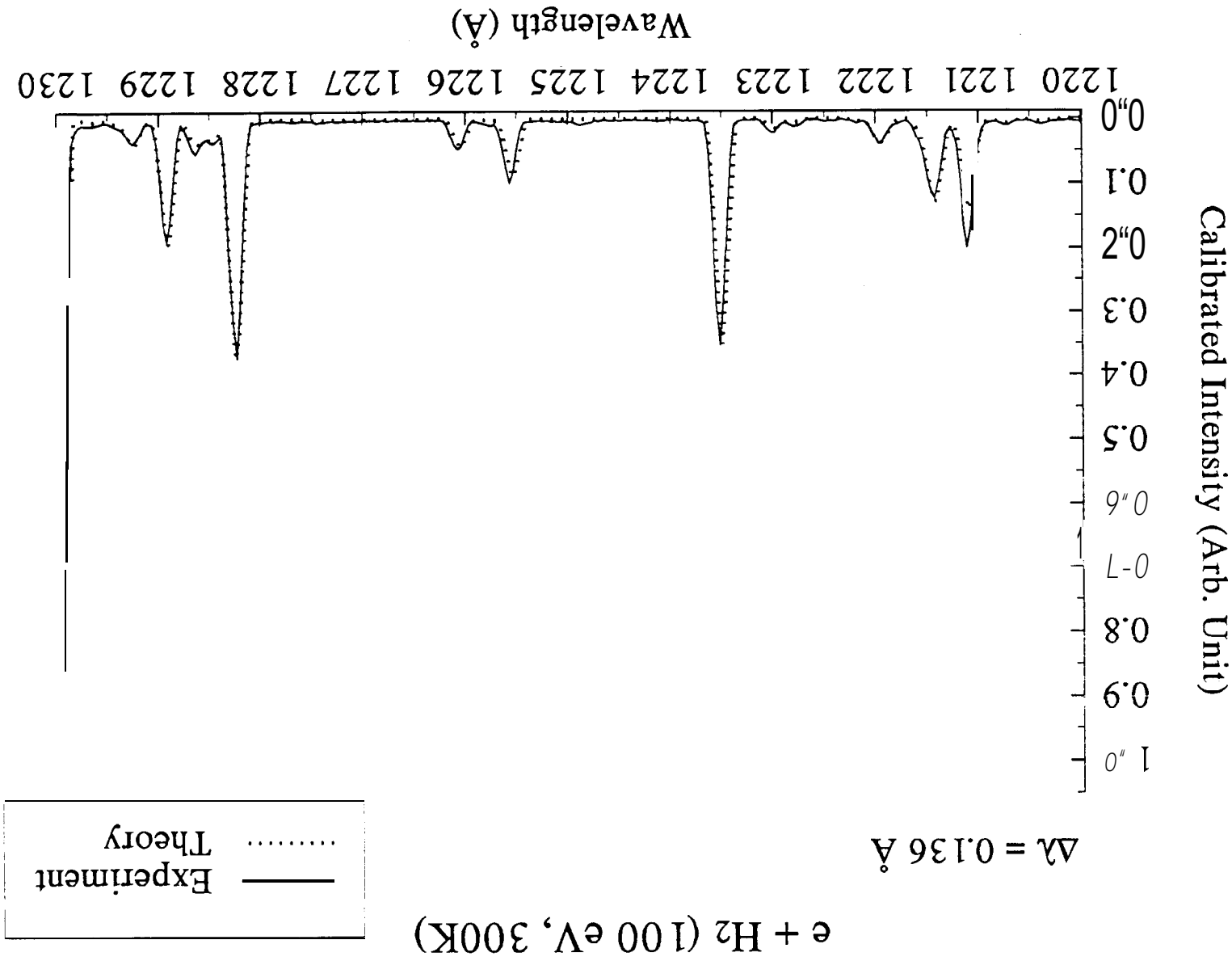
$\lambda = 0.136 \text{ \AA}$



$e + \text{H}_2$ (100 eV, 300K)

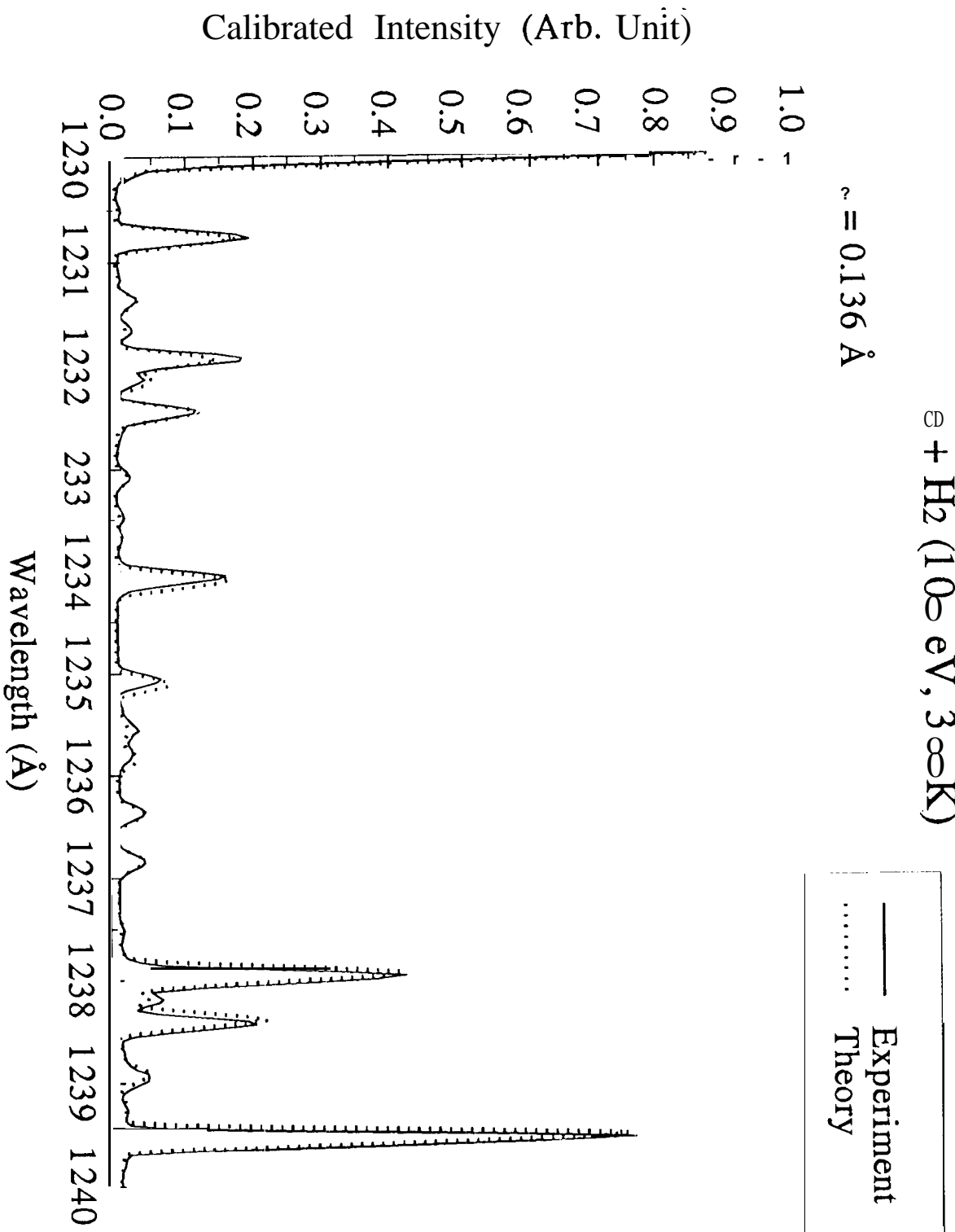
$\Delta\lambda = 0.136 \text{ \AA}$





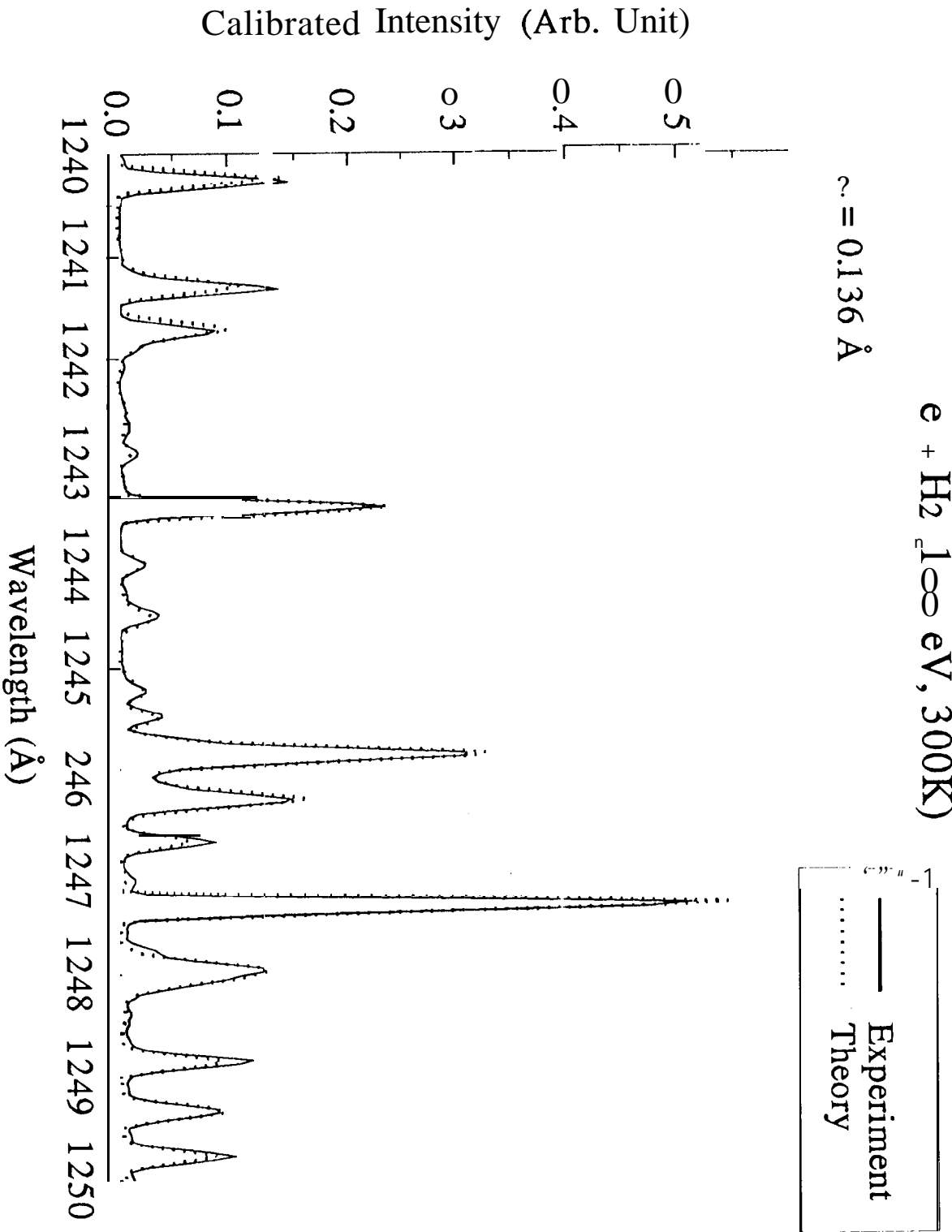
$e + H_2$ (100 eV, 300K)

$\lambda = 0.136 \text{ \AA}$



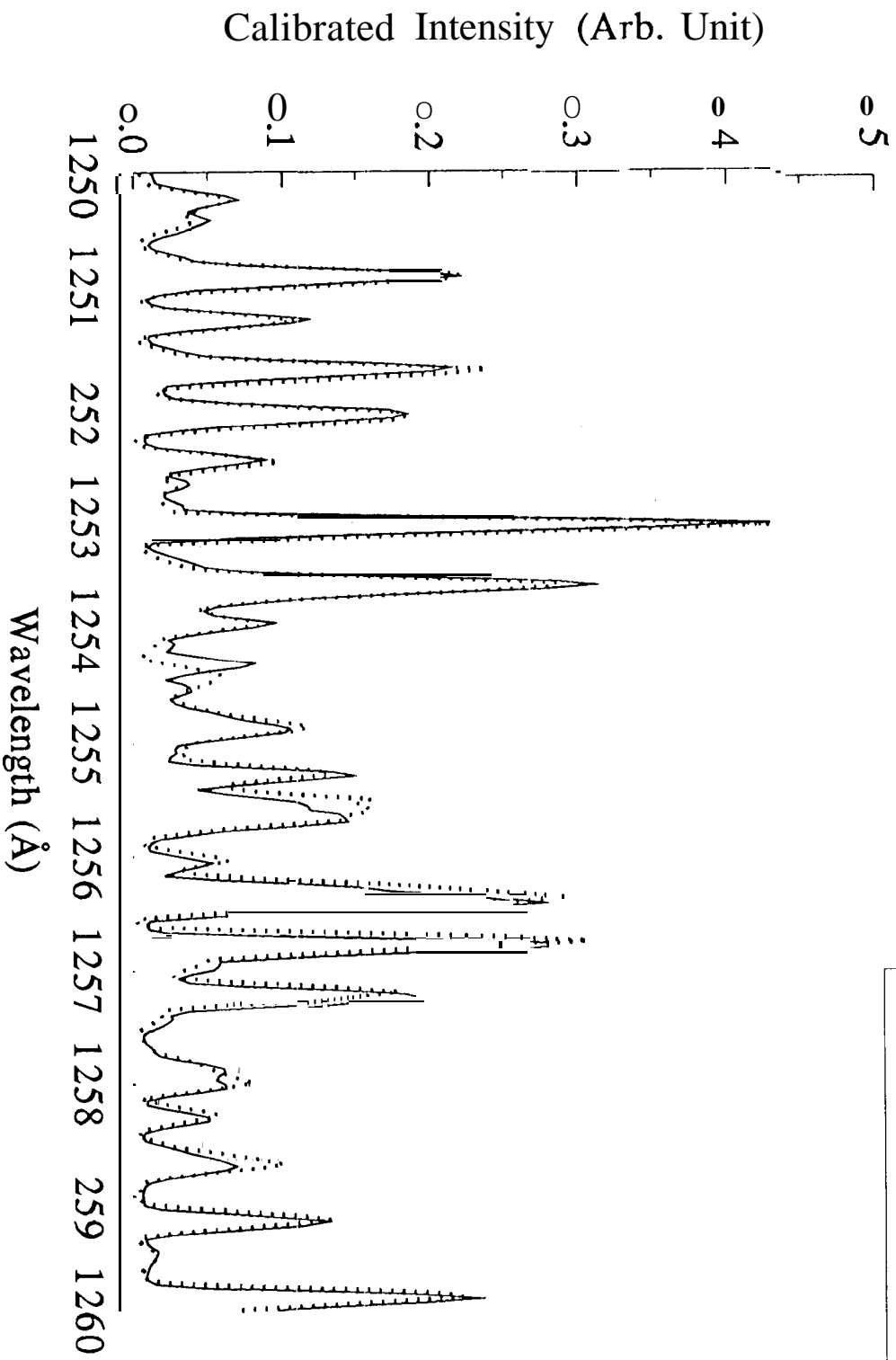
$e + H_2$ λ_{∞} eV, 300K)

$\lambda = 0.136 \text{ \AA}$



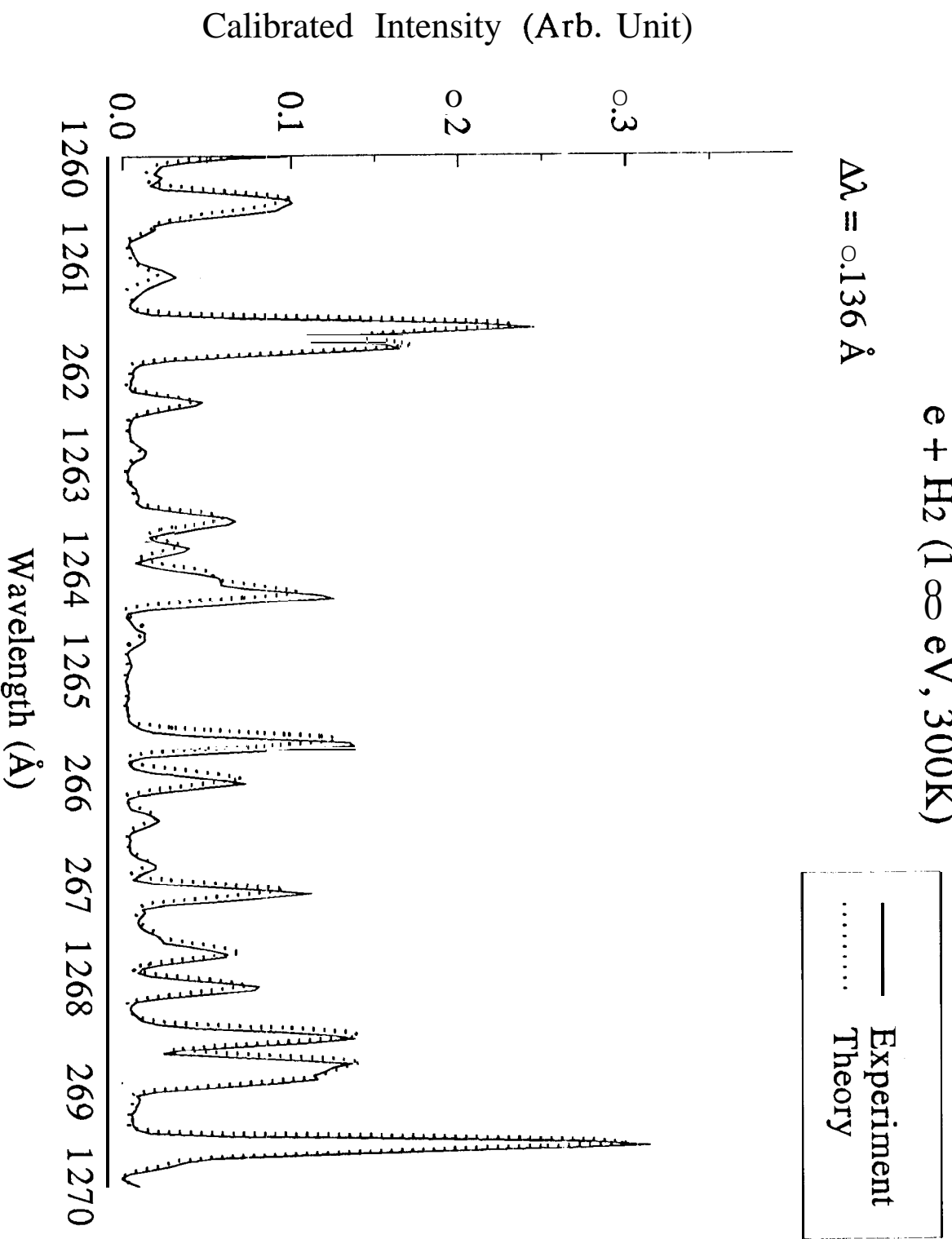
e + H₂ (100 eV, 300K)

$\lambda = 0.136 \text{ \AA}$



$e + H_2$ (1∞ eV, 300K)

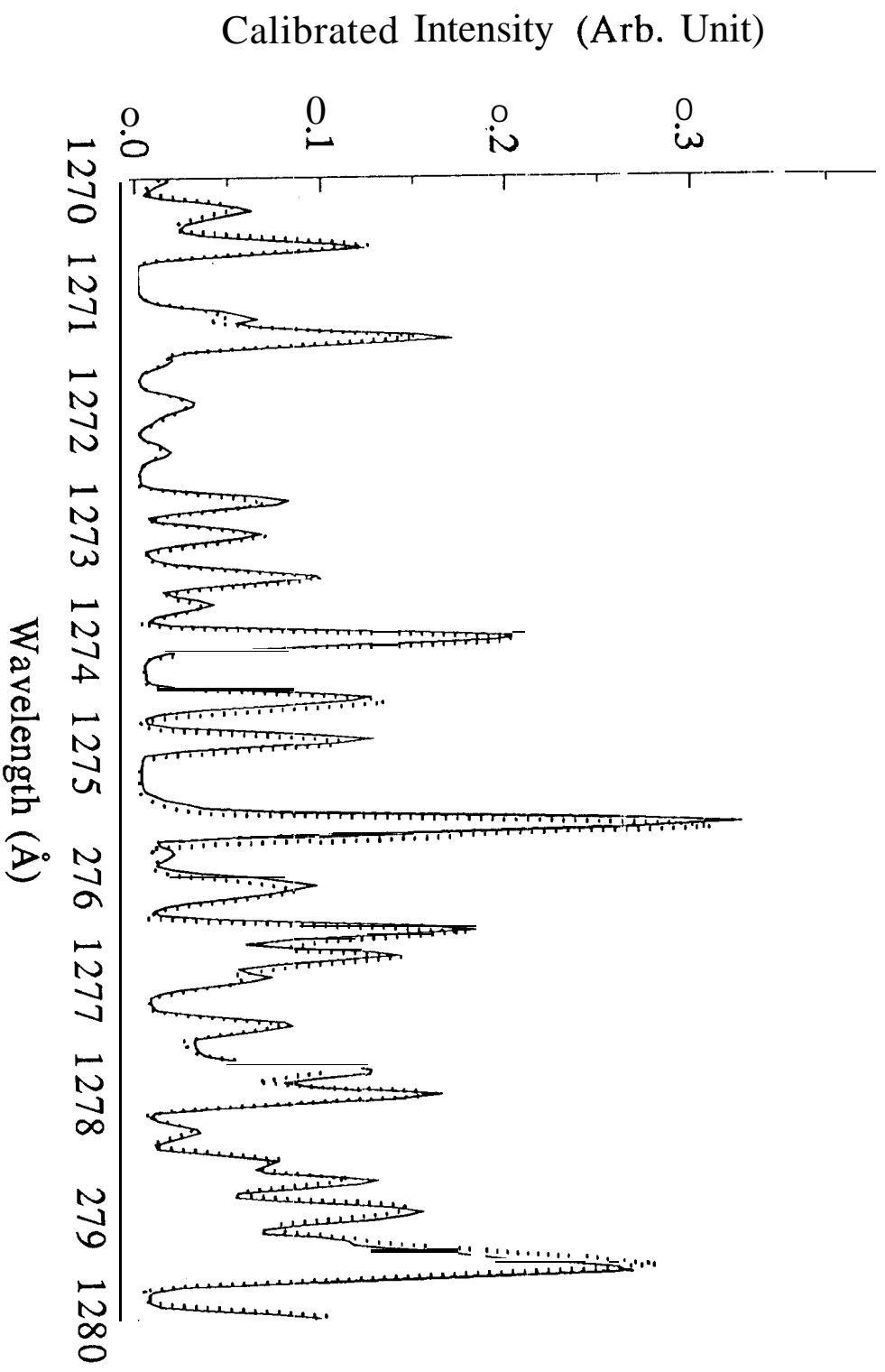
$\lambda = 0.136 \text{ \AA}$



$e + H_2$ (100 eV, 300K)

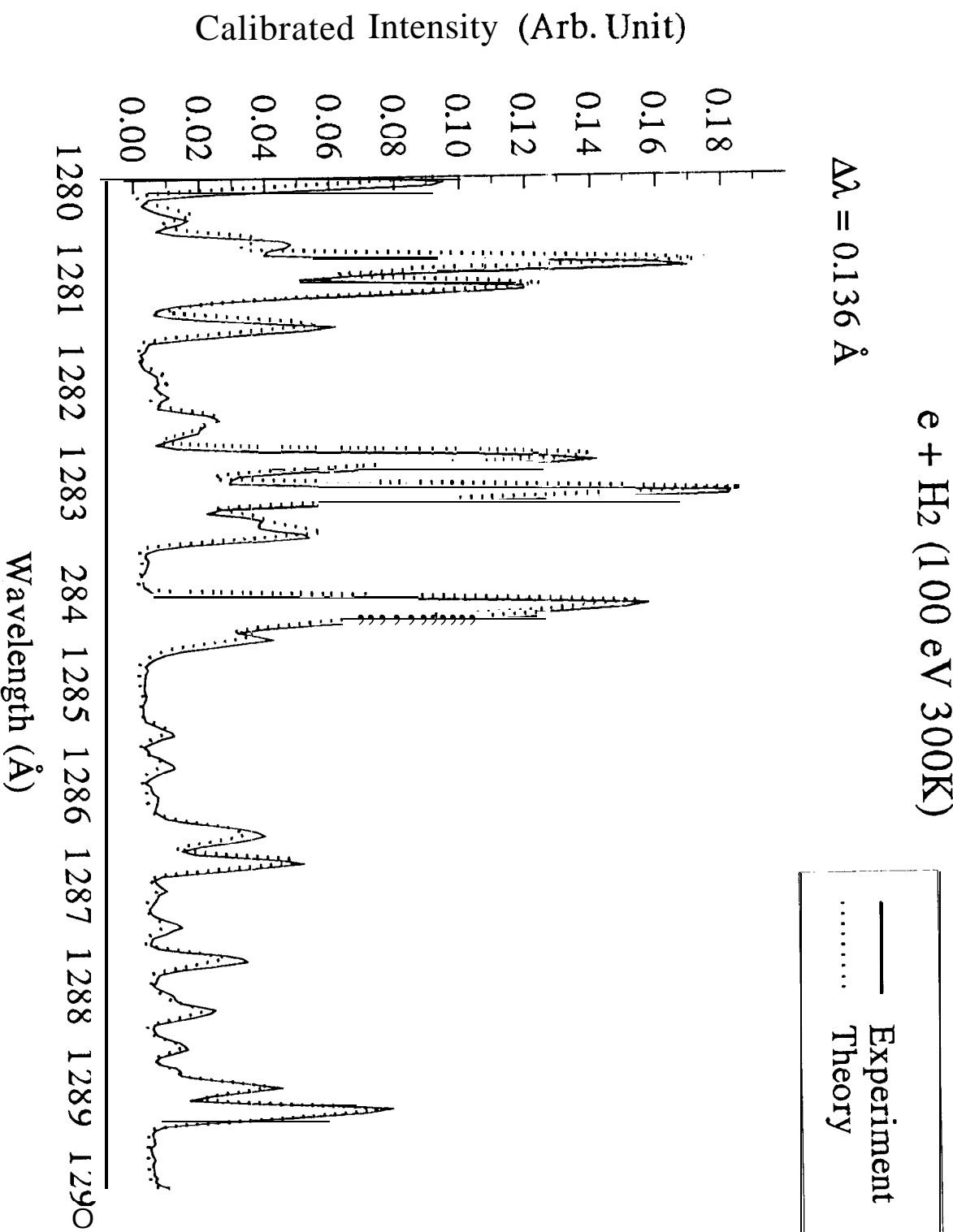
$\Delta\lambda = 0.136 \text{ \AA}$

— Experiment
- - - Theory



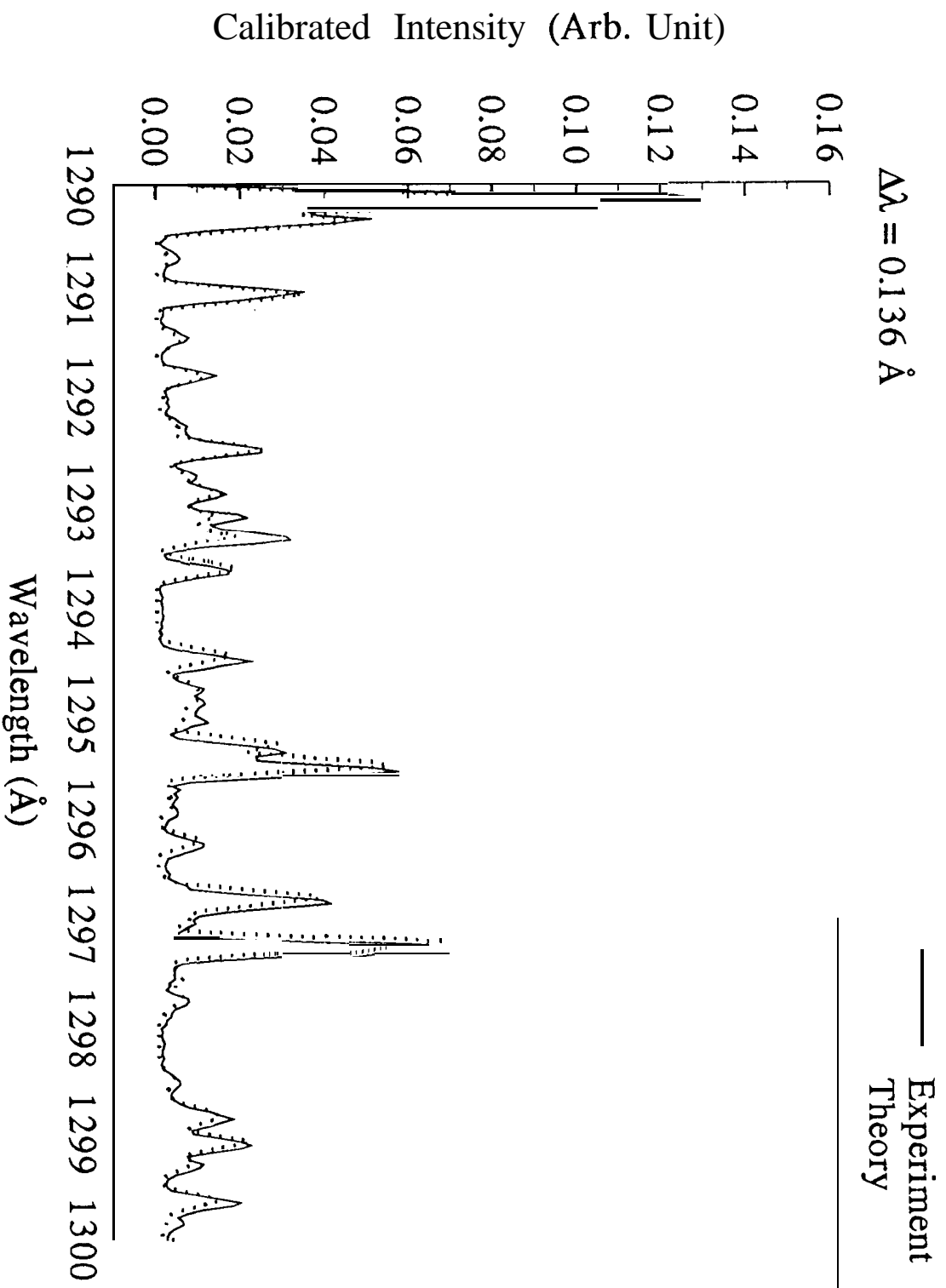
$e + \text{H}_2$ (100 eV 300K)

$\Delta\lambda = 0.136 \text{ \AA}$



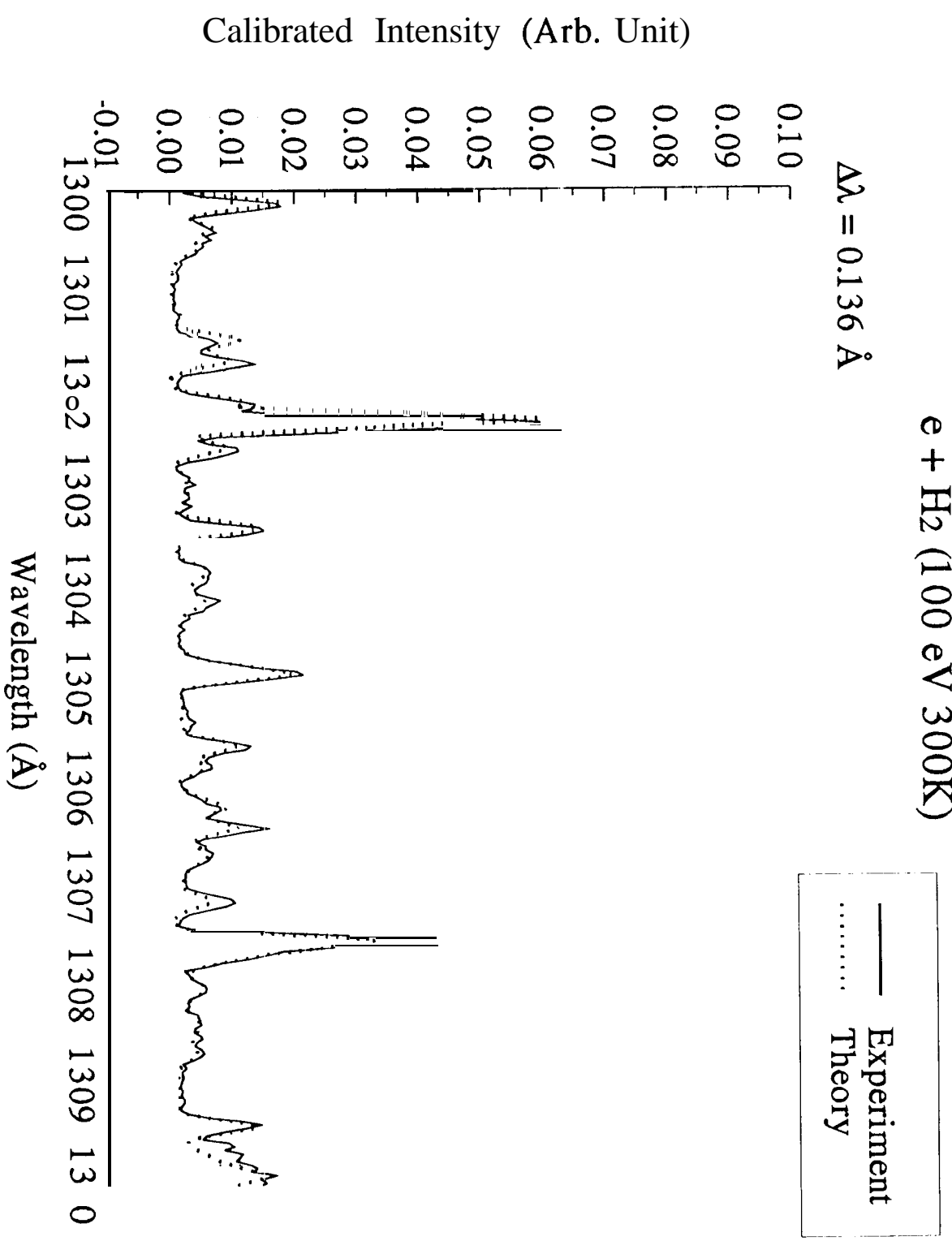
$e + H_2$ (1∞ eV 300K)

$\Delta\lambda = 0.136 \text{ \AA}$



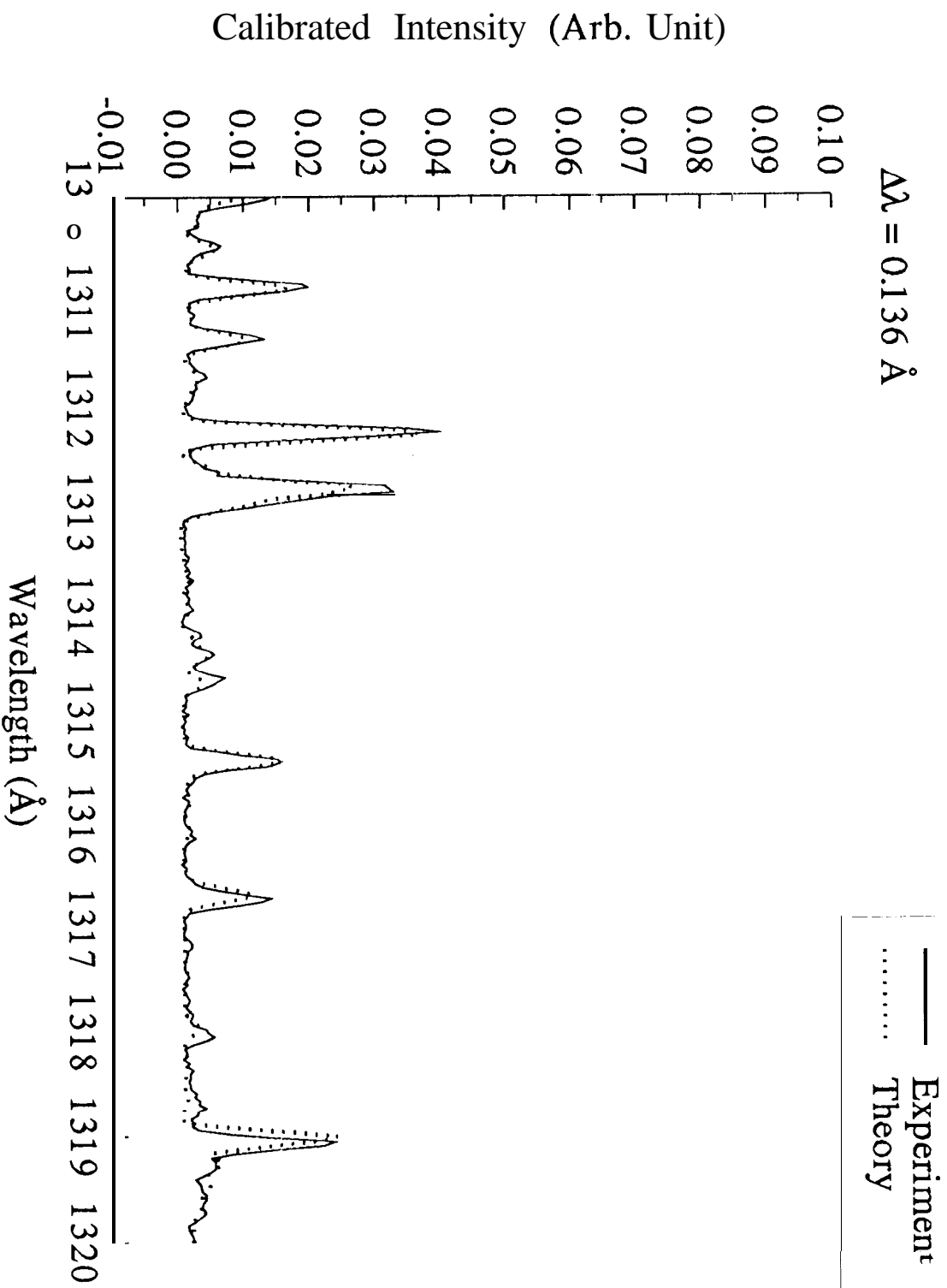
e + H₂ (100 eV 300K)

$\Delta\lambda = 0.136 \text{ \AA}$



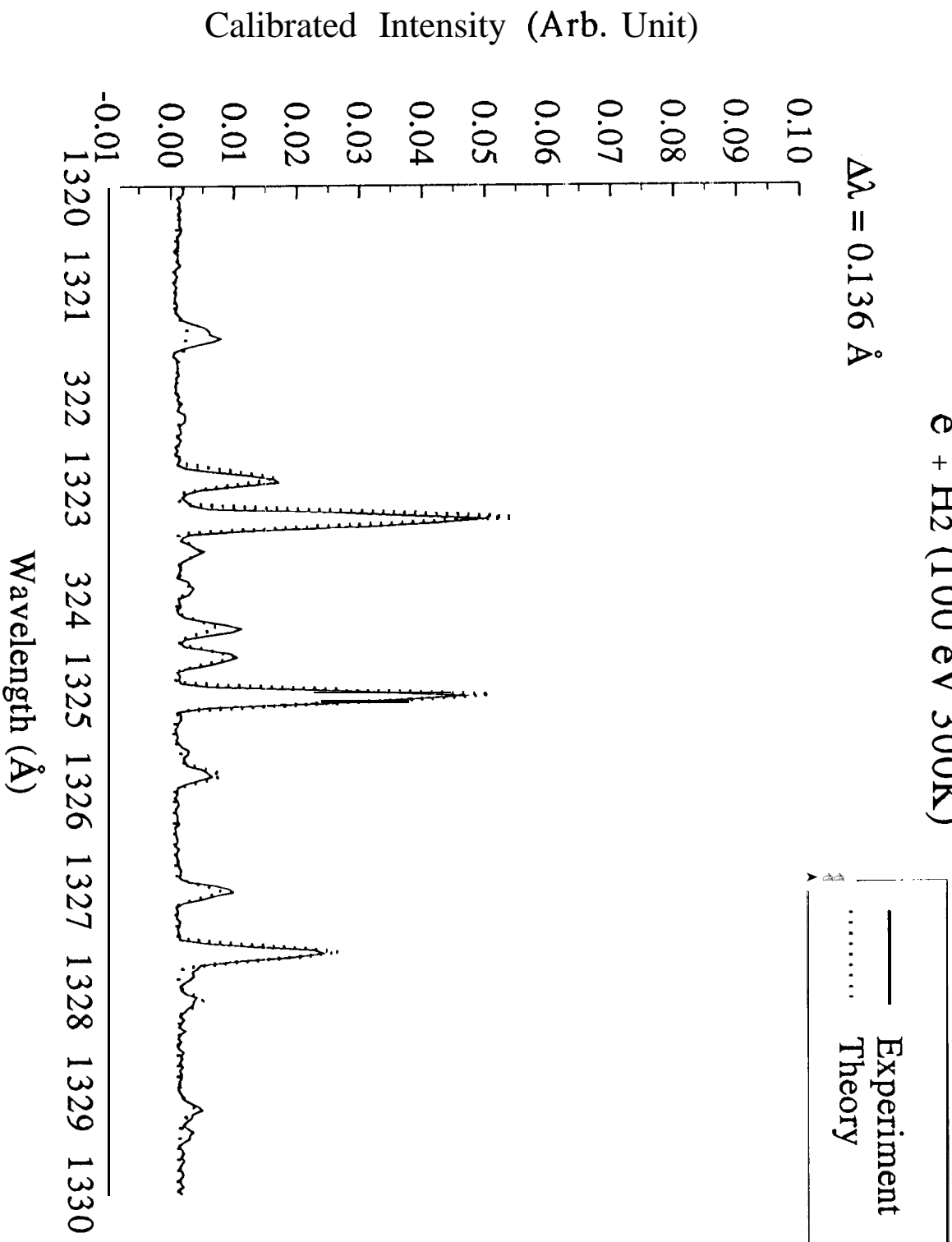
$e + H_2$ (100 eV 300K)

$\Delta\lambda = 0.136 \text{ \AA}$



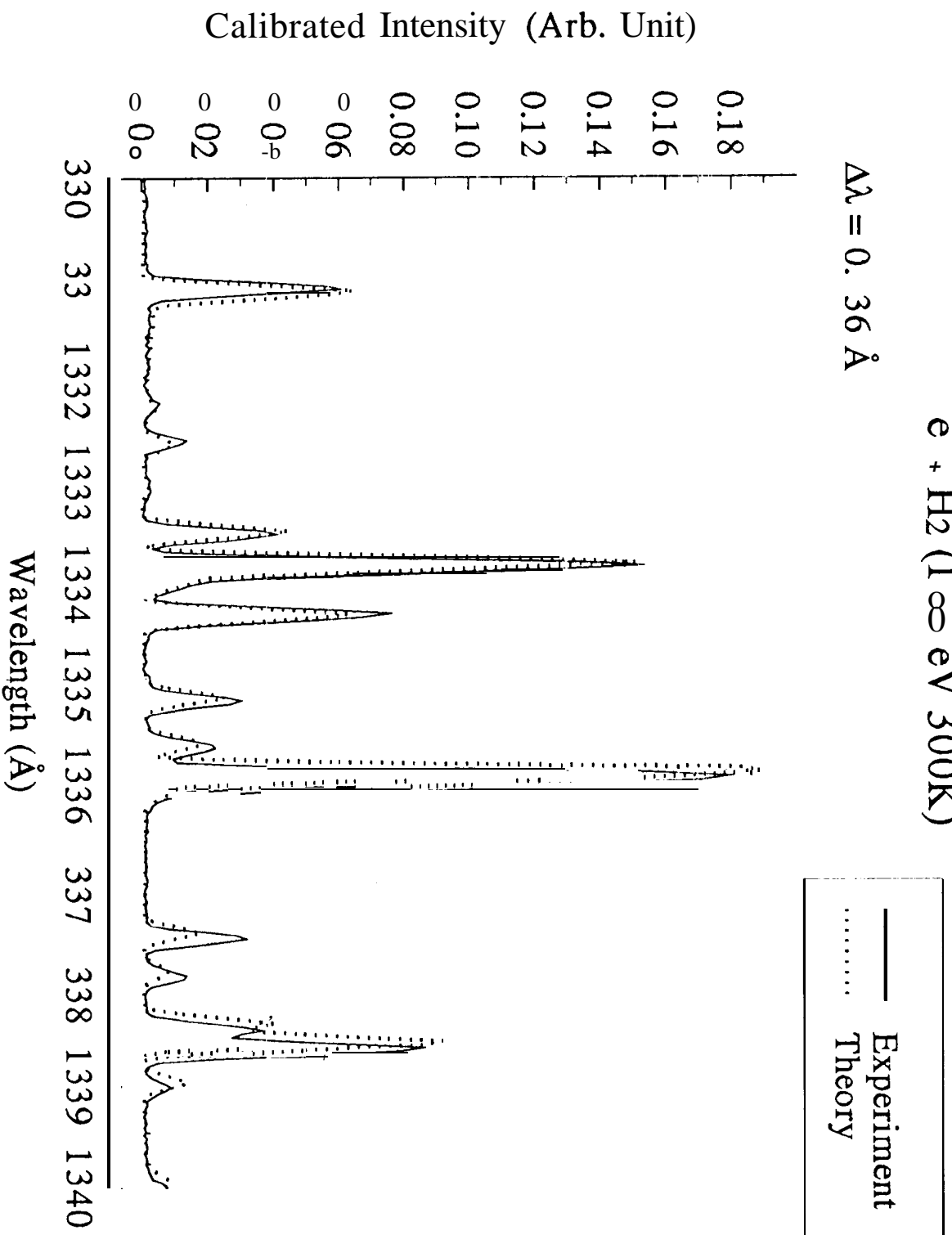
$e + H_2$ (100 eV 300K)

$\Delta\lambda = 0.136 \text{ \AA}$



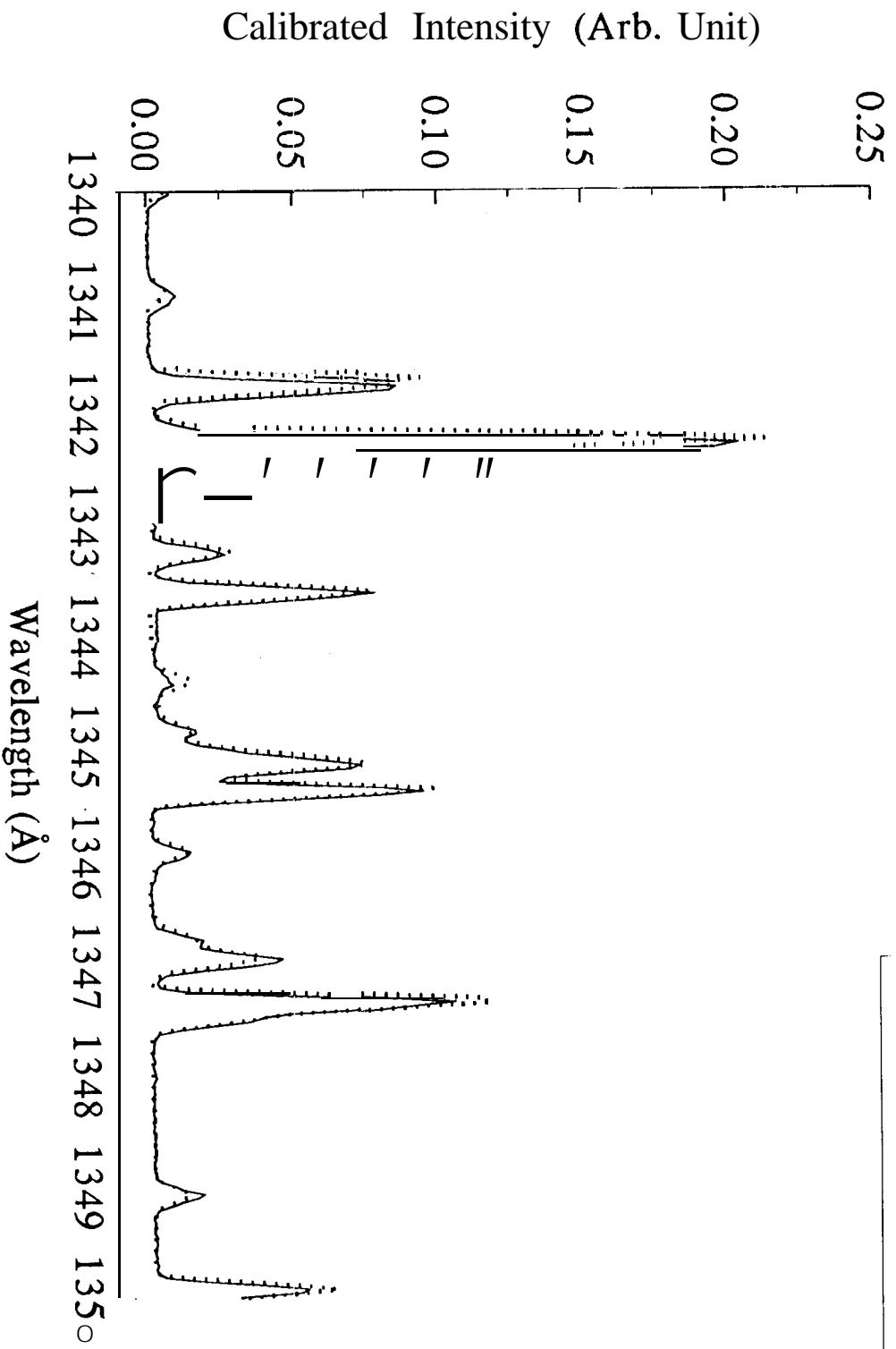
$e + H_2$ (1∞ eV 300K)

$\Delta\lambda = 0.36 \text{ \AA}$



$D + H_2$ 100 eV 300K)

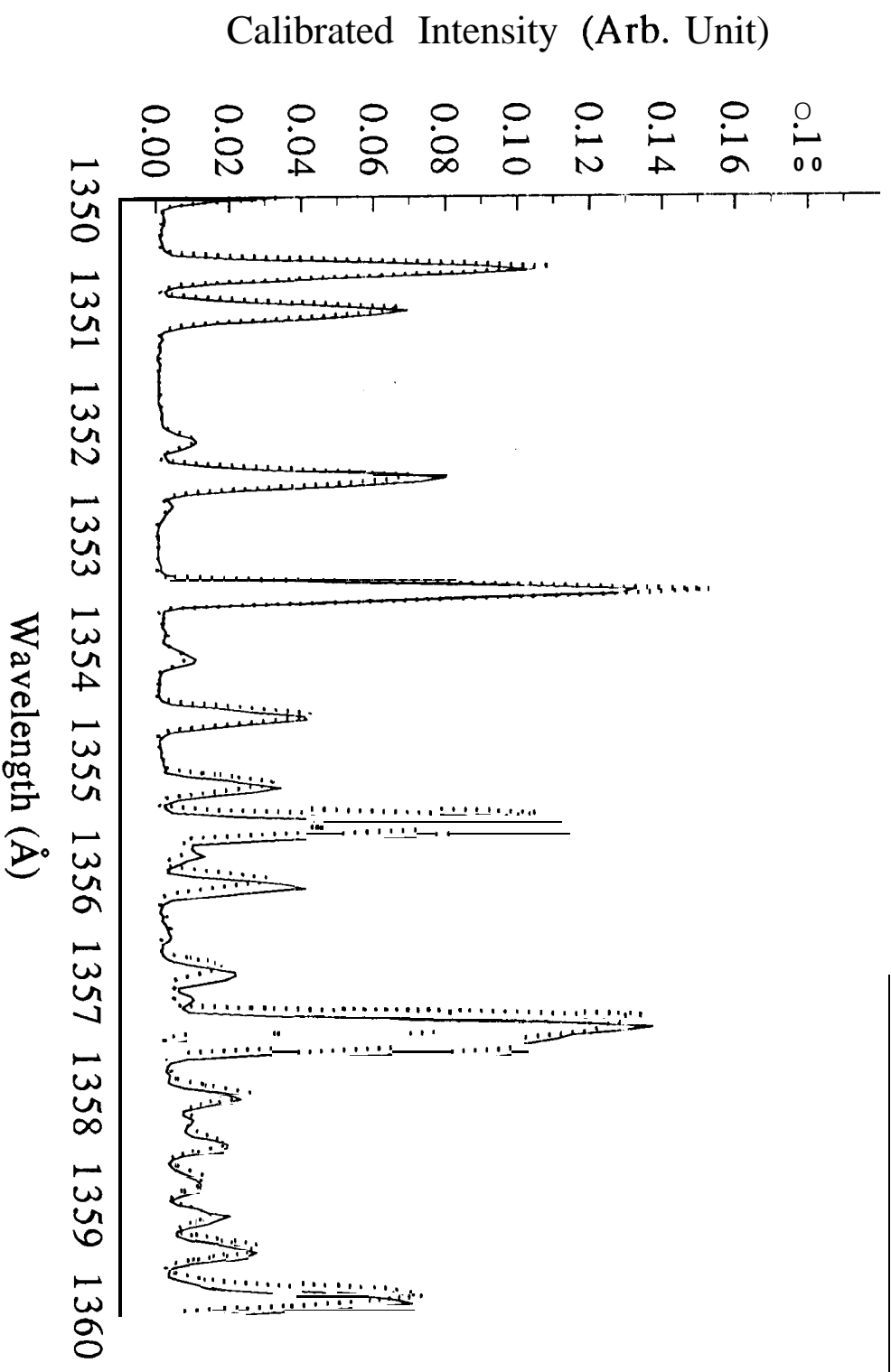
$\Delta\lambda = 0.136 \text{ \AA}$



e + H₂ (1∞ eV 300K)

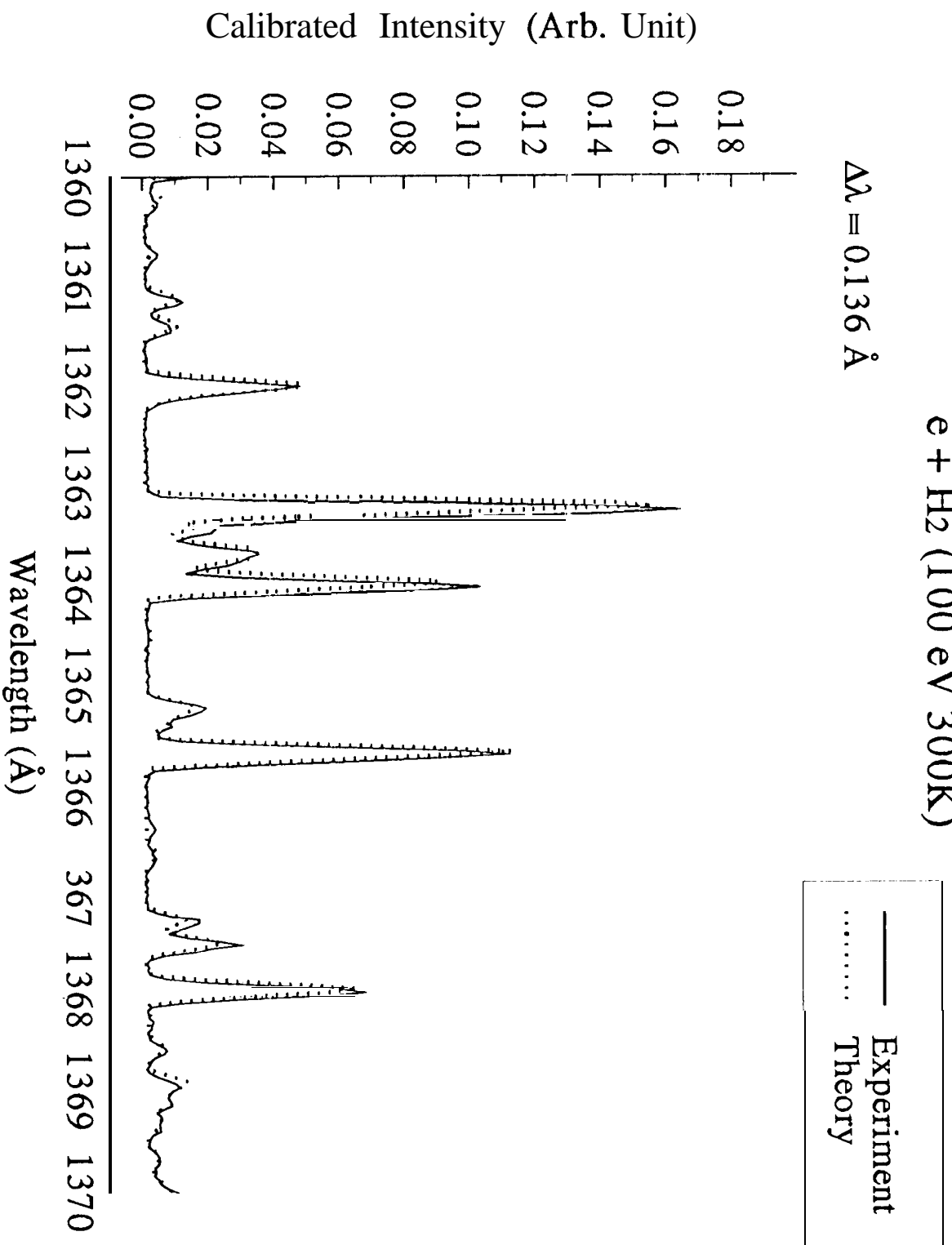
$\Delta\lambda = 0.136 \text{ \AA}$

— Experiment
..... Theory



e + H₂ (100 eV 300K)

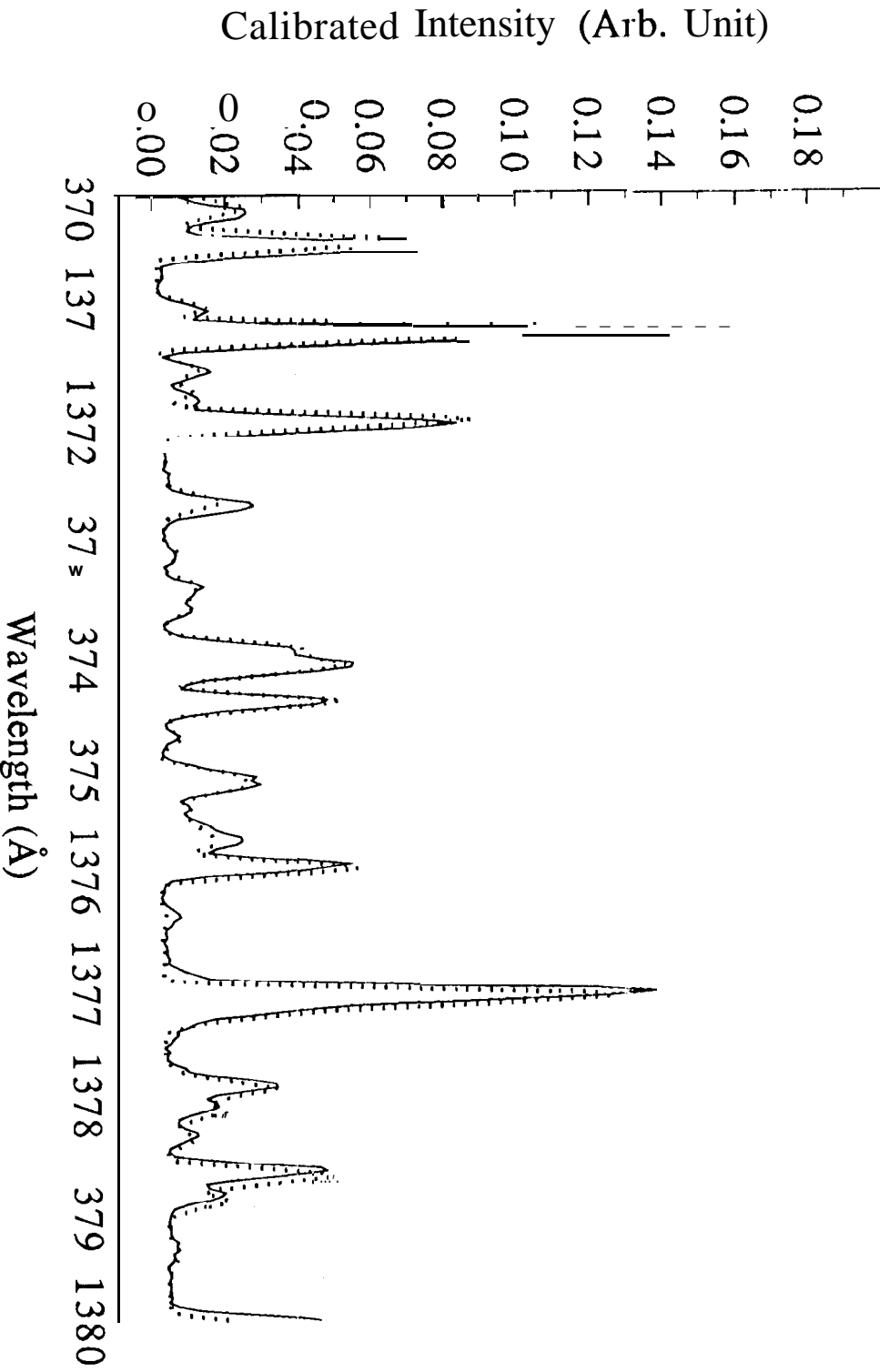
$\Delta\lambda = 0.136 \text{ \AA}$

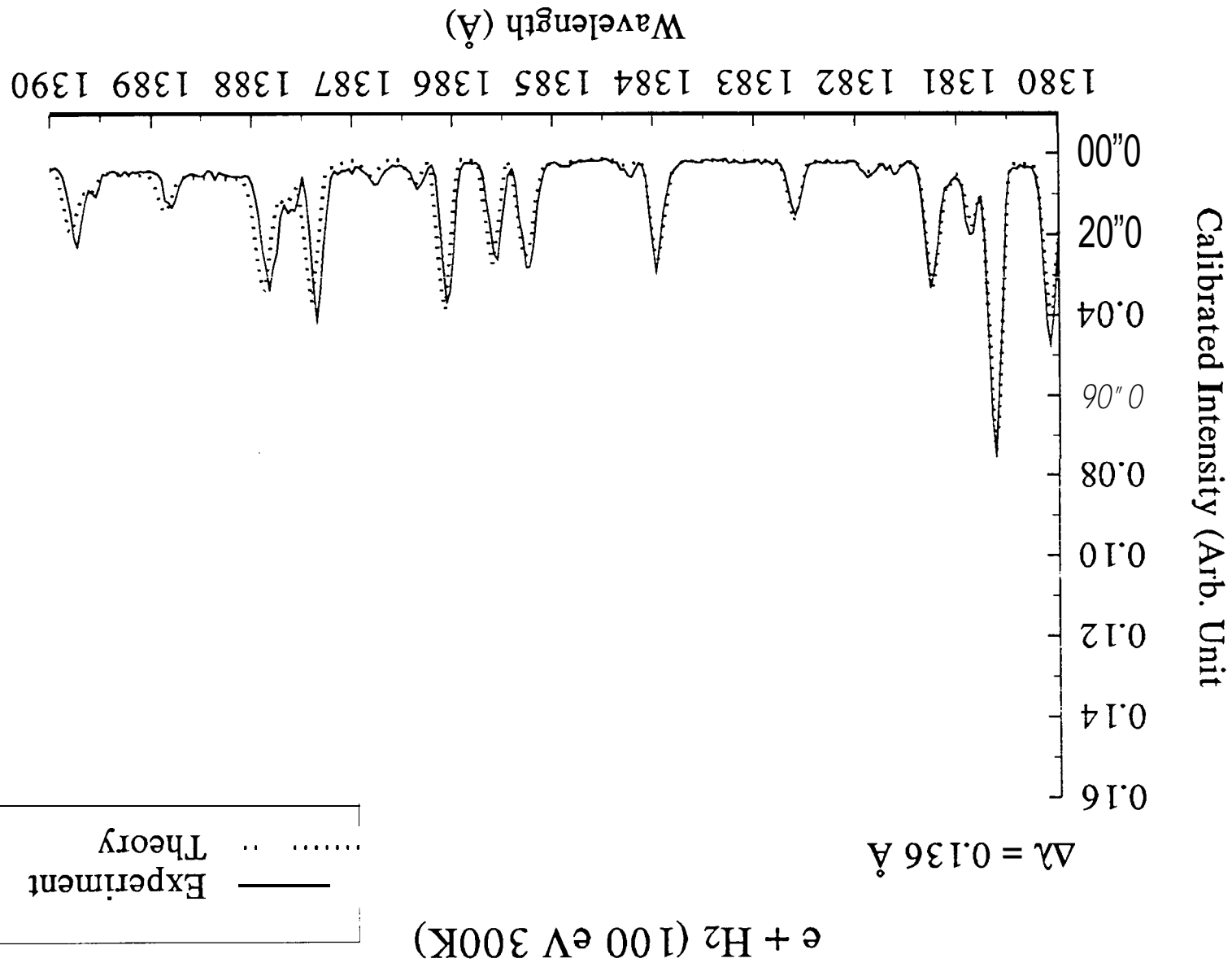


$e + H_2$ (100 eV 300K)

$\Delta\lambda = 0.136 \text{ \AA}$

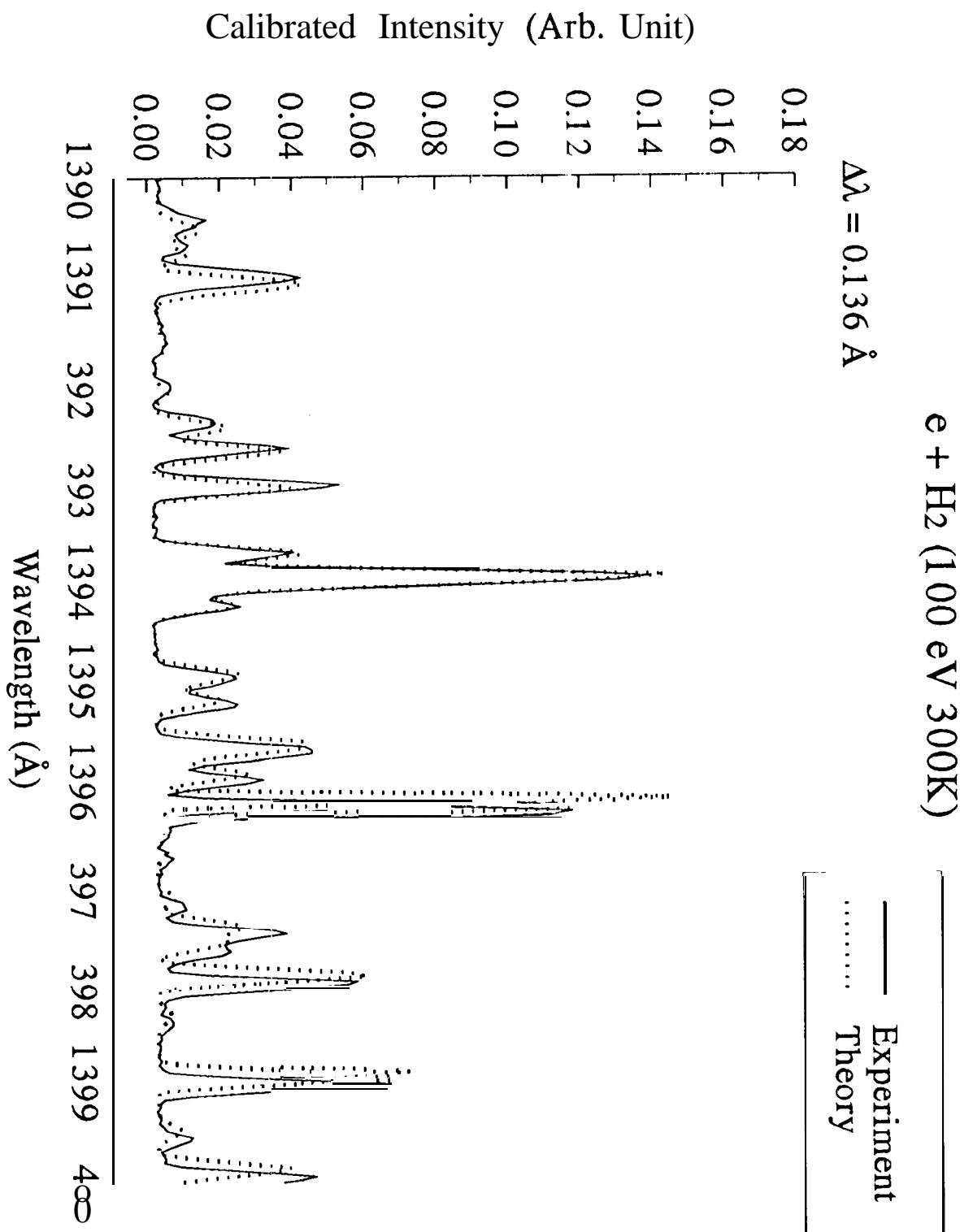
— Experiment
· Theory





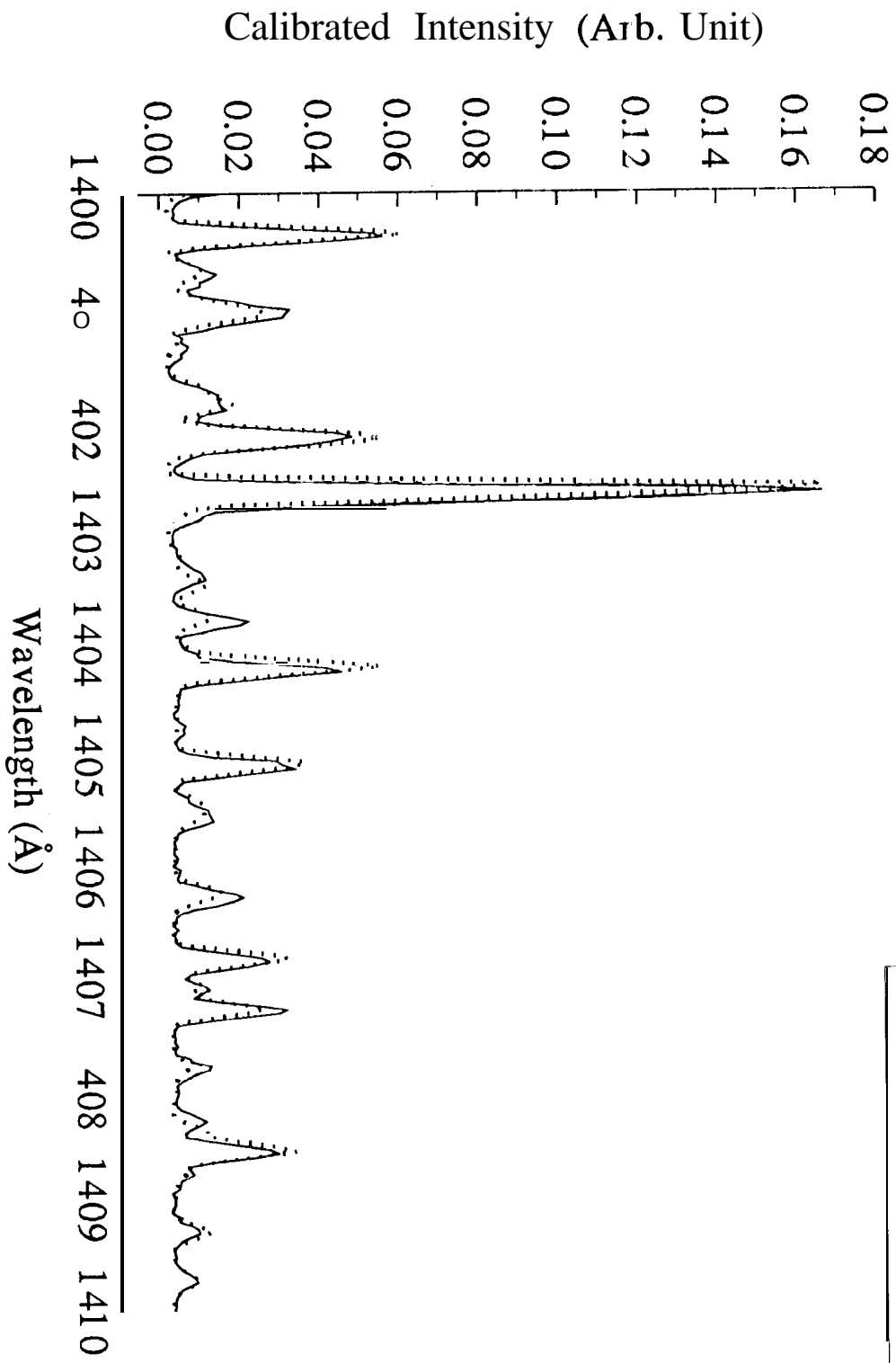
e + H₂ (100 eV 300K)

$\Delta\lambda = 0.136 \text{ \AA}$



e + H₂ (100 eV 300K)

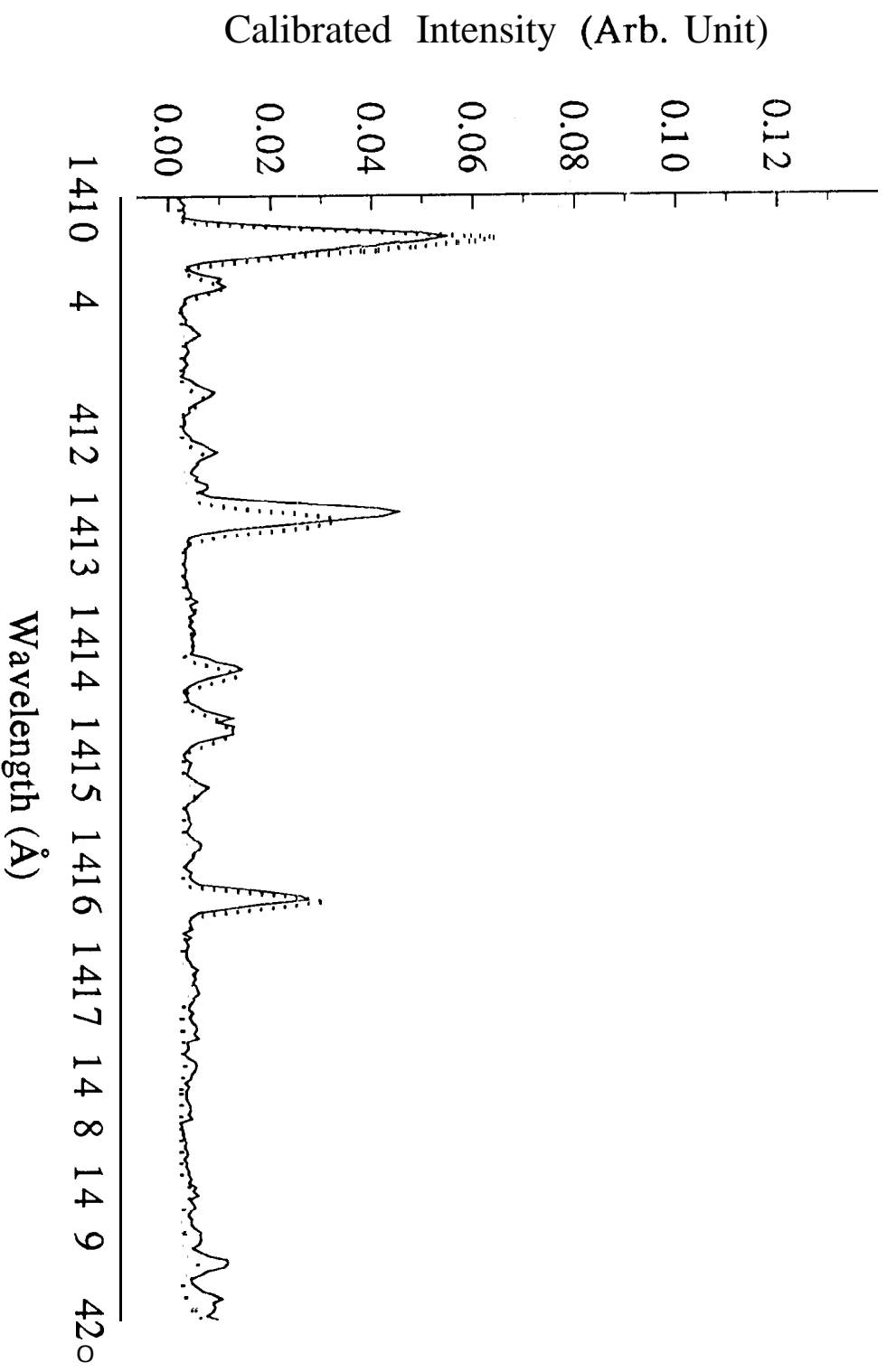
$\Delta\lambda = 0.136 \text{ \AA}$



e + H₂ (100 eV 300K)

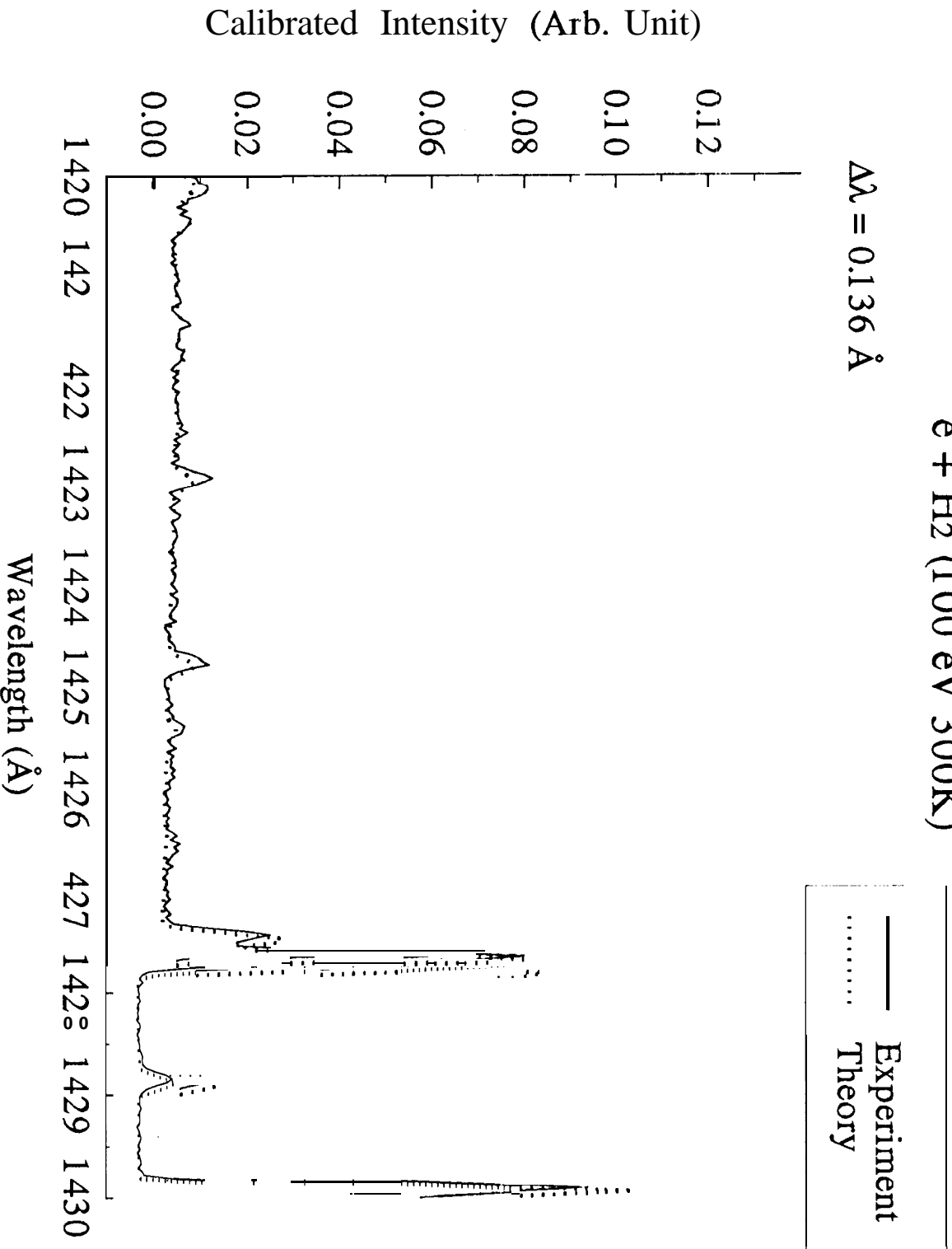
$\Delta\lambda = 0.136 \text{ \AA}$

— Experiment
— Theory



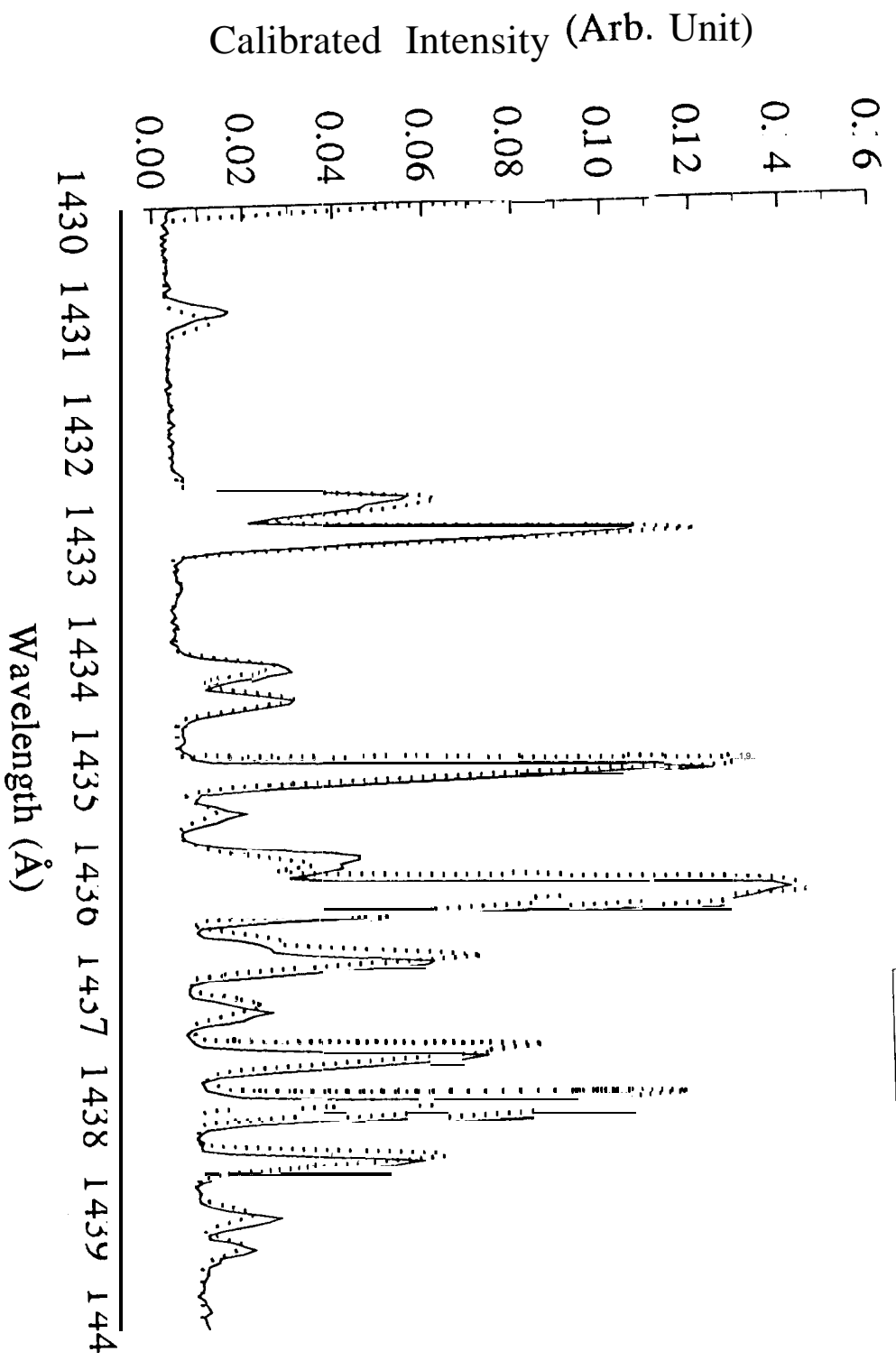
e + H₂ (100 eV 300K)

$\Delta\lambda = 0.136 \text{ \AA}$



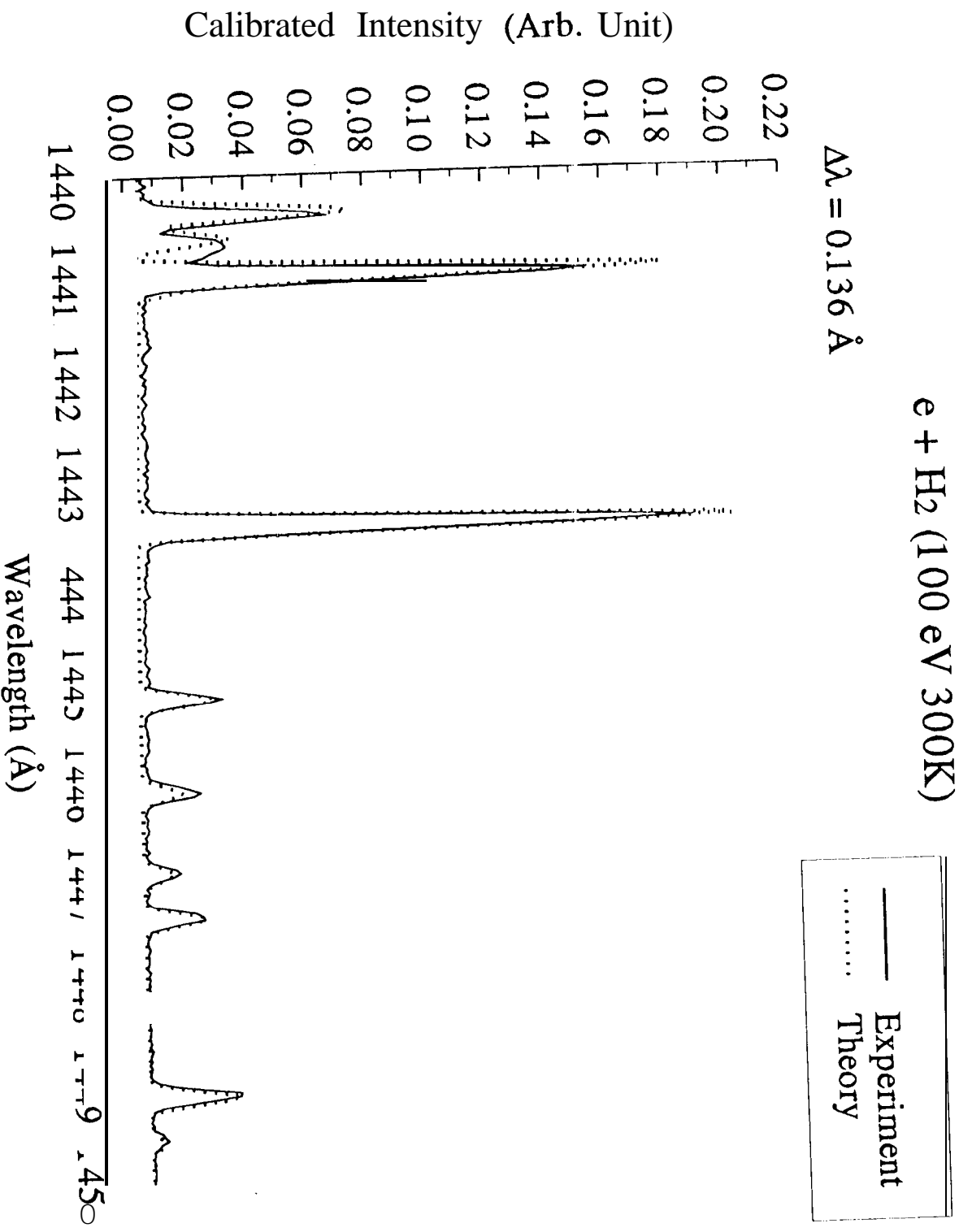
e + H₂ (100 eV 300K)

$\lambda = 0.136 \text{ \AA}$



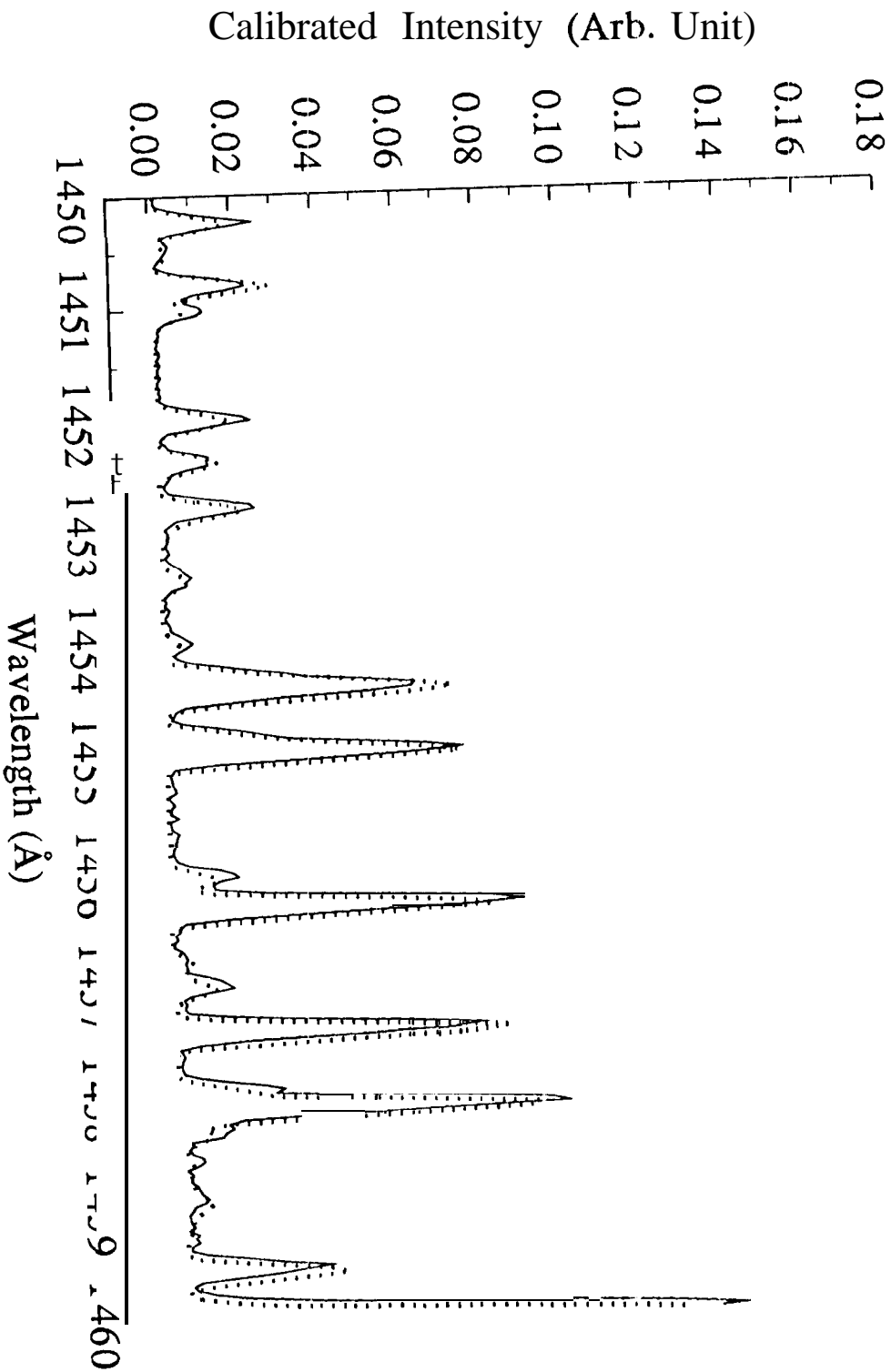
e + H₂ (100 eV 300K)

$\lambda = 0.136 \text{ \AA}$



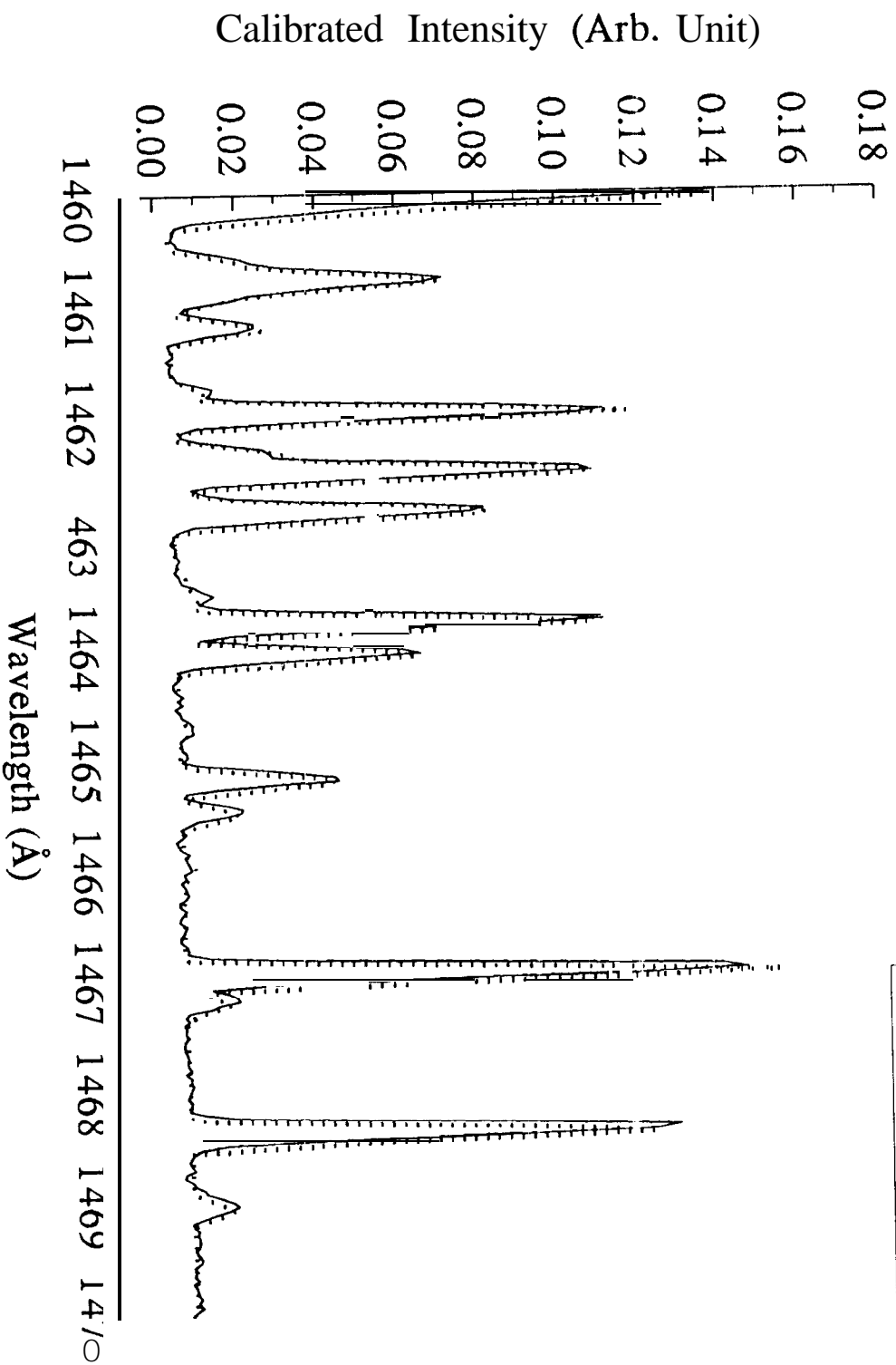
e + H₂ (100 eV 300K)

$\Delta\lambda = 0.136 \text{ \AA}$



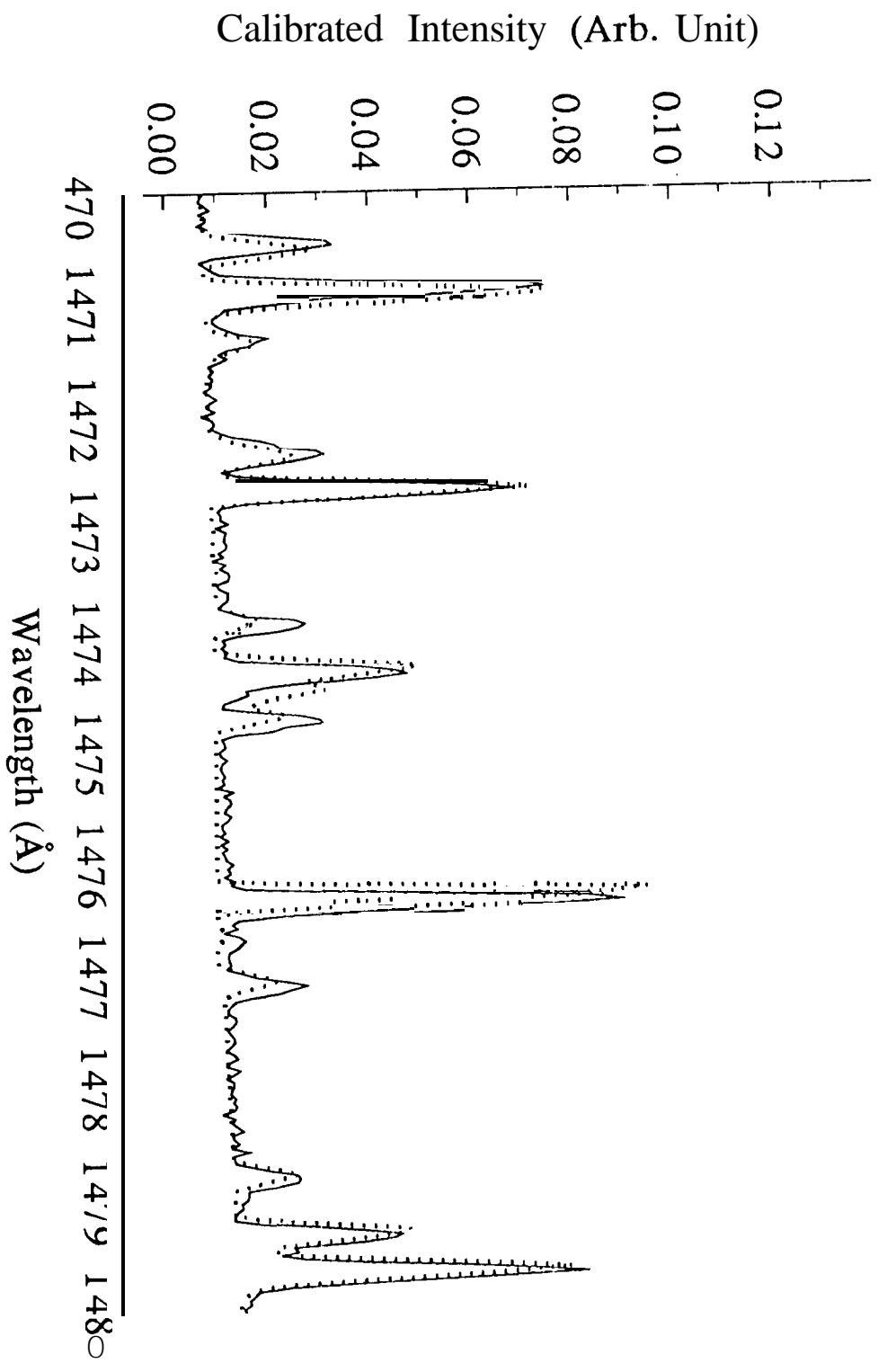
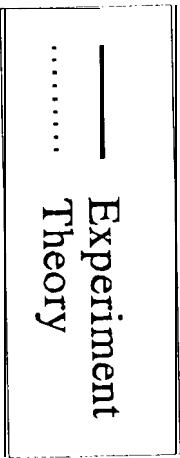
$e + H_2$ (100 eV 300K)

$\Delta\lambda = 0.136 \text{ \AA}$



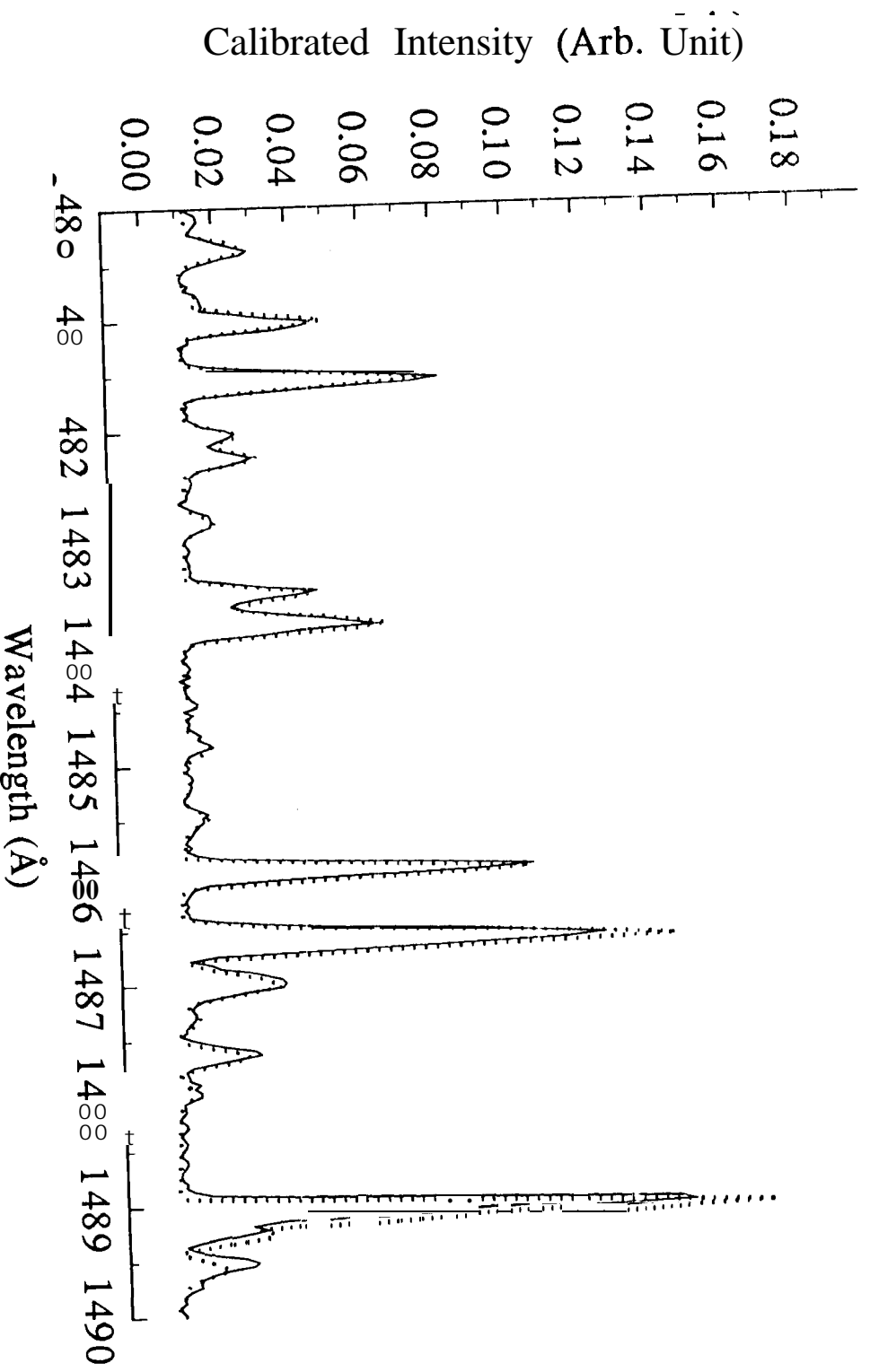
$e + H_2$ (100 eV 300K)

$\lambda_{H\alpha} = 136 \text{ \AA}$



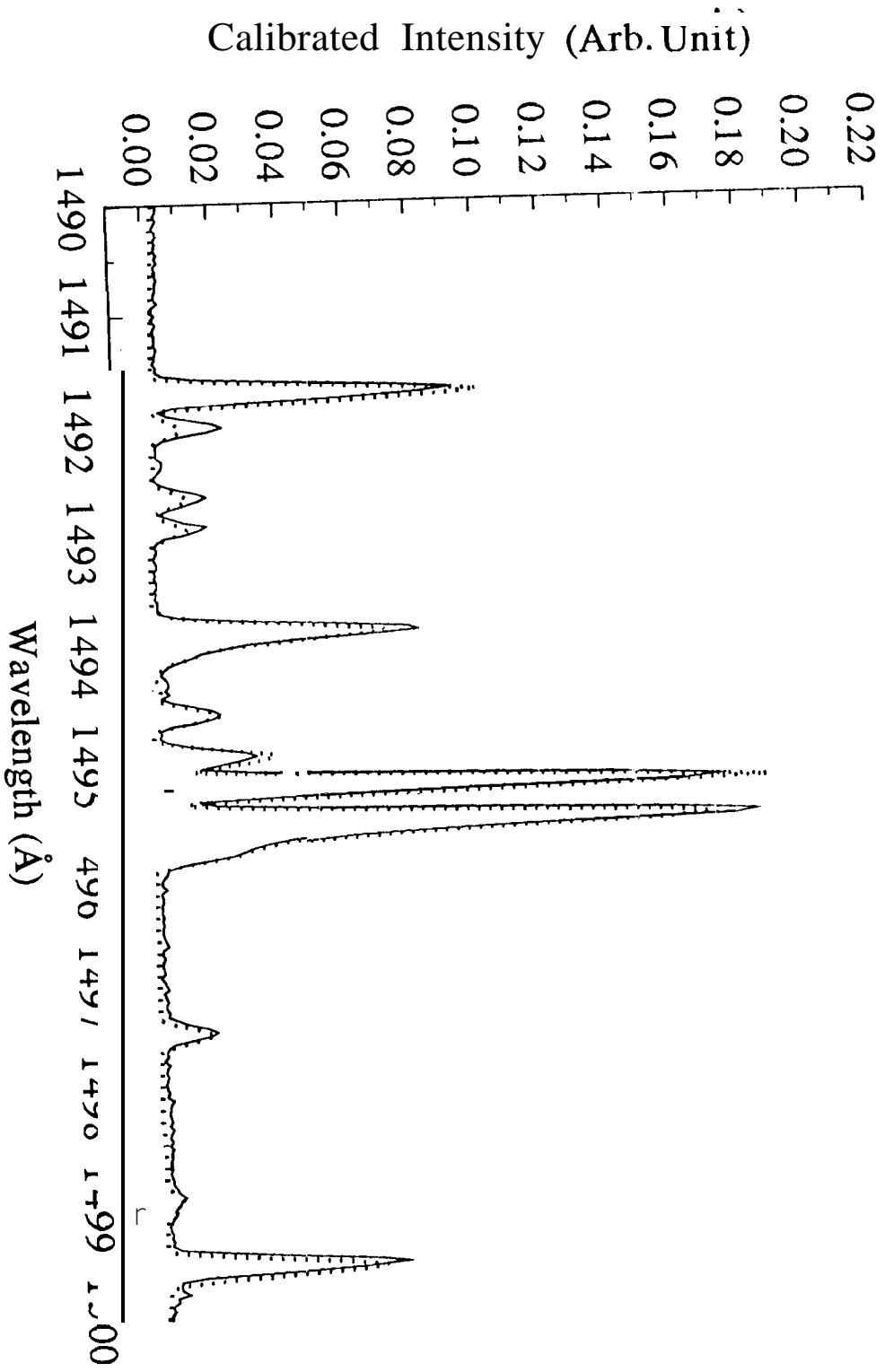
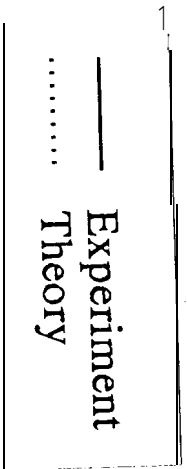
e + H₂ (100 eV 300K)

$\Delta\lambda = 0.136 \text{ \AA}$



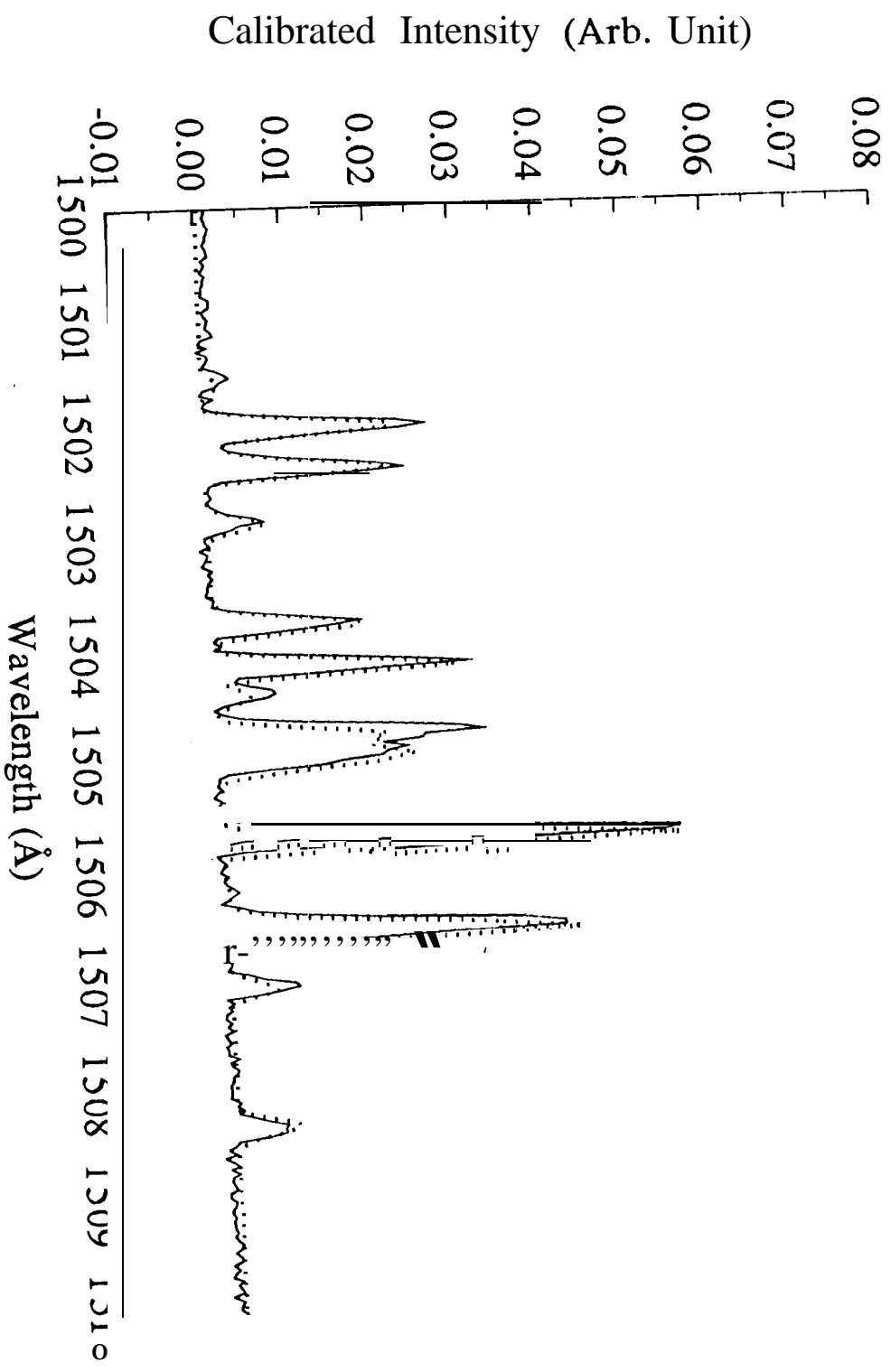
e + H₂ (100 eV 300K)

$\Delta\lambda = 0.136 \text{ \AA}$



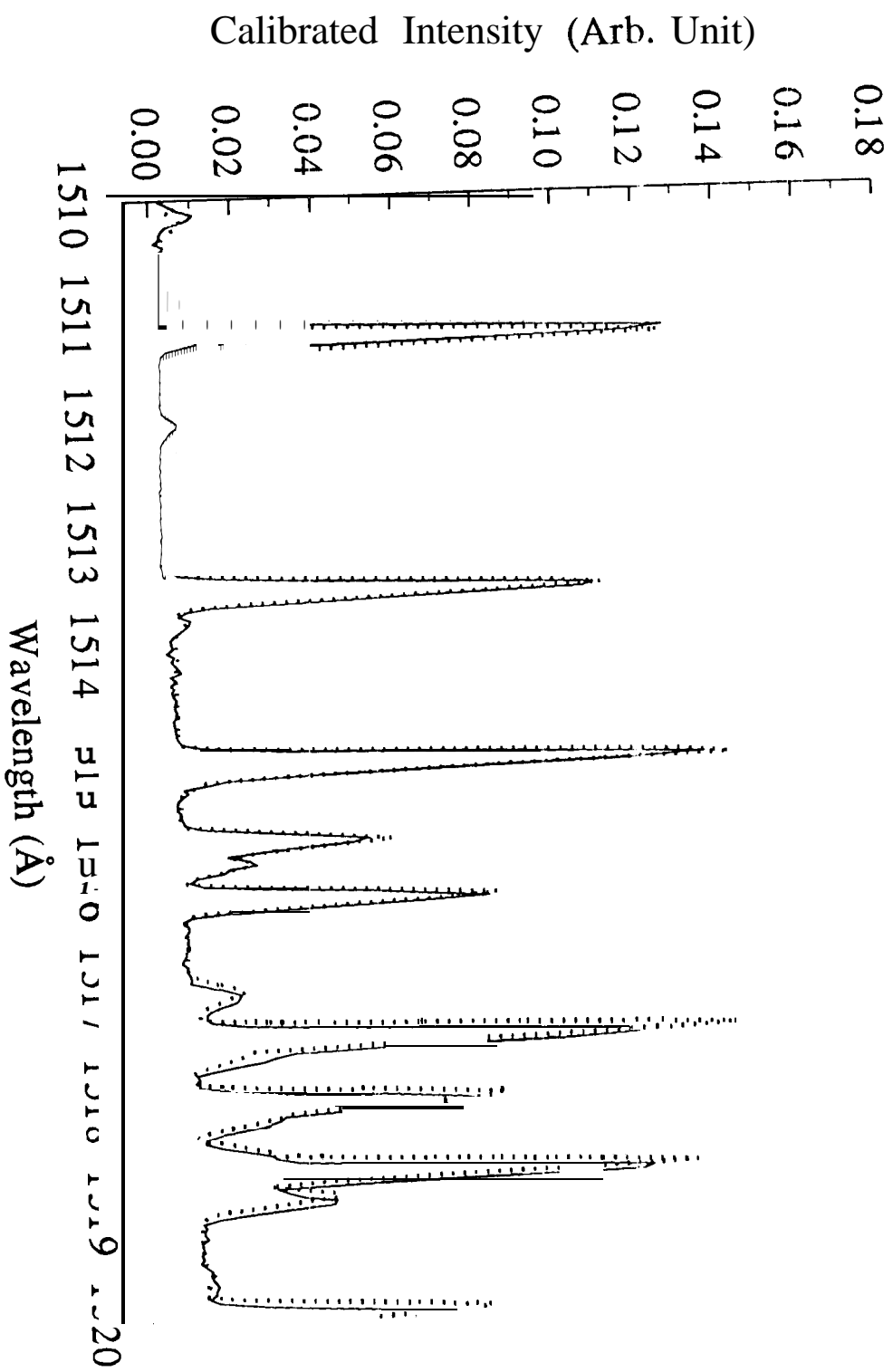
$e + H_2$ (100 eV 300K)

$\lambda = 0.136 \text{ \AA}$



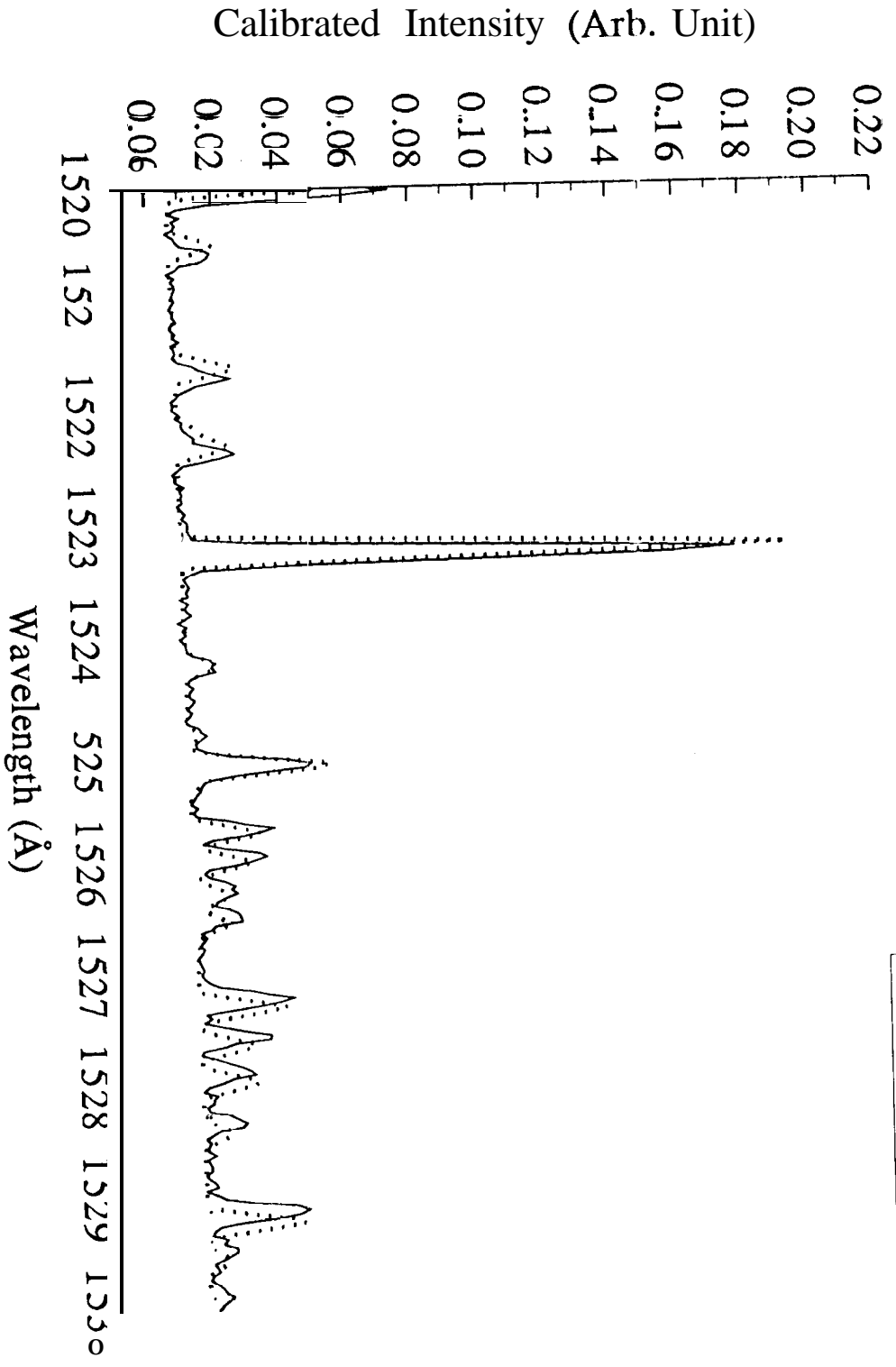
$\Theta + \text{H}_2 \text{ } ^1\infty \text{ eV } 300\text{K}$

$\Delta\lambda = 0.136 \text{ \AA}$



$e + H_2$ (1∞ eV 300K)

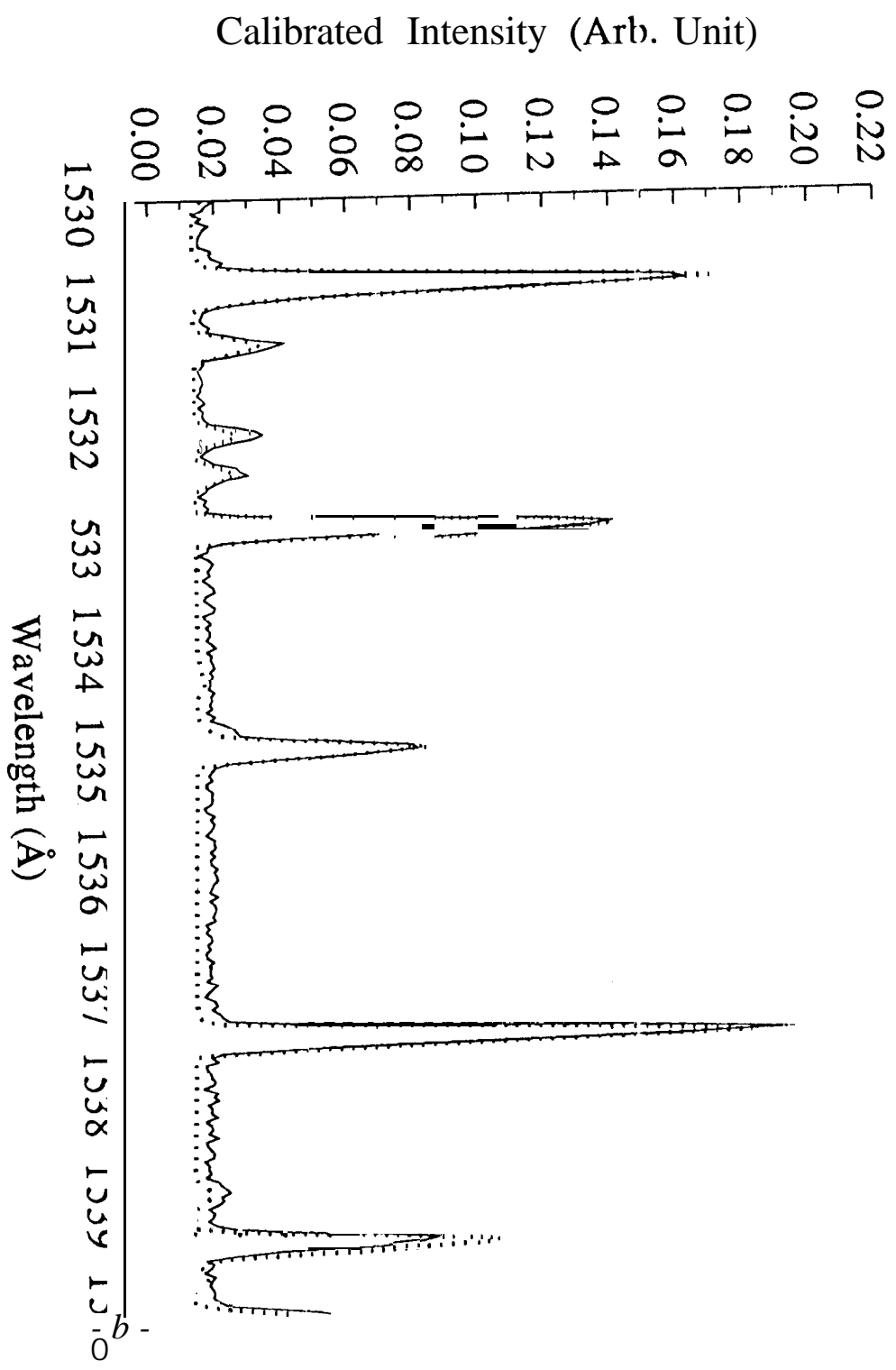
$\Delta\lambda = 0.136 \text{ \AA}$



e + H₂ (100 eV 300K)

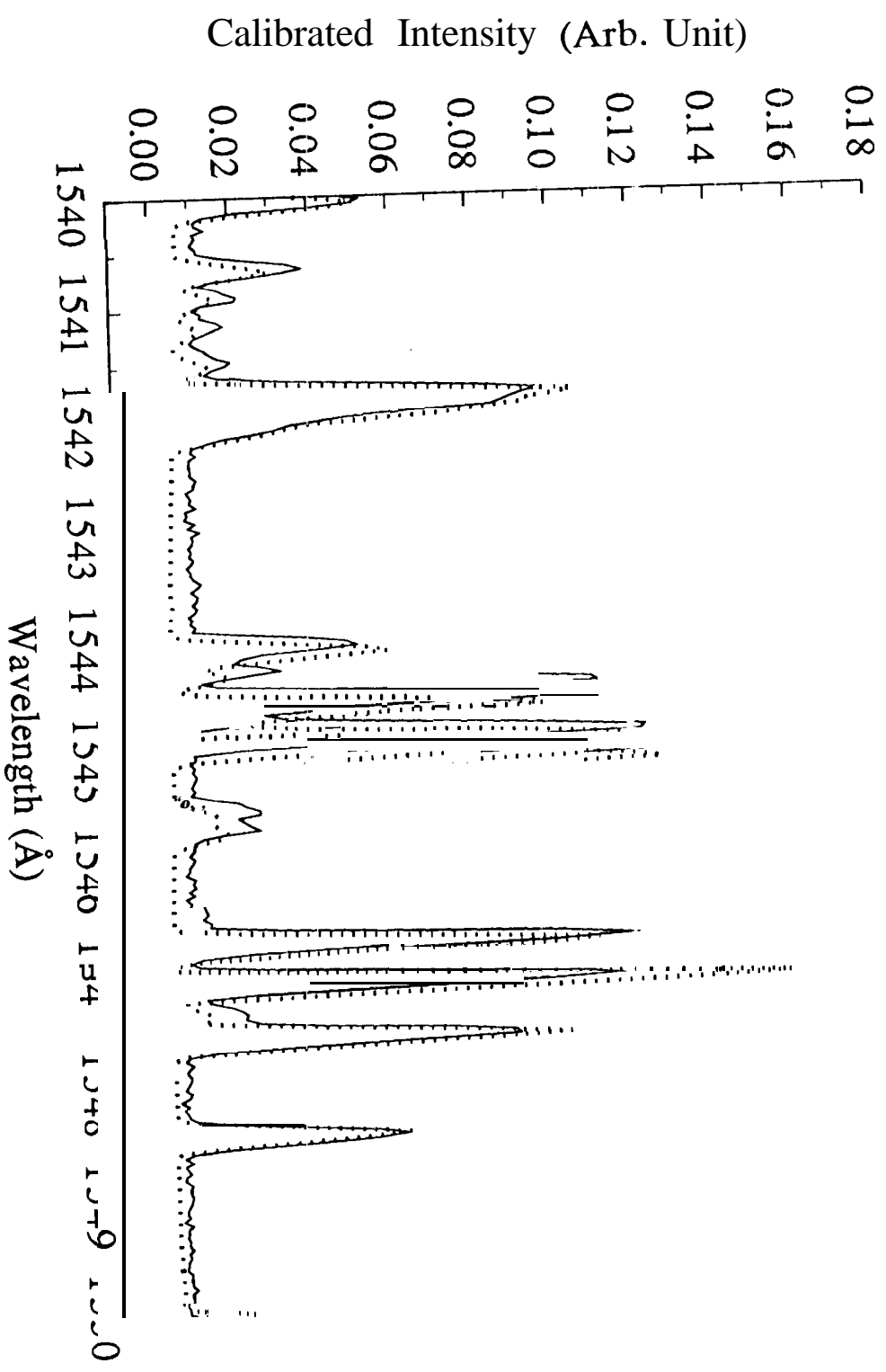
$\Delta\lambda = 0.136 \text{ \AA}$

— Experiment
- - - Theory



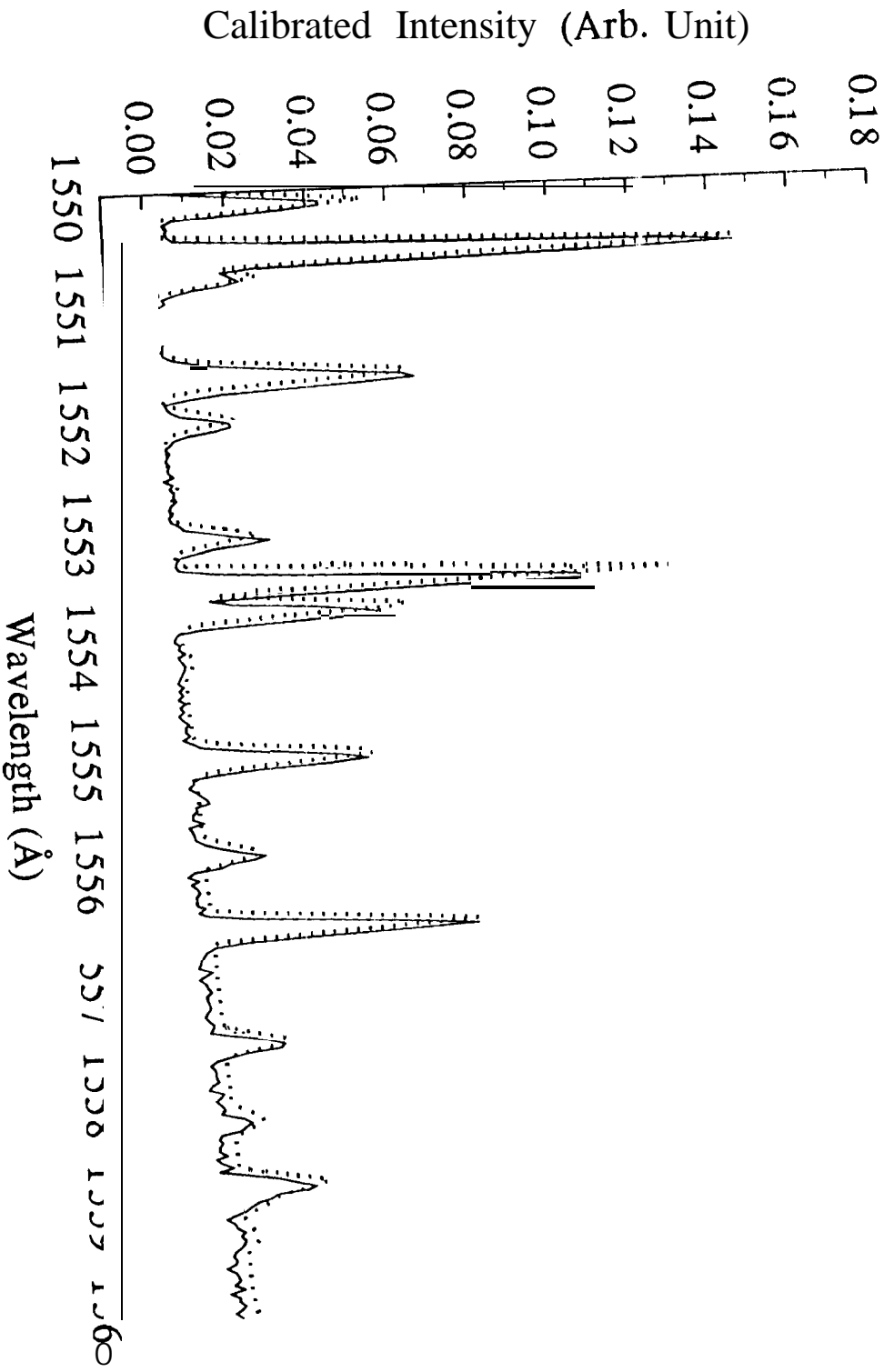
e + H₂ (100 eV 300K)

$\lambda = 0.136 \text{ \AA}$



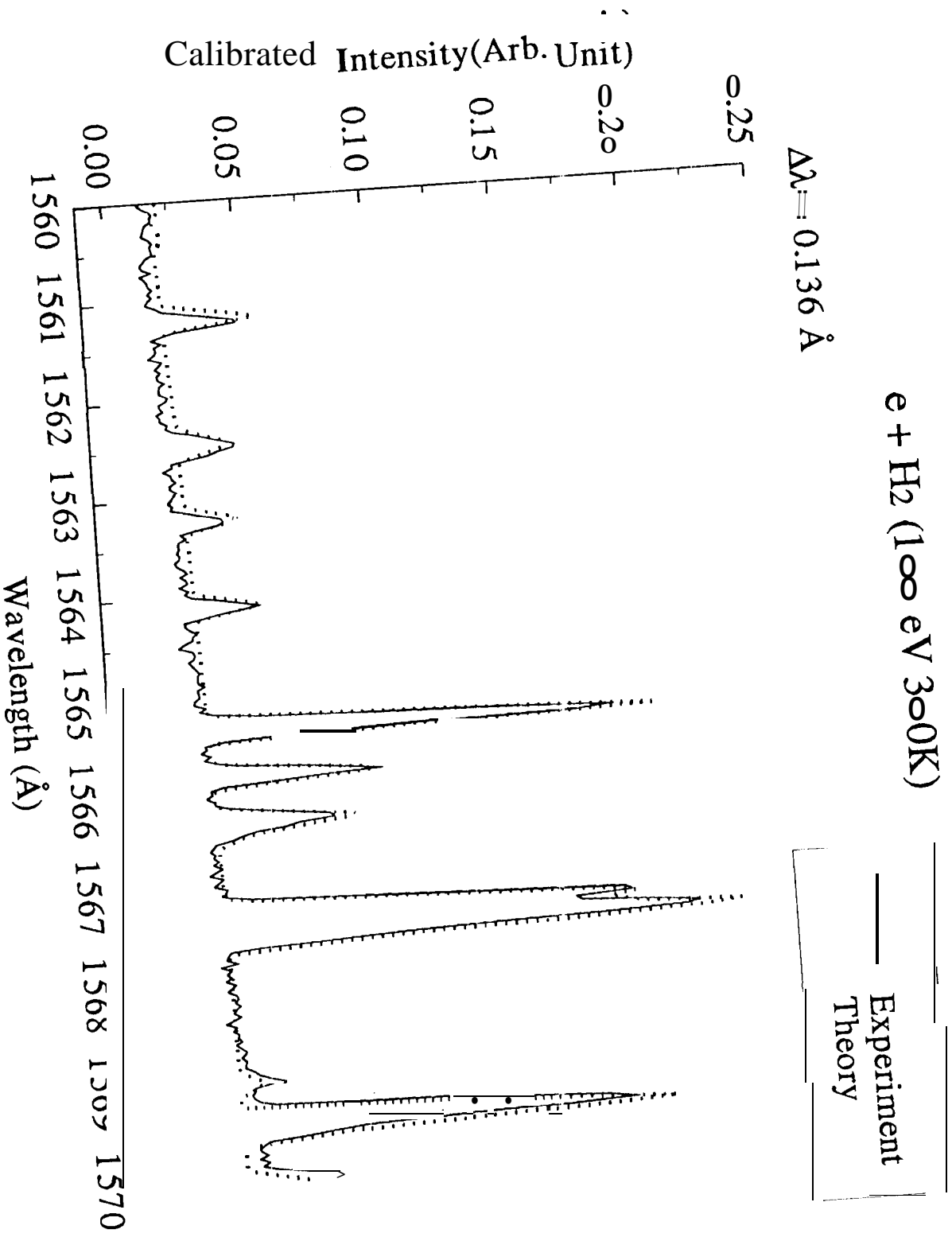
$e + H_2$ (1∞ eV 300K)

$\lambda = 0.136 \text{ \AA}$



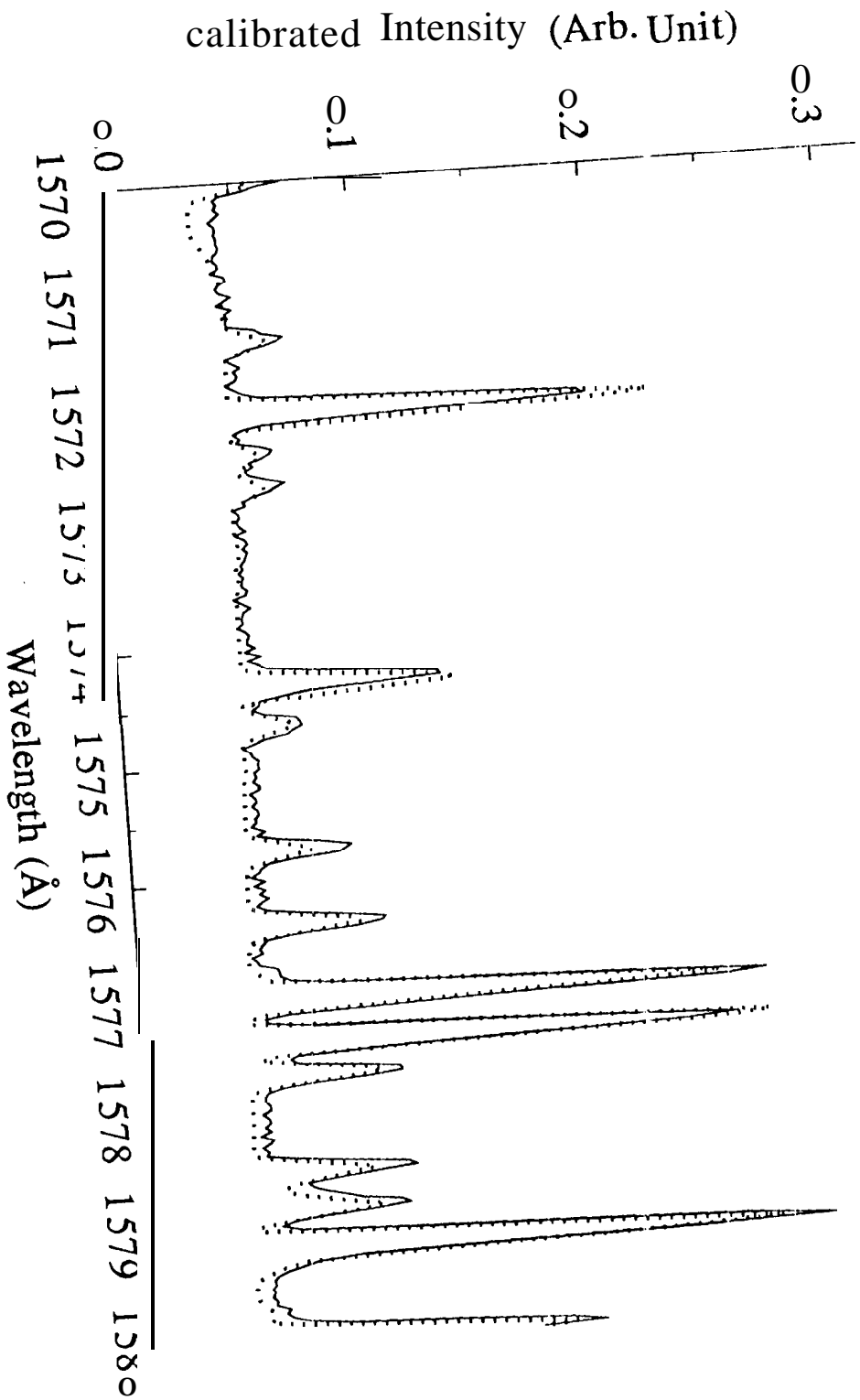
$e + H_2$ (100 eV 300K)

$\Delta\lambda = 0.136 \text{ \AA}$



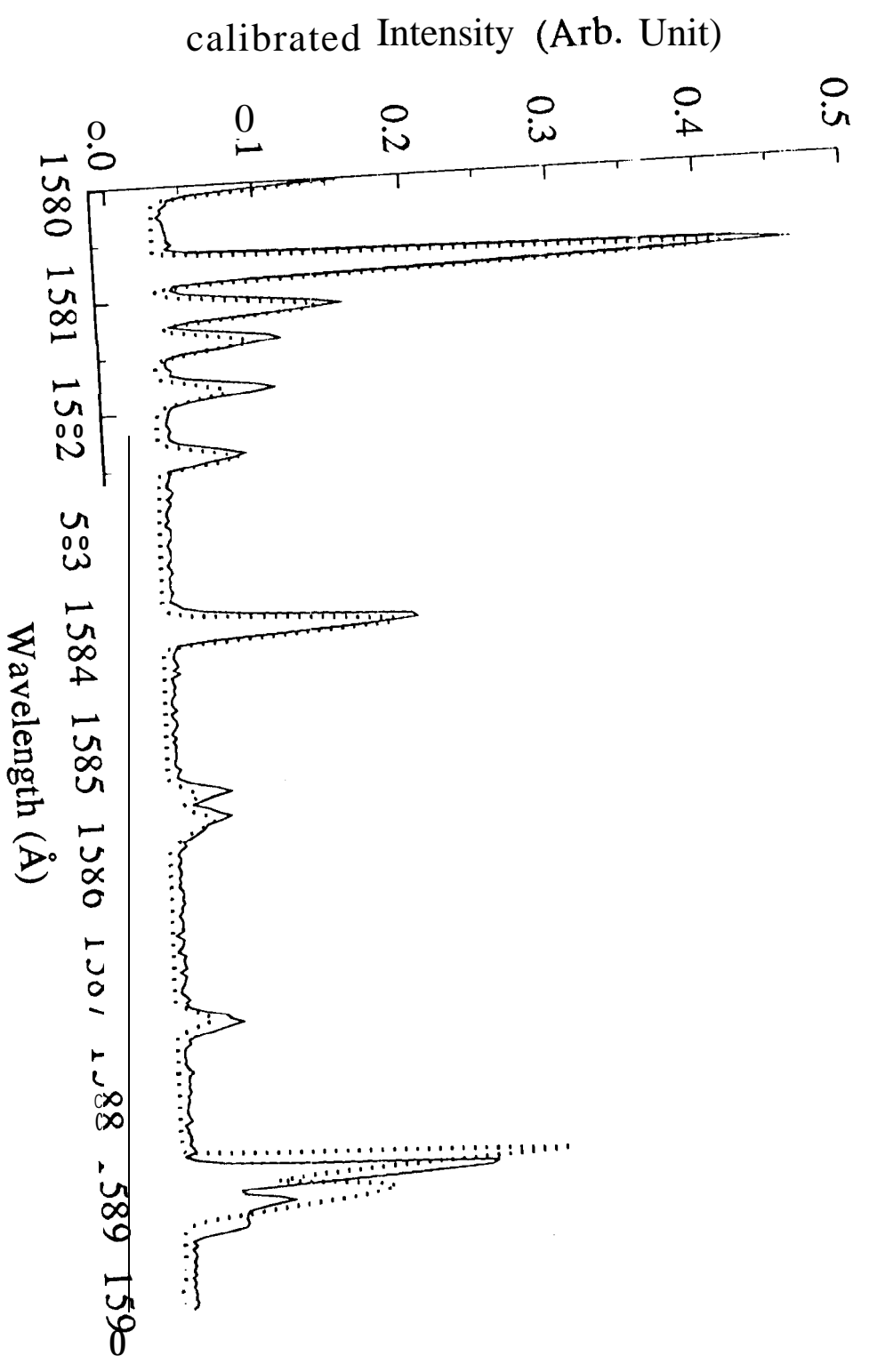
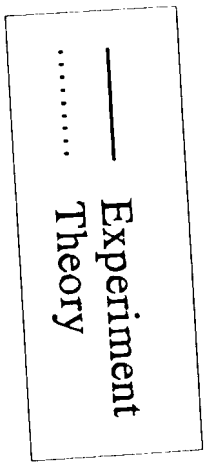
$e + H_2$ (100 eV 300K)

$\lambda = 0.136 \text{ \AA}$



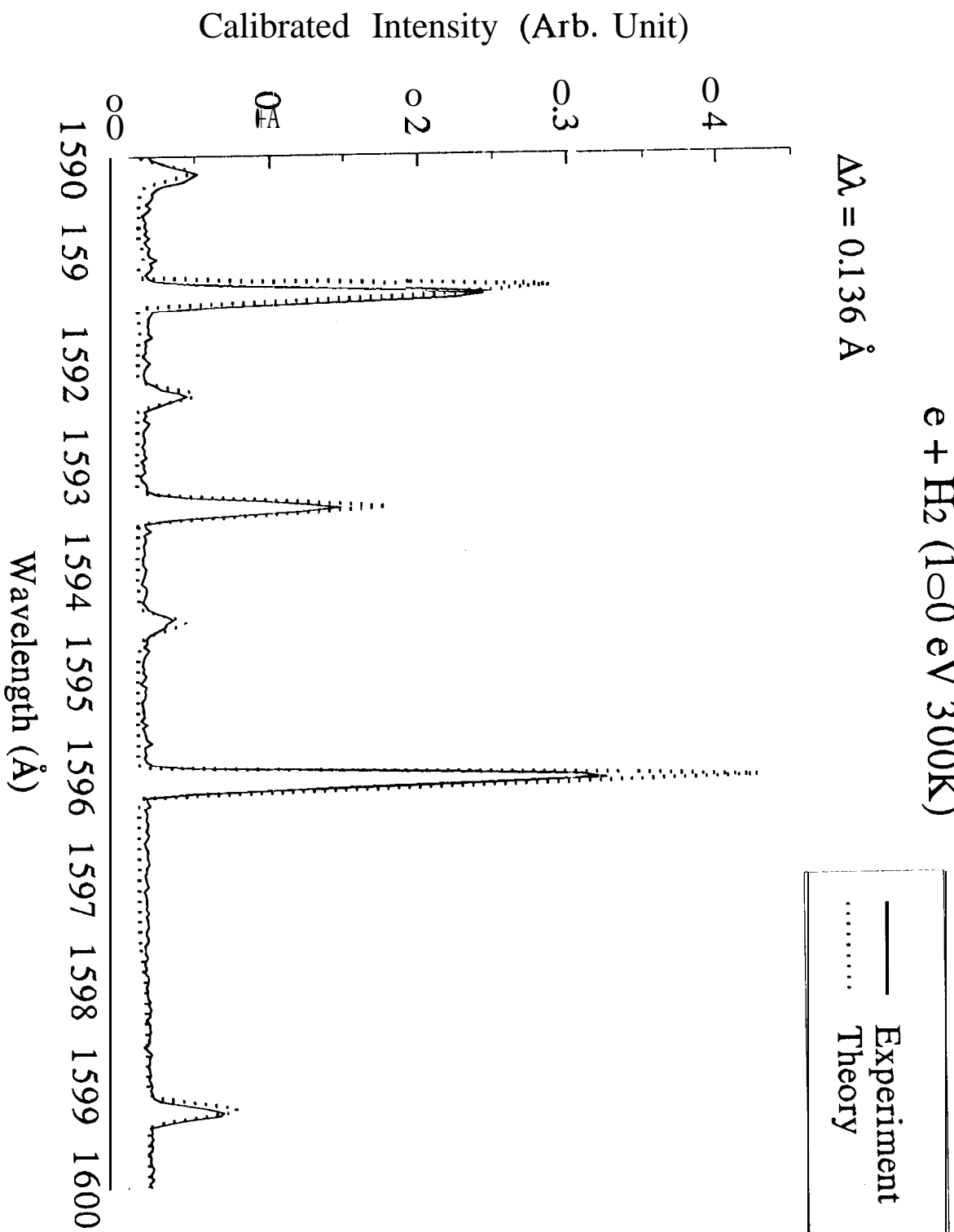
e + H₂ (100 eV 300K)

$\Delta\lambda = 0.136 \text{ \AA}$



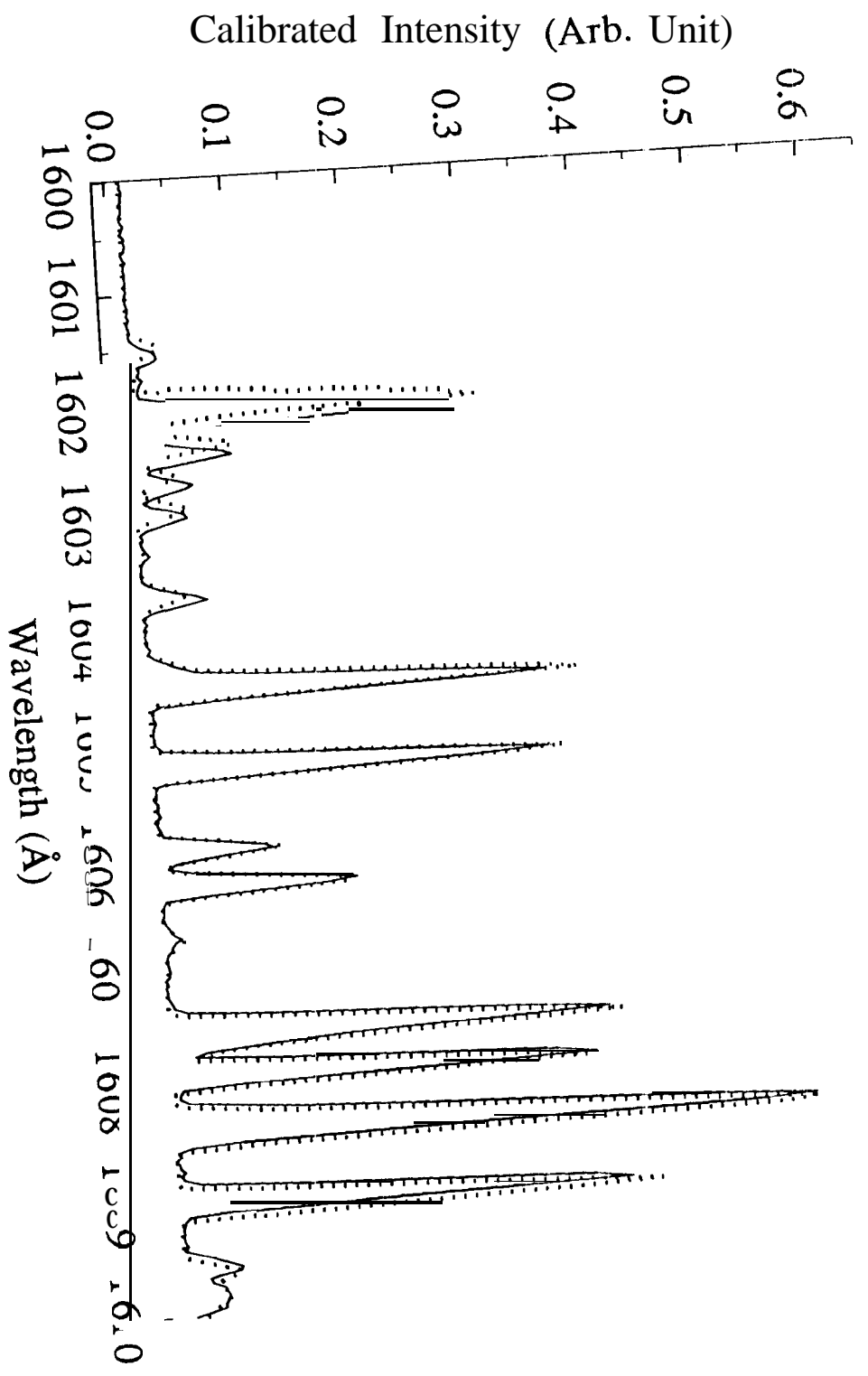
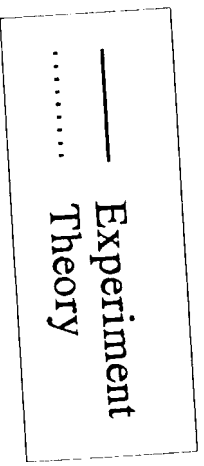
e + H₂ (100 eV 300K)

$\Delta\lambda = 0.136 \text{ \AA}$



$e + H_2$ (1.00 eV 300K)

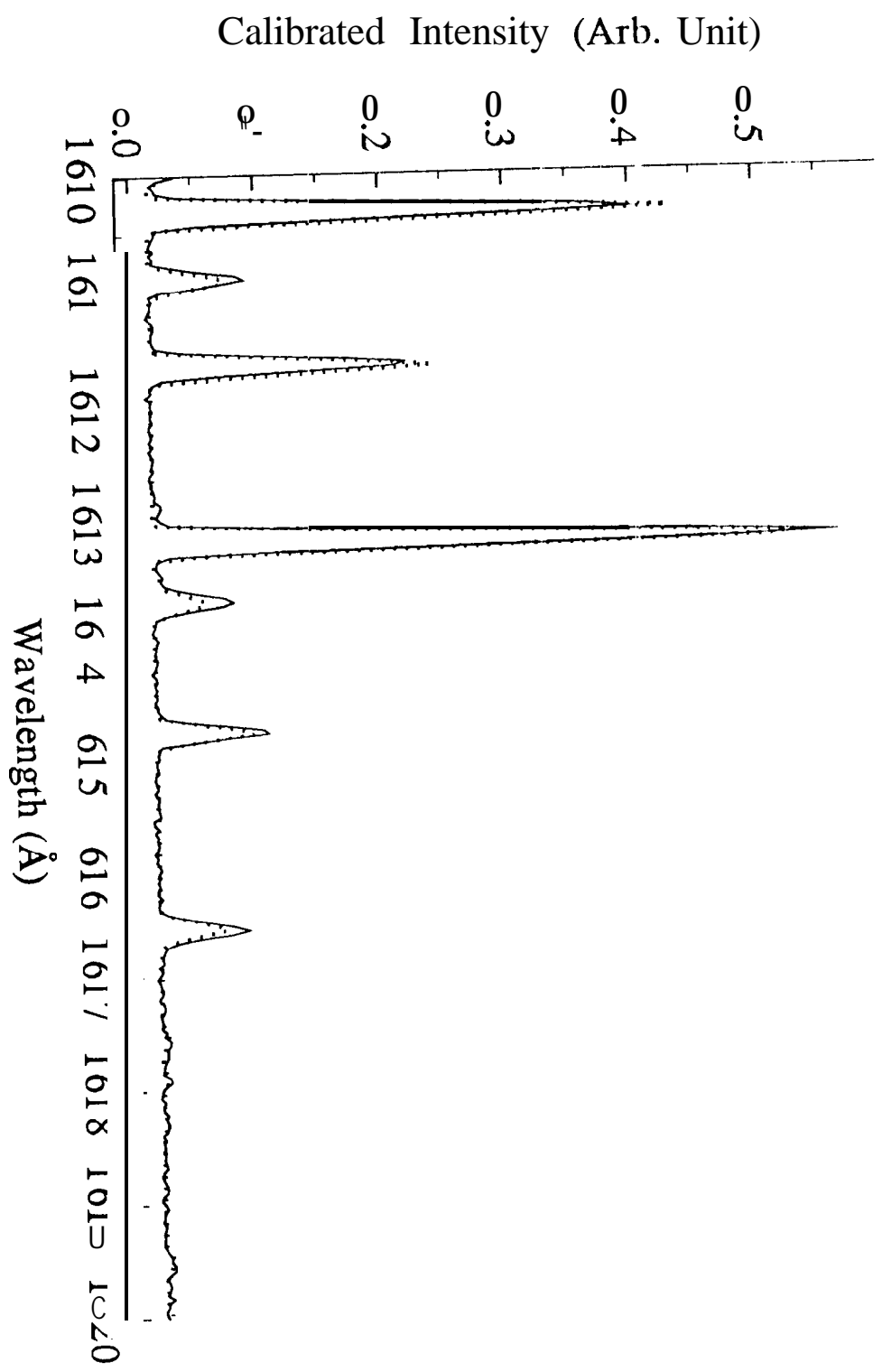
$\Delta\lambda = 0.136 \text{ \AA}$



$\text{S} + \text{H}_2$ (100 eV 300K)

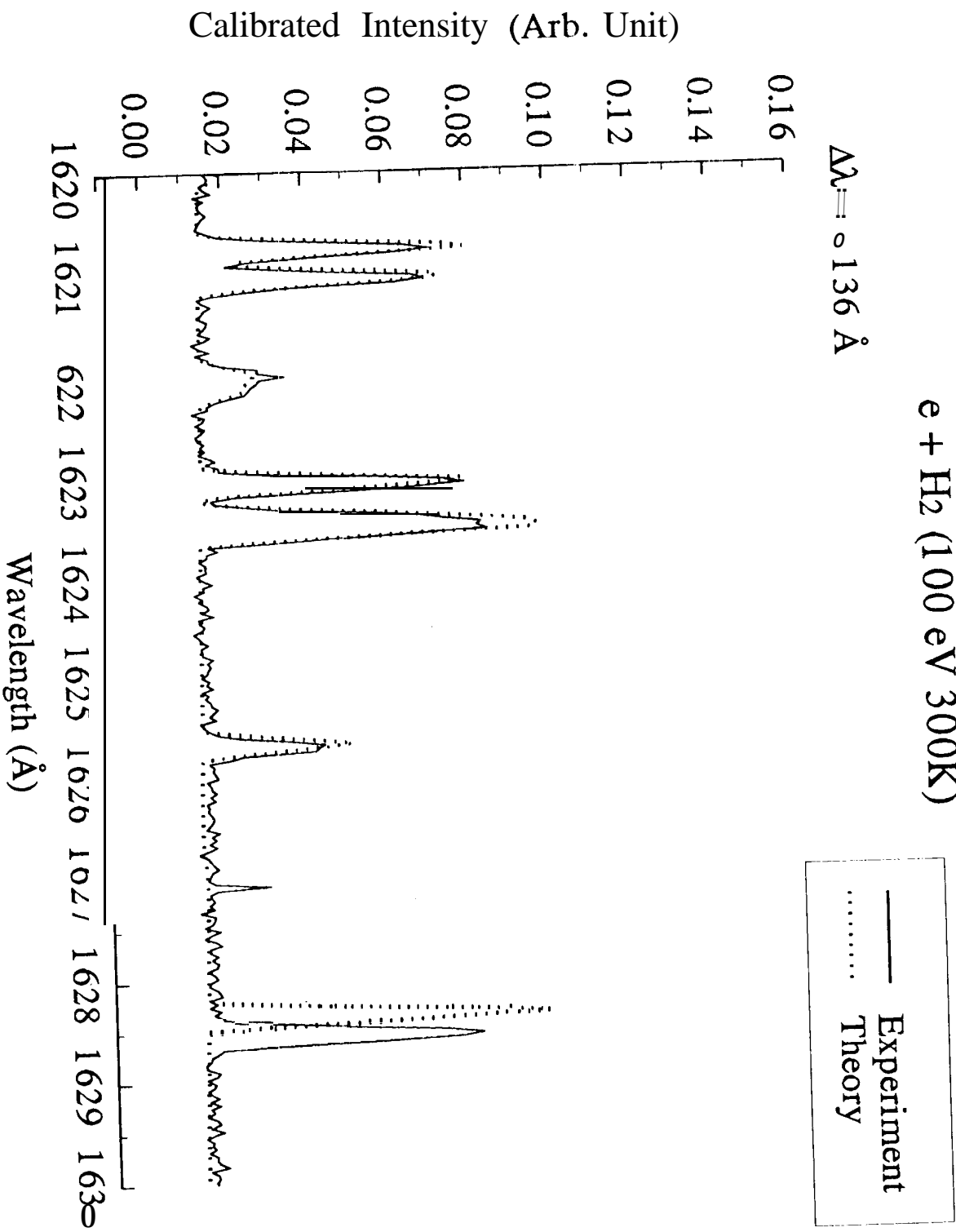
$\Delta\lambda = 0.136 \text{ \AA}$

— Experiment
· Theory



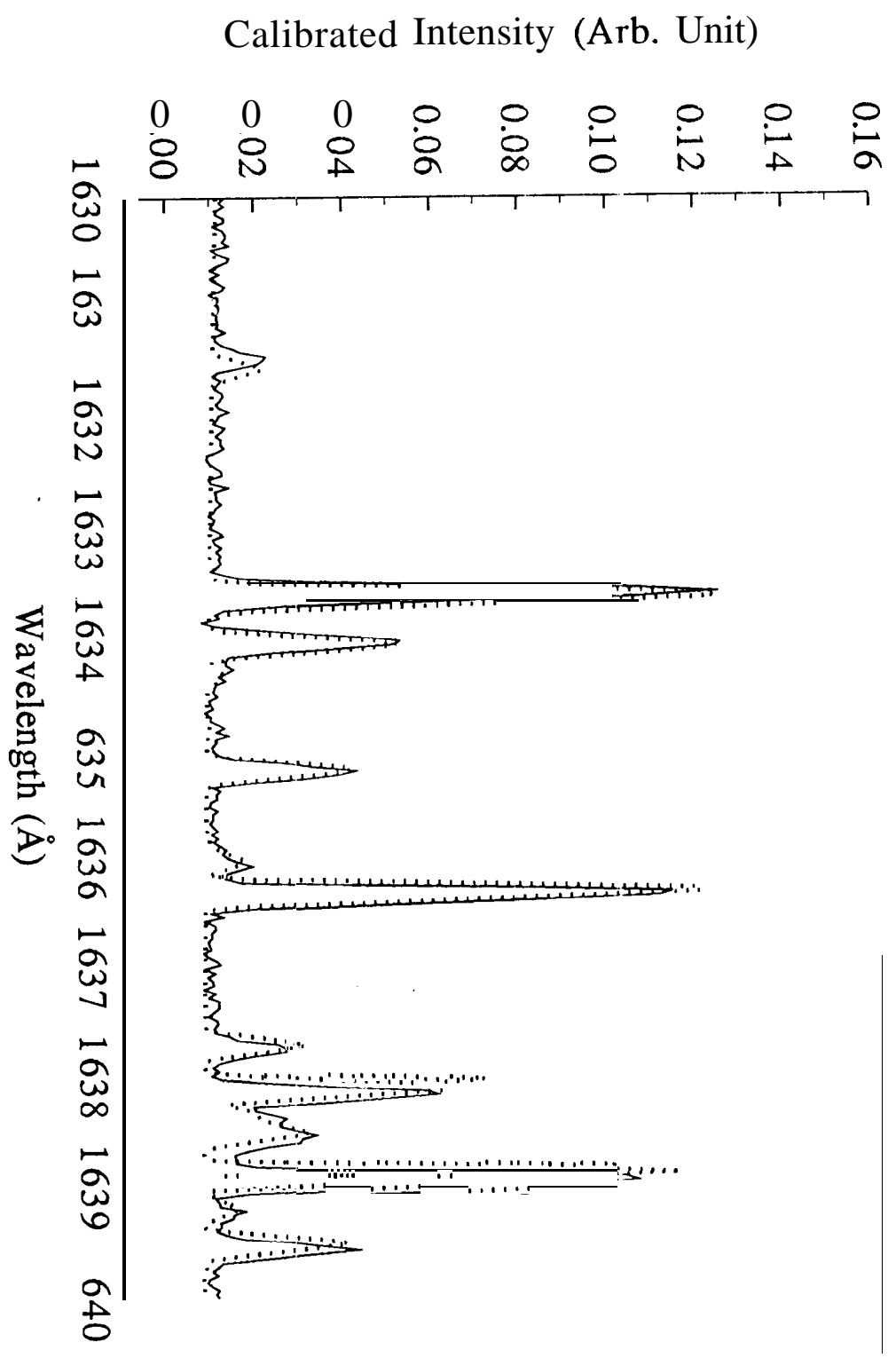
e + H₂ (100 eV 300K)

$\lambda_{\text{ref}} = 136 \text{ \AA}$



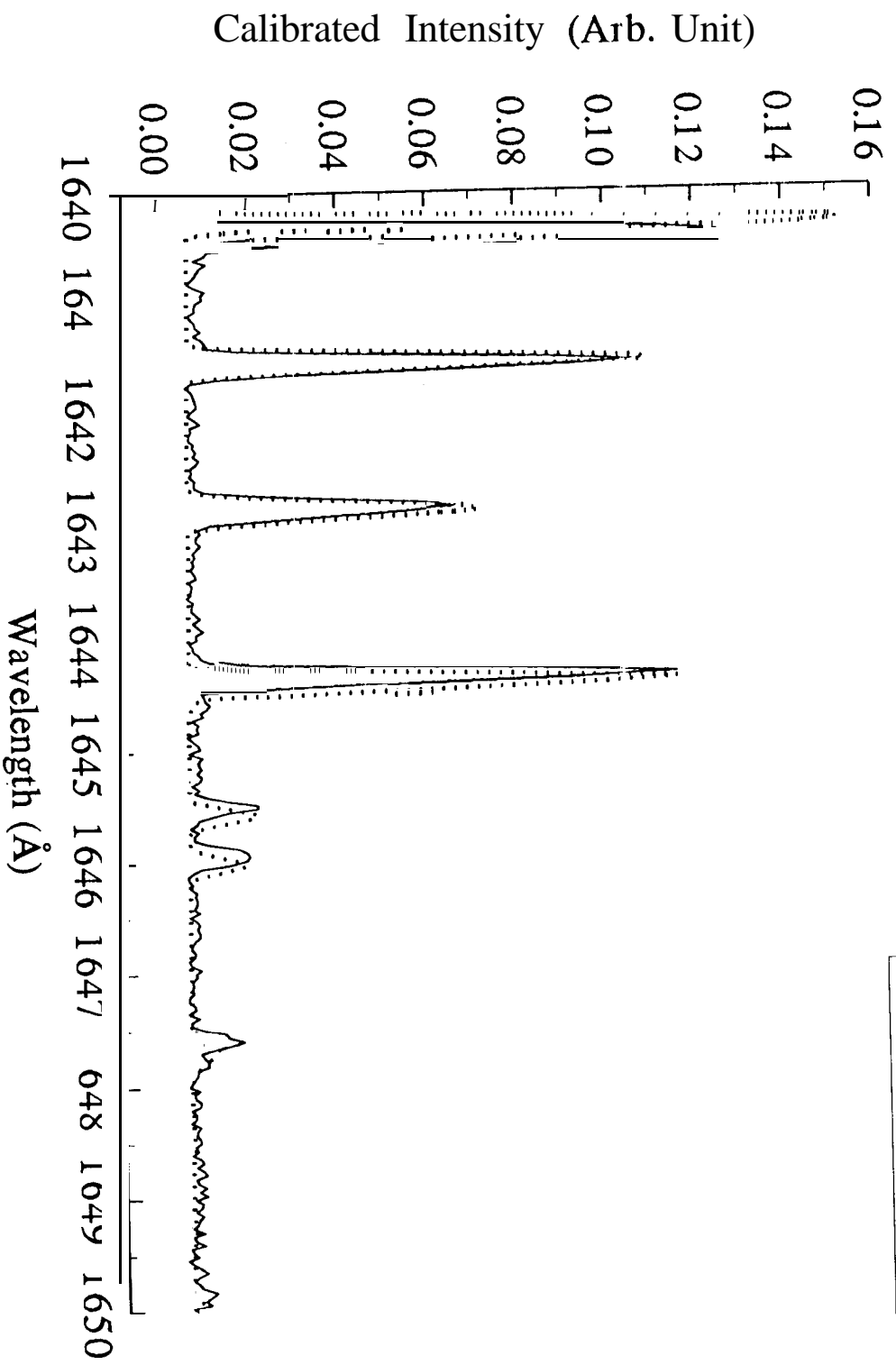
e + H₂ (100 eV 300K)

$\Delta\lambda = 0.136 \text{ \AA}$



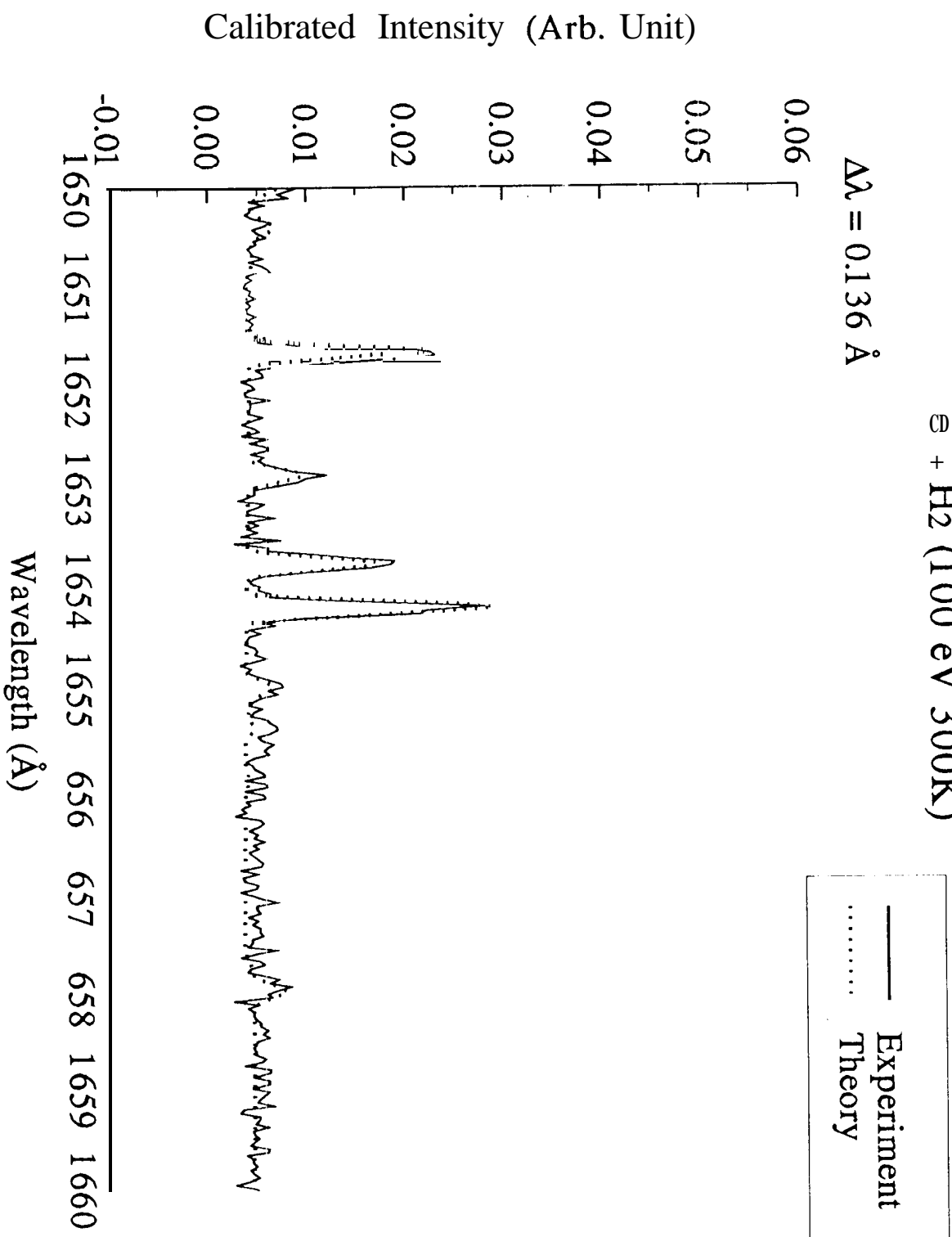
$e + H_2$ (100 eV 300K)

$\Delta\lambda = 0.136 \text{ \AA}$



$\epsilon + \text{H}_2$ (100 eV 300K)

$\Delta\lambda = 0.136 \text{ \AA}$



$e + H_2$ (100 eV 300K)

$\lambda = 0.136 \text{ \AA}$

— Experiment
— Theory

